



**NTNU – Trondheim**  
Norwegian University of  
Science and Technology

# Characterization of wave slamming forces for a truss structure within the framework of the WaveSlam project

**Ignacio Eugenio Rausa**  
**Heredia**

Coastal and Marine Civil Engineering

Submission date: June 2014

Supervisor: Michael Muskulus, BAT

Co-supervisor: Sebastian Schafhirt, BAT  
Øivind Arntsen, BAT

Norwegian University of Science and Technology  
Department of Civil and Transport Engineering





## **TESI DE MÀSTER**

### **Màster**

**MASTER EN ENGINYERIA DE CAMINS, CANALS I PORTS**

### **Títol**

**CHARACTERIZATION OF WAVE SLAMMING FORCES FOR A TRUSS  
STRUCTURE WITHIN THE FRAMEWORK OF THE WAVESLAM PROJECT**

### **Autor**

**RAUSA HEREDIA, IGNACIO EUGENIO**

### **Tutor**

**PROF.DR. MICHAEL MUSKULUS**

### **Intensificació**

**OFFSHORE STRUCTURES**

### **Data**

**13 /06 /2014**





Report Title:	Date: 13 <sup>th</sup> June, 2014		
Characterization of wave slamming forces for a truss structure within the framework of the WaveSlam project	Number of pages (incl. appendices): 180		
	Master Thesis	X	Project Work
Name: Rausa Heredia, Ignacio Eugenio			
Professor in charge/supervisor: Prof. Dr. Michael Muskulus Prof. Dr Øivind Arntsen, PhD. Sebastian Schafhirt			
Other external professional contacts/supervisors: Kasper Wåsjør			

**Abstract:**

The foundations of offshore wind turbines in shallow water are predominantly truss structures which are exposed to wave slamming forces. In these situations the design of the structure is governed by high and rapid impacts which usually are larger than Morison forces. These forces depend, among other parameters, on the slamming factor  $C_s$  that has been ranged by most researchers between  $\pi$  -  $2\pi$ . So far, several researches about slamming forces have been done for monopod structures, but still a long way to go regarding truss structures.

This master thesis is based on the WaveSlam project in which an instrumented multi-membered truss model has been subjected to hundreds of both regular and irregular waves. The experiments have been performed in the large wave flume at FZK Hannover in 2013. The tested structure was equipped with force transducers along the bracings and columns that measured the structure response from the breaking waves.

The initial goal of this research project is to characterize the breaking wave forces acting on the front bracings in order to get the slamming factors associated to them. For that purpose the structure tested in Hannover has been modelled and validated in a finite element model in ANSYS (1:8).

An initial analysis of the data shows an average time delay in the impact of the wave front. This time delay is around 0.003 s for the points located at the same height in the front bracings.

Using the recreation of the truss structure in ANSYS a wave run test is analyzed. Throughout a fitting procedure, the response from ANSYS and from the data are matched with a relative error of 3%. The wave loads have been defined as uniform loads with a triangular force time history acting along the bracings. The total load duration for those breaking wave loads goes from 0.0049 to 0.007 seconds. These values agree with the expected duration found in the literature.

From this initial analysis a slamming factor of  $C_s = 4.78$  is found in the highest part of the front instrumented bracings. The characterization of more breaking wave loads is recommended in order to get an estimate of the largest slamming factor.

Keywords:

1. Truss structure
2. Inverse Problem
3. ANSYS
4. Slamming coefficients



*Bak skyene skinner alltid solen*  
*Behind the clouds the sun is always shining*





## **PREFACE**

This master thesis analyzes part of the data that have been obtained from the experiments on a truss structure, which was carried out in the Large Wave Channel, at Forschungszentrum Küste (FZK), Hannover, Germany in May and June, 2013. The objective of this master thesis is to estimate local wave forces during the initial instants of impact acting on the truss structure.

## **ACKNOWLEDGEMENT**

The work described in this publication was supported by the European Community's 7th Framework Programme through the grant to the budget of the Integrating Activity HYDRALAB IV, Contract no. 261520.

I would like to express my gratitude and my sincerest appreciation to those who helped me accomplish this study. I would like first to thank to the professor in charge: Michael Muskulus, and my other supervisors: Øivind Asgeir Arntsen and Sebastian Schafhirt for their useful comments and remarks throughout all the meetings that we have had.

Special thanks to Kasper Wåsjør for assisting me in the modelling process in ANSYS during my stay in Reinertsen, Trondheim. It would have been much more difficult without your valuable comments about any problem I came up. Thanks also to Matthias Kudella who helped me in the reconstruction of the test structure.

Finally, special recognition and gratitude comes out to my family for their support, encouragement and motivation throughout all this way. Last but not least, I would like to thank to all my friends, especially to Marc Garcia and Silvia Medina for your support and advice.

## **DISCLAIMER**

This document reflects only the authors' views and not those of the European Community. This work may rely on data from sources external to the HYDRALAB IV project Consortium. Members of the Consortium do not accept liability for loss or damage suffered by any third party as a result of errors or inaccuracies in such data. The information in this document is provided "as is" and no guarantee or warranty is given that the information is fit for any particular purpose. The user thereof uses the information at its sole risk and neither the European Community nor any member of the HYDRALAB IV Consortium is liable for any use that may be made of the information.

Ignacio Eugenio Rausa Heredia,

Department of Civil and Transport Engineering, NTNU, June 2014.



## **TASK DESCRIPTION**

For the Master's thesis during the spring semester 2014, the student shall to estimate local wave forces acting on a truss structure during the first milliseconds of wave impact, using measurement data from the WaveSlam experiment performed at Forschungszentrum Küste in 2013 (Hannover, Germany).

So, the main goal of this project shall to find the wave forces acting on the structure from the responses recorded in the Large Wave Flume.

A finite element model of the structure (large scale 1:8) shall be developed and validated in ANSYS. The measurements shall be statistically analyzed and wave forces shall be estimated by matching the response on the numerical model.

Finally from the estimation of the acting wave loads the slamming factor shall be calculated.

The following tasks will be addressed:

- Literature study
- Statistical analysis of local measurements on the bracings
- To develop a finite element model for a transient analysis in ANSYS. This part is the core of the Master Thesis and will be developed in collaboration with Reinertsen SA.
- Validating and updating the numerical model for the local response on the bracings and a global response as well.
- Estimating wave forces.
- Characterization of slamming factors in the front bracings.



## SUMMARY

The foundations of offshore wind power energy are mainly classified whether the wind turbines are located in deep water or in shallow water (<25m water depth).

The design of the foundations in deep water requires the study of the non-breaking wave forces. These wave forces have been extensively studied and Morison's equation (1) (Morison, et.al, 1950) is the most used equation to calculate them:

$$dF = dF_D + dF_M = \frac{1}{2} \rho_w C_D D |u| u dz + \rho_w \frac{\pi D^2}{4} C_M \frac{du}{dt} dz \quad (1)$$

where  $\rho_w$  is the water density,  $C_D$  is the drag coefficient,  $D$  is the diameter,  $u$  is the water particle velocity,  $d$  is the water depth and  $C_M$  is the inertia coefficient.

The Morison's equation is composed by the action of quasi-static inertia and drag forces.

For shallow water the slamming forces (2) have to be added to the Morison's forces and these three components: drag forces, inertia forces and slamming forces define completely the action of the wave. The forces produced from the breaking wave are supposed to be dominant in front of Morison's forces.

$$F_s = C_s \rho_w \lambda \eta_b C_b^2 R \quad (2)$$

where  $C_s$  is the slamming factor,  $\rho_w$  is the water density,  $\lambda \eta_b$  is defined as the length of impact;  $R$  is the radius of the element and  $C_b$  is the wave celerity.

Among all these factors, there is one which has been particularly investigated throughout many years, especially on a single vertical and inclined pile. This factor is the well-known slamming factor  $C_s$ , and for different researches it has been ranged from  $\pi - 2\pi$ . Regarding to truss structures not so many researches have been done so far.

The estimation of this factor represents the ultimate goal of this master thesis and can be easily calculated once the breaking wave load has been properly defined.

The thesis is based on the experiments carried out last year in the Large Wave Flume in Hannover. A truss structure was built up in Large scale (1:8) and tested for different waves. The structure is equipped with force transducers along the bracings and on the front legs as well.

From the responses recorded on different transducers along the truss structure an estimation of the wave loads acting on it should be found through a fitting procedure using the model in ANSYS, which will recreate the structure tested in the Large Wave Flume.

This method is known in the literature as Inverse problem.

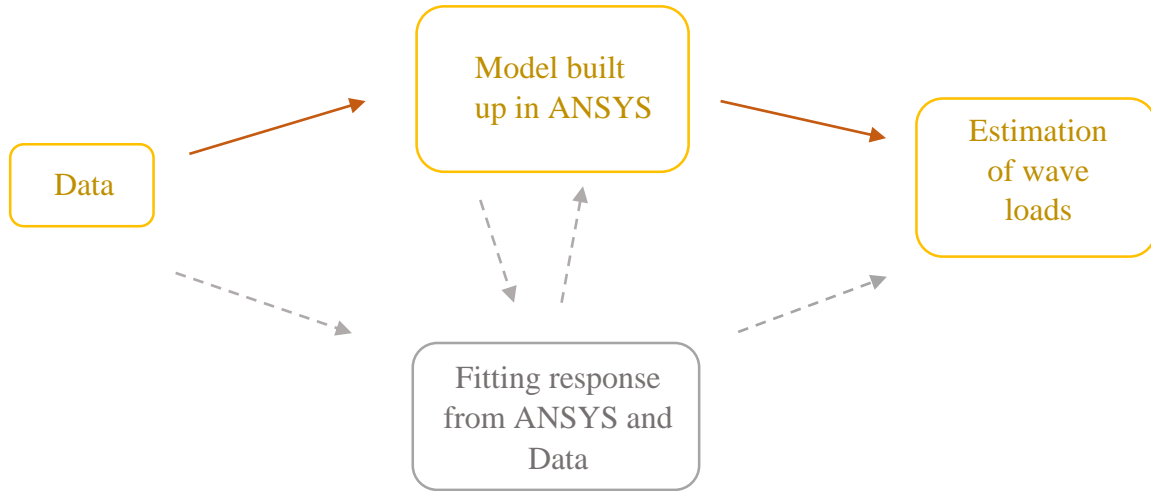


**Figure 0.1: Scheme of an Inverse problem**

Therefore, the modelling of the structure is a center part of the thesis due to the fact that a reliable model is necessary to get closer estimates for the breaking wave loads and consequently for the slamming factors. To trust in the model a validation process has been applied both for local and global response. The truss structure was exposed to regular waves and different hammer tests were applied as well. The response from these hammer test located on different parts of the structure have been used to validate and update the model in ANSYS.

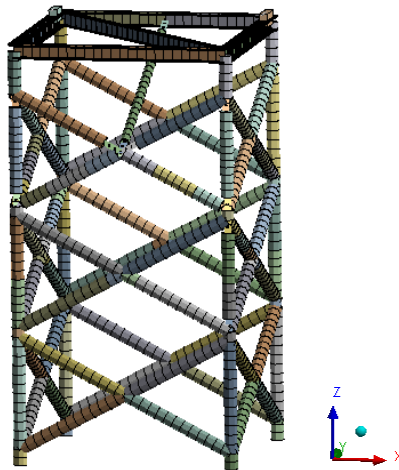


**Figure 0.2: Representation of the model built up in ANSYS**

For the validation process a good fit for the initial peaks of the response from ANSYS was required. Several sensitivity analysis have been done in order to improve this initial response both for the front instrumented bracings and the overall response.

This process has modified the following material properties in the ANSYS model with respect to the initial set-up in the Large Wave Flume:

- Density and Young Modulus at the front instrumented bracings
- Young Modulus of the instrumented columns
- Density of the upper beam connecting the front instrumented bracings to the top back side of the structure.

Moreover, during the data processing some inconsistencies have been found for the two total force transducers located at the top of the structure. This strange behavior occurs for all hammer tests carried out on 11<sup>th</sup> and 24<sup>th</sup> June, 2013. The response of these transducers seems limited to a certain value and no higher values are recorded, whereas the ANSYS response of those points is not limited at all. This behavior is not appreciated when wave larger loads impact the structure during the wave tests.

Other calibration errors in different local force transducers were discovered and reported to Mattias Kudella, one of the people who was in charge of this WaveSlam experiment.

A preliminary statistical analysis has been carried out for both force and time response. From that analysis a certain asymmetry of the front wave is appreciated. For the force transducers located at the same height there is an existing average time delay in the maximum response at around 0.0027 s.

Several uncertainties in some aspects such as: curling factor, possibility of wall effects, run-up effect, accurate determination of Morison forces and whether the wave breaks a few meters before the structure, just in front, or at the back side generates large dispersion on the results.

Once the model in ANSYS has been calibrated and locally and globally validated, the study of the wave loads acting on the front bracings is carried out for the *wave test 2013061414*.

A complementary analysis using what is called as the frequency response function (FRF) is used to get more understanding of the impact load and as was expected it shows a triangular force time history with a very short peak time. This method allows to get the impulse force from the measured response and it will be further explained in the following chapters.

The initial response is filtered down in order to only analyze the impulse response. A fitting procedure has been carried out in order to reduce the deviation between the data and ANSYS results. Four uniform wave loads have been applied along different parts of the bracings simulating the breaking wave. The time duration of all four wave loads is ranged from 0.005 to 0.007 s, and it has been found as one of the main governing parameters of the response.

Finally, for the case studied a slamming coefficient of 4.78 is found in the highest part of the instrumented front bracings.





## TABLE OF CONTENTS

<b>ABSTRACT .....</b>	<b>I</b>
<b>PREFACE .....</b>	<b>III</b>
<b>TASK DESCRIPTION .....</b>	<b>IV</b>
<b>SUMMARY .....</b>	<b>V</b>
<b>TABLE OF CONTENTS.....</b>	<b>VIII</b>
<b>LIST OF FIGURES .....</b>	<b>XI</b>
<b>LIST OF TABLES .....</b>	<b>XV</b>
<b>1. INTRODUCTION.....</b>	<b>1</b>
<b>2. BACKGROUND AND LITERATURE REVIEW .....</b>	<b>2</b>
<b>2.1 Introduction .....</b>	<b>2</b>
<b>2.2 Literature review.....</b>	<b>2</b>
2.2.1 <i>Morison Equation</i> .....	2
2.2.2 <i>Slamming forces</i> .....	3
2.2.2.1 <i>Wave particle velocity <math>C_b</math></i> .....	5
2.2.2.2 <i>Curling factor <math>\lambda</math></i> .....	5
2.2.2.3 <i>Slamming coefficient <math>C_s</math></i> .....	6
2.2.2.4 <i>Duration of the slamming force, <math>\tau</math></i> .....	7
<b>3. WAVESLAM EXPERIMENTAL TEST SET-UP .....</b>	<b>9</b>
<b>3.1 Set-up of the experiments .....</b>	<b>9</b>
<b>3.2 Definition of the coordinate system .....</b>	<b>11</b>
<b>3.3 Sampling frequencies .....</b>	<b>11</b>
<b>4. ANALYSIS OF THE RESULTS ON THE FRONT BRACINGS .....</b>	<b>12</b>
<b>4.1 Introduction .....</b>	<b>12</b>
<b>4.2 Hammer test analysis .....</b>	<b>13</b>
<b>4.3 Analysis of the results.....</b>	<b>15</b>
4.3.1 <i>Force analysis</i> .....	19
4.3.2 <i>Time delay</i> .....	22
<b>5. MODELLING OF THE STRUCTURE IN ANSYS .....</b>	<b>25</b>
<b>5.1 Introduction .....</b>	<b>25</b>
<b>5.2 Finite Element Method and Software used.....</b>	<b>25</b>
<b>5.3 Theory .....</b>	<b>26</b>

<b>5.4 Geometry</b> .....	<b>27</b>
5.4.1 <i>Cross sections</i> .....	31
5.4.2 <i>Connections</i> .....	32
<b>5.5 Materials</b> .....	<b>36</b>
<b>5.6 Hydrodynamic added mass</b> .....	<b>37</b>
5.6.1 <i>Structure under the water level (St-37_BSWL)</i> :.....	39
5.6.2 <i>Instrumented leg, Pole 3</i> .....	41
<b>5.7 Boundary conditions</b> .....	<b>42</b>
5.7.1 <i>Lower part</i> .....	42
5.7.2 <i>Upper part</i> .....	43
<b>5.8 Mesh</b> .....	<b>46</b>
<b>5.9 Modal Analysis</b> .....	<b>48</b>
<b>5.10 Damping Ratio</b> .....	<b>50</b>
<b>6. VALIDATION OF THE MODEL</b> .....	<b>55</b>
<b>6.1 The impulse hammer test</b> .....	<b>55</b>
<b>6.2 Transient Analysis</b> .....	<b>56</b>
<b>6.3 Local response analysis of the instrumented front bracings</b> .....	<b>56</b>
6.3.1 <i>Definition of hammer test studied on bracings</i> .....	57
6.3.2 <i>Analysis of the results on the bracings</i> .....	57
<b>6.4 Global response of the structure</b> .....	<b>74</b>
6.4.1 <i>Definition of Hammer test studied</i> .....	75
6.4.2 <i>Analysis of the global response</i> .....	76
<b>7. CHARACTERIZATION OF THE DYNAMIC WAVE FORCES ACTING ON THE BRACINGS</b> .....	<b>89</b>
<b>7.1 Introduction</b> .....	<b>89</b>
<b>7.2 Case of study: Wave test 2013061414</b> .....	<b>89</b>
7.2.1 <i>Interpretation of the study case</i> .....	92
7.2.2 <i>Treatment of the signal</i> .....	94
7.2.3 <i>Inverse Fast Fourier Transform, IFFT</i> .....	97
7.2.4 <i>Sensitivity Analysis</i> .....	99
7.2.4.1 <i>Parameters to calibrate</i> .....	101
7.2.5 <i>Slamming coefficients</i> .....	112
7.2.5.1 <i>Lower part of the front bracing, FTBF01-04</i> .....	113

7.2.5.2 Upper part of the front bracing, FTBF02-03.....	113
<b>8. CONCLUSIONS AND RECOMENDATIONS.....</b>	<b>114</b>
<b>8.1 Recommendations for further work.....</b>	<b>116</b>
<b>REFERENCES.....</b>	<b>117</b>
<b>LIST OF SYMBOLS.....</b>	<b>119</b>
<b>APPENDICES .....</b>	<b>A</b>
APPENDIX A .....	A-1
APPENDIX B .....	B-1
APPENDIX C .....	C-1
APPENDIX D .....	D-1
APPENDIX E .....	E-1



## LIST OF FIGURES

Figure 0.1: Scheme of an Inverse problem.....	VI
Figure 0.2: Representation of the model built up in ANSYS.....	VI
Figure.2.1: Definition of parameters for calculating wave slamming forces for Wagner <sup>1</sup> and von Karman <sup>2</sup> theories.....	4
Figure 2.2: Definition of impact force on a vertical circular cylinder (IEC 61400-3, 2009).....	5
Figure 2.3: Estimation of curling factor $\lambda$ for maximum loading case and different inclinations.....	6
Figure 2.4: Time history of the line force for different theories (Wienke & Oumeraci, 2005).....	7
Figure 3.1: Test set-up in the Large Wave Flume.....	9
Figure 3.2: Front view of the structure. Location of the transducers on the bracings and columns..	10
Figure 4.1: Hammer impulse at position 7 and responses recorded at FTBF01-02-03-04.....	13
Figure 4.2: Hammer impulse at position 8 and responses recorded at FTBF01-02-03-04.....	13
Figure 4.3: Hammer impulse at position 9 and responses recorded at FTBF01-02-03-04.....	14
Figure 4.4: Decomposition of the response Wave Test 20130614-13 [105-106s].....	16
Figure 4.5: The bracing response spectrum at FTBF01 from a hammer test located at position n°09.....	17
Figure 4.6: The total response spectrum obtained from a hammer test located at position n°8. Hammer test 2406201325.....	17
Figure 4.7: Filtered response for a cut-off frequency of 800 Hz. Wave test: 20130614-08- [140-142s].....	18
Figure 4.8: Filtered response for a cut-off frequency of 400 Hz. Wave test: 20130614-08- [140-142].....	18
Figure 4.9: Filtered response for a cut-off frequency of 50 Hz. Wave test: 20130614-08 [140-142s].....	18
Figure 4.10: Convergence Analysis of degree's filter.....	19
Figure 4.11: Impulse response along the front bracings for different wave crest height.....	21
Figure 4.12: Analysis for the time delay of the maximum response achieved for different wave crest height.....	23
Figure 4.13: Response for Wave test: 20130614-08 on the bracings.....	24
Figure 4.14: Response for Wave test: 20130614-08 on the columns.....	24
Figure 5.1: Isometric view of the structure.....	28
Figure 5.2: Dimensions of the front side of the structure.....	29
Figure 5.3: Dimensions of the right side of the structure.....	30
Figure 5.4: View from an upper position.....	30
Figure 5.5: Cross section of the normal tubes and instrumented bracings.....	31
Figure 5.6: Cross section of the tube that connects the upper front bracings to the backside of the structure and the beams at the top of the structure.....	31
Figure 5.7: Cross section of the diagonal beam located at the top of the structure and cross section for the instrumented columns. Units in mm.....	32
Figure 5.8: Front view of the front instrumented bracings and instrumented columns.....	33
Figure 5.9: Front view in ANSYS.....	33
Figure 5.10: Front view in AUTOCAD showing the bracing and legs transducers.....	34

Figure 5.11: Back view of the front bracings.....	34
Figure 5.12: Cross sections of the connections between instrumented front bracings and instrumented legs. ....	35
Figure 5.13: Representation of the structure modelled in ANSYS .....	35
Figure 5.14: Added mass coefficient as function of Kc number for smooth (solid line) and rough (dotted line) cylinder. ....	39
Figure 5.15: Details of the lower supports on AUTOCAD.....	42
Figure 5.16: Detail of the FTTF03 in the Large Wave channel in Hannover, Germany .....	43
Figure 5.17: Supports (1), (2) and (3) corresponding to the left part of the structure. ....	44
Figure 5.18: Real view from the Large Wave Flume.....	44
Figure 5.19: Total Force transducers in ANSYS. ....	45
Figure 5.20: Fixed supports at the top of the structure, ANSYS.....	46
Figure 5.21: Convergence analysis of different mesh sizes. ....	47
Figure 5.22: Representation of the mesh size 50 which has 1938 elements. ....	48
Figure 5.23: Vibration modes 1 and 2 respectively.....	49
Figure 5.24: Vibration modes 3 and 6 respectively.....	49
Figure 5.25: Proportional damping scheme. ....	51
Figure 5.26: Half-power bandwidth method description .....	52
Figure 5.27: Time force response at FTTF01. Wave Test: 20130624-18.....	53
Figure 5.28: Time force response at FTTF01 in ANSYS for different damping ratios .....	54
Figure 6.1: Hammer test 2406201325 at position n°8.....	57
Figure 6.2: Hammer test 2406201328 at position n°11.....	57
Figure 6.3: Description of hammer test 8 in ANSYS.....	58
Figure 6.4: Comparison between data and ANSYS response at FTBF01 for hammer test 8.....	59
Figure 6.5: Comparison between data and ANSYS response at FTBF02 for hammer test 8.....	59
Figure 6.6: Comparison between data and ANSYS response at FTBF03 for hammer test 8.....	59
Figure 6.7: Comparison between data and ANSYS response at FTBF04 for hammer test 8.....	60
Figure 6.8: Time response at FTBF01-FH from the hammer test n° 08.....	60
Figure 6.9: Spectrum at FTBF01 of the response hammer test located at position n°8 .....	61
Figure 6.10: Frequency of the front bracings from a modal analysis in ANSYS (1).....	61
Figure 6.11: Frequency of the front bracings from a modal analysis in ANSYS (2).....	62
Figure 6.12: Value of the dynamic response compare to the static for different ratios of impact duration and Eigen frequency of any element. (Naess, 2011).....	63
Figure 6.13: Details of the instrumented bracings designed in ANSYS. ....	63
Figure 6.14: Boundary conditions for a beam.....	64
Figure 6.15: Comparison between the data and ANSYS response at FTBF01-FH from hammer test at 8. Sensitivity analysis I.....	65
Figure 6.16: Comparison between the data and ANSYS response at FTBF02-FH from hammer test at 8. Sensitivity analysis I.....	66
Figure 6.17: Comparison between the data and ANSYS response at FTBF03-FH from hammer test at 11. Sensitivity analysis I.....	66
Figure 6.18: Comparison between the data and ANSYS response at FTBF04-FH from hammer test at 11. Sensitivity analysis I.....	66

Figure 6.19: Comparison between the data and ANSYS response at FTBF01-FH from hammer test at 8. Sensitivity analysis II. ....	69
Figure 6.20: Comparison between the data and ANSYS response at FTBF02-FH from hammer test at 8. Sensitivity analysis II. ....	69
Figure 6.21: Comparison between the data and ANSYS response at FTBF03-FH from hammer test at 11. Sensitivity analysis II. ....	69
Figure 6.22: Comparison between the data and ANSYS response at FTBF04-FH from hammer test at 11. Sensitivity analysis II. ....	70
Figure 6.23: Comparison between the data and ANSYS response at FTBF01-FH from hammer test at 8. Sensitivity analysis III. ....	71
Figure 6.24: Comparison between the data and ANSYS response at FTBF2-FH from hammer test at 8. Sensitivity analysis III. ....	72
Figure 6.25: Comparison between the data and ANSYS response at FTBF3-FH from hammer test at 11. Sensitivity analysis III. ....	72
Figure 6.26: Comparison between the data and ANSYS response at FTBF4-FH from hammer test at 11. Sensitivity analysis III. ....	72
Figure 6.27: Eigen frequency of the front bracings after validation of the local response. ....	74
Figure 6.28: Hammer test at position number 2. ....	75
Figure 6.29: Hammer test at position number 5. ....	75
Figure 6.30: Comparison between data and ANSYS global response at FTTF01-02 from hammer test n°5. Initial set-up. ....	77
Figure 6.31: Comparison between data and ANSYS global response at FTTF03-04 from hammer test n°5. Sensitivity analysis I. ....	78
Figure 6.32: Comparison between data and ANSYS global response at FTTF01-02 from hammer test n°2. Sensitivity analysis I. ....	79
Figure 6.33: Comparison between data and ANSYS global response at FTTF01-03 from hammer test n°5. Sensitivity analysis II. ....	81
Figure 6.34: Comparison between data and ANSYS global response at FTTF01-03 from hammer test n°2. Sensitivity analysis II. ....	81
Figure 6.35: Comparison between data and ANSYS global response at FTTF01-03 from hammer test n°5. Sensitivity analysis III. ....	83
Figure 6.36: Comparison between data and ANSYS global response at FTTF01-03 from hammer test n°2. Sensitivity analysis III. ....	83
Figure 6.37: Comparison between data and ANSYS global response at FTTF01-03 from hammer test n°8. Final set-up. ....	86
Figure 6.38: Comparison between data and ANSYS global response at FTTF01-03 from hammer test n°11. Final set up. ....	86
Figure 6.39: Comparison between data and ANSYS global response at FTTF01-03 from hammer test n°8. Modifications at the upper beam. ....	87
Figure 6.40: Comparison between data and ANSYS global response at FTTF01-03 from hammer test n°8. Modifications at the upper beam. ....	87
Figure 7.1: Representation of the wave height at water gauge WG S9 located at the front of the structure. ....	90
Figure 7.2: Wave at the structure of Wave Test: 20130614-14 [132-135s] ....	90
Figure 7.3: Front view of the wave impact area. ....	91

Figure 7.4: Force-time response for the front bracings. .... 91

Figure 7.5: Force time response for the instrumented columns ..... 92

Figure 7.6: Force response and correlations on the instrumented bracings for Wave test 2013061414 at 132-135s. .... 93

Figure 7.7: Response decomposition at FTBF01-FH for a cut-off frequency of 34.85 Hz..... 95

Figure 7.8: Response decomposition at FTBF03-FH for a cut-off frequency of 34.85 Hz..... 95

Figure 7.9: Force response at FTBF01 for different cut-off frequencies ..... 96

Figure 7.10: Response decomposition at FTBF03-FH for a cut-off frequency of 18 Hz..... 97

Figure 7.11: IFFT of the response at FTBF03-FH. .... 98

Figure 7.12: Filtered response with a cut-off frequency of 150 Hz. .... 99

Figure 7.13. Location of the uniform wave load at the lower left front bracing. .... 100

Figure 7.14: Characterization of the wave load. .... 100

Figure 7.15: Representation of the two impact areas produced by the delay on the impact along different points on the front bracings. .... 102

Figure 7.16: Representation of the responses for different peak time values. .... 103

Figure 7.17: Comparison between the Data response and ANSYS at FTBF01-FH for run test I... 104

Figure 7.18: Comparison between the Data response and ANSYS at FTBF01-FH for run test II. 104

Figure 7.19: Comparison between the Data response and ANSYS at FTBF01-FH for run test III. 104

Figure 7.20. The maximum response to a suddenly applied triangular force time history (Naess) 105

Figure 7.21: Comparison between the Data response and ANSYS at FTBF04-FH for run test I... 106

Figure 7.22: Comparison between the Data response and ANSYS at FTBF04-FH for run test II. 107

Figure 7.23: Comparison between the Data response and ANSYS at FTBF04-FH for run test III. 107

Figure 7.24: Comparison between the Data response and ANSYS at FTBF02-FH for run test I... 109

Figure 7.25: Comparison between the Data response and ANSYS at FTBF02-FH for run test II. 109

Figure 7.26: Comparison between the Data response and ANSYS at FTBF02-FH for run test III. 109

Figure 7.27: Comparison between the Data response and ANSYS at FTBF03-FH for run test I... 111

Figure 7.28: Comparison between the Data response and ANSYS at FTBF03-FH for run test II. 111

Figure 7.29: Comparison between the Data response and ANSYS at FTBF03-FH for run test III. 111

Figure 0.1: Right lateral view of the truss structure taking as reference the wave direction ..... B-1

Figure 0.2: Left lateral view of the truss structure taking as reference the wave direction..... B-2

Figure 0.3: Approximate location of hammer points. .... B-3

Figure 0.4: Deviation on the response for samplings analyzed at FTBF01-FH..... C-8

Figure 0.5: Summarize of the Half power bandwidth method applied using different hammer tests D-



## LIST OF TABLES

Table 2.1: Slamming coefficient found by different authors and distribution of the impact force. ....	6
Table 2.2: Guidelines for the design of offshore structures. ....	7
Table 2.3: Findings for the total duration of the slamming force from different authors. ....	8
Table 3.1: Sampling frequencies .....	11
Table 4.1: Location of force cell transducers .....	12
Table 4.2: Location of water gauge at the structure. ....	12
Table 4.3: Description of the time delay response and force decay .....	14
Table 4.4: Delay of the maximum positive response .....	15
Table 4.5: Analysis of the degree of filter .....	19
Table 4.6: Properties of the waves analyzed for all 10 tests .....	20
Table 4.7: Impulse average response of different wave heights along the bracings .....	20
Table 4.8: Time delay of the maximum responses along the bracing and columns.....	22
Table 5.1: Properties of all the cross sections. ....	32
Table 5.2: Instrumented bracings [x1, one cell transducer for every instrumented part] .....	36
Table 5.3: Instrumented legs. Pole 3 is partially submerged below still water level (BSWL).....	36
Table 5.4: Properties of the materials.....	37
Table 5.5: Properties of the elements located below the still water level .....	39
Table 5.6: Geometry of all the structure below the SWL.....	39
Table 5.7: Properties of the part of the structure submerged. ....	40
Table 5.8. Consideration of water flooded structure .....	40
Table 5.9: Properties of the partial instrumented leg situated below the still water level.....	41
Table 5.10: Contribution of the different parts of the structure to the total mass. ....	41
Table 5.11: Features of all four total force transducers.....	45
Table 5.12: Boundary conditions at each support. ....	46
Table 5.13: Evolution of the error varying the mesh size. ....	47
Table 5.14: The main mode shapes are defined .....	48
Table 5.15: Average damping ratio found using Half power bandwidth method .....	52
Table 5.16: Mass and stiffness coefficients for different damping ratios .....	53
Table 6.1: Values for the Transient Analysis .....	56
Table 6.2: Properties of the impulse load and the Eigen frequency of the bracings for the model tested and ANSYS.....	62
Table 6.3: Eigen frequency of the front bracings for different boundary conditions.....	64
Table 6.4: First sensitivity analysis for the local response on the instrumented bracings. ....	68
Table 6.5: Second sensitivity analysis for the local response on the instrumented bracings. ....	70
Table 6.6: Third sensitivity analysis for the local response on the instrumented bracings .....	73
Table 6.7: Material properties set-up after local validation on the instrumented bracings. ....	77
Table 6.8: First sensitivity analysis for the global response on the structure.....	80
Table 6.9: Second sensitivity analysis for the global response on the structure .....	82
Table 6.10: Third sensitivity analysis for the global response on the structure .....	84
Table 6.11: Material properties of the Final set-up .....	85
Table 6.12: Sensitivity analysis for the global response on the structure for hammer test 8 and 11. 88	

Table 7.1: Wave parameters corresponding to 2013061414 run test.....	89
Table 7.2: Wave's cases studied with different peak time .....	103
Table 7.3: Characterization of wave loads studied for FTBF01 .....	103
Table 7.4: Sensitivity analysis of FTBF01-FH .....	106
Table 7.5: Characterization of wave loads studied for FTBF04 .....	106
Table 7.6: Sensitivity analysis of FTBF04-FH .....	108
Table 7.7: Characterization of wave loads studied for FTBF02 .....	108
Table 7.8: Sensitivity analysis of FTBF02-FH .....	110
Table 7.9: Characterization of wave loads studied for FTBF03 .....	110
Table 7.10: Sensitivity analysis of FTBF03-FH .....	112
Table 7.11: Slamming factors for the lower part of the bracings.....	113
Table 7.12: Slamming factors for the upper part of the bracings.....	113
Table 0.1. Maximum impulse response values in the front bracings transducers for tests n°11 and 13 on the 13 June, 2013.....	C-1
Table 0.2. Maximum impulse response values in the front bracings transducers for tests n°2-4-8and 13 on the 14 June, 2013.....	C-2
Table 0.3. Maximum impulse response values in the front bracings transducers for tests n°23-16-25 and 24 on the 14 June, 2013 .....	C-3
Table 0.4. Time response values for the highest force response in the front bracings transducers and columns for tests n°11 and 13 on the 13 June, 2013 .....	C-4
Table 0.5. Time response values for the highest force response in the front bracings transducers and columns for tests n°2 -4-8 and 13 on the 14 June, 2013.....	C-5
Table 0.6. Time response values for the highest force response in the front bracings transducers and columns for tests n°23 16-25-and 24 on the 14 June, 2013.....	C-6
Table 0.7. Average values for the response and deviation associated to each one .....	C-7
Table 0.8 Proportional damping ratios for different frequencies .....	D-1

## 1. INTRODUCTION

The wind power is one of the most fast growing energy source. The first offshore wind project around the world was set up in Denmark during the beginning of the 1990s. Since that time, Europe has become the world leader in offshore energy production.

Even though in Norway, roughly all the electric energy is coming from hydroelectric power, it has a lot of potential with respect to offshore wind power and the EU targets for 2020 implies a massive installation of offshore wind power. Initial investment estimations say that around € 125 billion for installation of 50 GW offshore wind in European seas will be needed.

When the installation of these wind turbines is referred to shallow water (<20 m water depth) the foundations might be exposed to slamming forces of breaking waves, typically plunging breaking waves.

Nowadays the main models available to estimate the slamming forces arising from breaking waves are monopods. Reinertsen A/S, Trondheim, has been involved in the design of truss support structures for wind turbines on the Thornton Bank, Belgian Coast. Calculations based on monopods show that the impulsive forces from the plunging waves might be governing factors of the truss structure and the foundations.

The goal of the proposed project is to investigate the slamming forces from plunging breaking waves on truss structures placed in shallow water and to improve the method to calculate those forces through model tests.

For this purpose large scale (1:8) tests were carried out at the Large Wave Flume in Hannover, Germany in 2013, in order to recreate plunging breaking waves and to study the responses from these breaking wave forces.

The simulation of the model tested using a finite element method software will allow to study and characterize through a fitting analysis, which have been the wave forces acting on the structure and determine the respective slamming coefficients. So far only monopod structures have been extensively studied so, this project undoubtedly represents a significant step for the study of the slamming forces on truss structures.

Since these slamming forces seem to be predominant in front of the Morison forces a better comprehension of the slamming coefficients will improve the estimates for these harsh loads and finally, might lead to an optimization of the guidelines for the design of truss support structures in shallow water.

## 2. BACKGROUND AND LITERATURE REVIEW

### 2.1 Introduction

The determination of wave slamming forces remains still today, after more than 85 years of study, a challenging topic. The main difficulties are related to the uncertainties and singularities of pressure and fluid velocity in the waterfront. During all these years it has been found that the slamming forces are proportional to the square wave celerity, the impact area of the wave, the water density, the radius of the element and a slamming coefficient.

Experimental results show significant scattering of wave slamming forces. This scattering might be produced by scale effects when the structure is scaled down to small scales around 1:80 – 1:50, different set ups and other uncertainties as could be asymmetry of waves in shallow water. The scale effects mentioned before are related to the less amount of entrained air in small scales than in reality. This situation might reduce the impact pressure.

### 2.2 Literature review

The wave forces acting on a single slender cylinder or by extension to truss structures can be described by three main components (3):

$$F_{wave} = F_M + F_D + F_S \quad (3)$$

where  $F_M$  refers to the inertia force per unit length,  $F_D$  denotes the drag forces per unit length and  $F_S$  denotes the contribution of a slamming force when the wave breaks at the structure. If the wave breaking is not occurring, the wave force is completely defined by the first two forces contribution.

#### 2.2.1 Morison Equation

It describes the wave force as the sum of the drag force per unit length and the quasi-static inertial forces. The total wave force can be obtained integrating the equation (4) along the length of the cylinder (Morison, et.al, 1950).

$$F_{wave} = F_M + F_D = \int_{-d}^{\eta} \frac{1}{2} \rho_w C_D D |u| u dz + \int_{-d}^{\eta} \rho_w \frac{\pi D^2}{4} C_M \frac{du}{dt} dz \quad (4)$$

The drag coefficient  $C_D$  and the inertia coefficient  $C_M$  are dependent on many parameters such as: surface roughness ratio, Carpenter number, Keulegan number, etc. These coefficients have to be empirically determined but recommended values are available in API RP 2A-WSD (2007).

### 2.2.2 Slamming forces

One of the first approach to determine the slamming forces was carried out by von Karman (1929). In von Karman model the airflow is considered not significant and other aspects as viscosity and surface tension are considered negligible. The consideration of the local flow acceleration predominant with respect to the gravitational acceleration when slamming occurs turns into gravity neglecting.

He considered a horizontal cylinder of infinite length. The cylinder is approximated by a flat plate with a width equal to the submerged part of the cylinder. von Karman method neglects the so-called pile-up effect, i.e. the raise of free surface elevation when the slamming occurs. The force on this plate is calculated (5) considering the potential flow below the plate and integrating the pressures.

This gives the following slamming force per unit length:

$$f_s(t) = V \rho_w \frac{\pi}{2} \frac{dc^2(t)}{dt} = \pi \rho_w R V^2 \left(1 - \frac{V}{R}t\right) \quad (5)$$

where  $V$  is the relative velocity between water and the body assumed to be constant, the length  $c$  is the distance between the intersection point of the cylinder and the still water level,  $R$  is the radius and  $\rho_w$  is the water density. See Figure (2.1)

The above equation can be rewritten by defining the slamming factor as follows (6):

$$C_s = \pi \left(1 - \frac{V}{R}t\right) \quad \rightarrow \quad f_s(t) = \rho_w C_s R V^2 \quad (6)$$

The slamming coefficient  $C_s$  becomes  $\pi$  when  $t = 0$ .

Three years later a method developed by Wagner (1932) takes into account the pile-up effect which had been neglected by von Karman. See figure 2.1.

The consideration of the pile-up effect implies a larger slamming force per unit length and following the von Karman theory explained before it results in (7):

$$f_s(t) = V \rho_w \frac{\pi}{2} \frac{dc^2(t)}{dt} = 2\pi \rho_w R V^2 \quad (7)$$

where the slamming coefficient  $C_s$  is  $2\pi$  and occurs at the initial moments of the slamming impact. The maximum line force calculated by Wagner is twice the maximum line force calculated by von Karman.

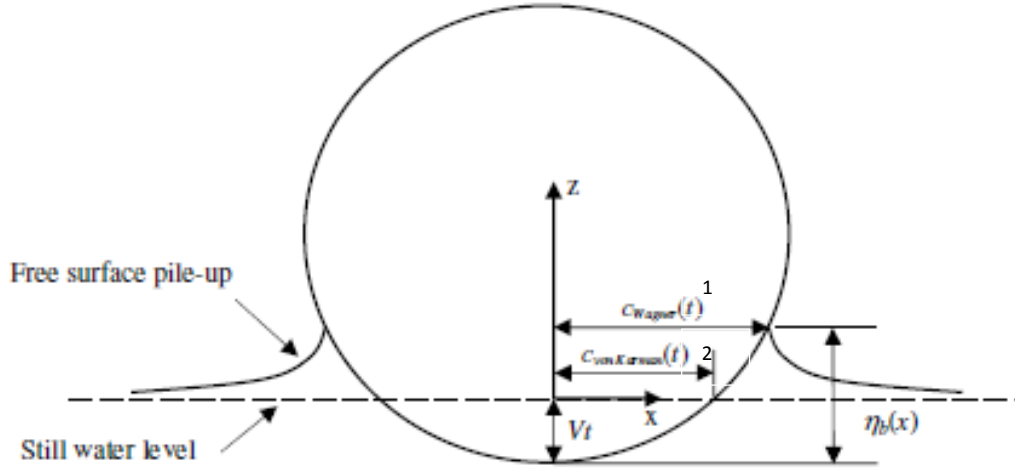


**Figure.2.1: Definition of parameters for calculating wave slamming forces for Wagner<sup>1</sup> and von Karman<sup>2</sup> theories.**

The approach of von Karman is adopted by different scientists as Goda et al (1966) and Tanimoto et al. (1986), (8), in order to estimate the slamming forces on vertical cylinders.

This total slamming force on a vertical cylinder is defined as:

$$F_s(t) = \rho_w \pi \left(1 - \frac{V}{R}t\right) R V^2 \lambda \eta_b = \lambda \eta_b f_s \quad (8)$$

where  $\lambda$  is defined as the curling factor and detail what is the part of the wave height  $\eta_b$  that makes a contribution for the slamming forces. The  $f_s$  part has been previously defined in equation (5) as the slamming force per unit of length. This theory assumes that the water front of a breaking wave over the height  $\lambda \eta_b$  is vertical and its celerity corresponds to the wave celerity, see Figure 2.2.

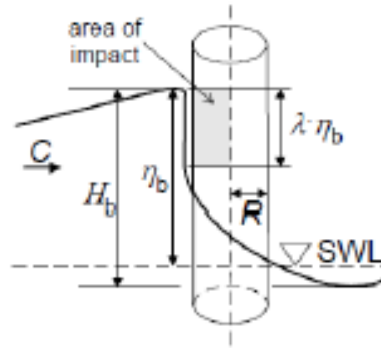


**Figure 2.2: Definition of impact force on a vertical circular cylinder (IEC 61400-3, 2009)**

All the above empirical results have in common that the slamming force  $F_s$  depends on physical parameters such as: water particle velocity  $V$ , curling factor  $\lambda$  and slamming coefficient  $C_s$ .

#### 2.2.2.1 Wave particle velocity $C_b$

The expressions showed above require the input of the water particle velocity at the free surface of a breaking wave. The wave breaks when the water particle velocity at the wave crest exceeds the wave celerity. It seems consistent that the water particle velocity  $V$  is close to the wave celerity (9). This statement is no longer valid when the wave breaks either much earlier before the structure or much later.

For shallow water the wave celerity can be defined as:

$$C_b = V = \sqrt{g(d + \eta_b)} \quad (9)$$

where  $d$  is the water depth,  $\eta_b$  is the free surface height from the still water level and  $g$  is the gravitational celerity.

#### 2.2.2.2 Curling factor $\lambda$

The curling factor (10) is another important parameter that defines the slamming force. It describes the area of impact of the plunging wave and is ranged between 0.4-1.

It is defined as:

$$\lambda = \frac{F_s}{C_s \rho_w R V^2} \quad (10)$$

Recent researches show the curling factor for vertical and inclined cylinders, Wienke and Oumeraci (2005). See Figure 2.3.

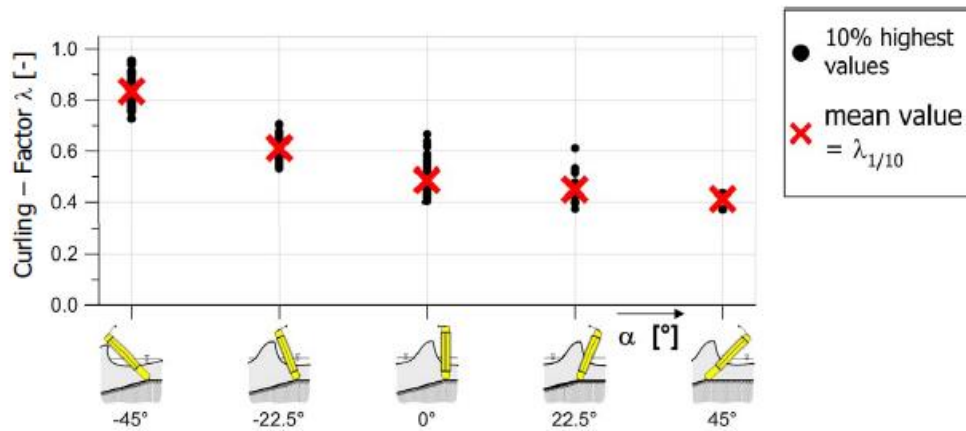


**Figure 2.3: Estimation of curling factor  $\lambda$  for maximum loading case and different inclinations**

For a vertical cylinder the mean value for the curling factor found is 0.46. This value is in between the proposed curling factor for plunging wave breakers defined by Goda, et.al (1966).

### 2.2.2.3 Slamming coefficient $C_s$

The slamming coefficient is one of the most investigated parameters related to the slamming forces.

According to von Karman this slamming coefficient is  $\pi$  whereas, for Wagner who considers pile-up effects turns into  $2\pi$ . Several researches have been done from 1932 until now. Mostly of them have considered a single vertical cylinder but others as Aune (2011) studied a truss structure.

In the following table there is an overview about the main findings for the slamming factor.

**Table 2.1: Slamming coefficient found by different authors and distribution of the impact force.**

Author	Slamming coefficient	Force distribution
<i>Karman (1929)</i>	$\pi$	Uniform
<i>Wagner (1932)</i>	$2\pi$	Uniform
<i>Goda (1966)</i>	$\pi$	Uniform
<i>Swaragi and Nochino (1986)</i>	$\pi$	Triangular
<i>Tanimoto (1986)</i>	$\pi$	Triangular
<i>Wienke and Oumeraci (2005)</i>	$2\pi$	Uniform
<i>Aune (2011)</i>	4.77	Uniform
<i>Xavier Ros (2011)</i>	4.3	Triangular
<i>Christy Ushanth (2013)</i>	3.3	Triangular



When it comes to the design process of an offshore structure, there are different standards dealing with prediction of design slamming factors. It is clearly seen that the determination of the slamming factor  $C_s$  plays an important role because the designed slamming forces are directly proportional to it. These standards are based mainly in the equation (8) for the slamming force per unit of length.

The main guidelines are defined in Table 2.2.

**Table 2.2: Guidelines for the design of offshore structures.**

Commonly used design guidelines	Recommended values for the Slamming coefficient
ABS (2010)	$\pi$
API RP 2A -WSD (2007) ; ISO 19902 (2007)	0.5 -1.7 $\pi$
DNV (2010a,b)	5.15
GL (2005) ; IEC 61400-3 (2009) ; ISO 21650 (2007)	2 $\pi$

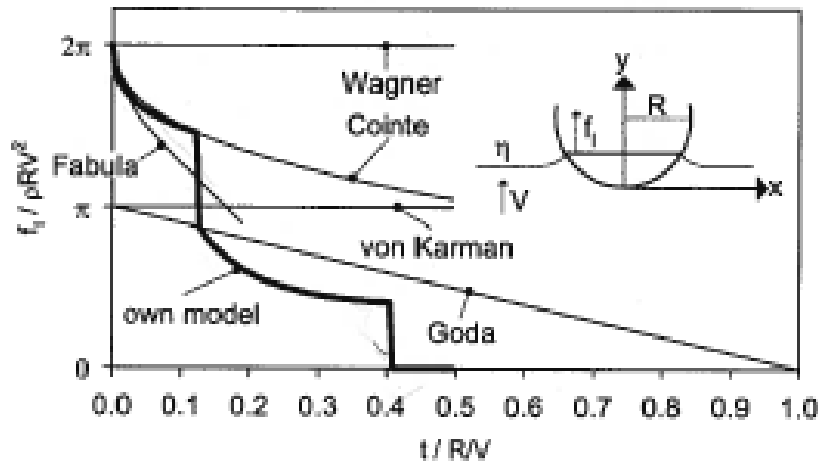


**Figure 2.4: Time history of the line force for different theories (Wienke & Oumeraci, 2005)**

#### 2.2.2.4 Duration of the slamming force, $\tau$

Another factor that has been studied for many researchers is the duration of the slamming impact. That duration is important for the characterization of the wave slamming forces and several expressions can be found in Table 2.3.

**Table 2.3: Findings for the total duration of the slamming force from different authors.**

Author	Duration of slamming force
<i>Von Karman (1929)</i>	$D/2u$
<i>Goda (1966)</i>	$D/2 C_b$
<i>Tanimoto (1986)</i>	$[0.5 - 0.25] D/C_b$
<i>Wienke and Oumeraci (2005)</i>	$(13/64) D/C_b$

Von Karman defined it using the water particle velocity  $u$  and the other researches considered it as the breaking wave celerity  $C_b$ .

### 3. WAVESLAM EXPERIMENTAL TEST SET-UP

#### 3.1 Set-up of the experiments

The truss structure built up for the experiment in Hannover, Germany (Large scale 1:8) was done following a previous small scale (1:50) model tests at NTNU.

This structure is not a truly representation of any structure done before but it was pretended to be similar to the one that Reinertsen designed for the Thornton bank.

The Large Wave Flume in Hannover is around 300 meters long, 5 m wide and has a depth of 7 m

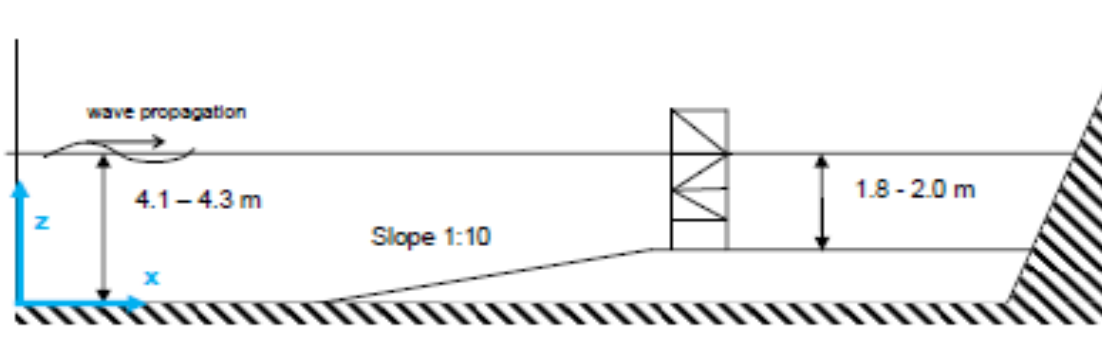


Figure 3.1: Test set-up in the Large Wave Flume

There was 1 wave gauge in the plane of the vertical front pile (WG S9), another at the vertical back pile (WG S11). In addition to that, 6 wave gauges and 3 Acoustic Doppler Velocity meter (ADV) were placed in line with the front leg of the structure.

The structure was equipped with force transducers. The Figure 3.2 shows the force transducers installed at the front. The structure was equipped with:

- 4 total force transducers, two at the top and two at the bottom measuring the total force on the structure.
- 10 local force transducers
- 12 XY force transducers measuring the total force on six bracings, 2 at the front bracings and the other 4 at the right and left sides respectively.

The total wave force transducers were provided by the Provider (FZK-GWK) and were similar to those used by Wienke and Oumeraci (2005). The other force transducers were provided by NTNU.

4 one-directional accelerometers were installed to record accelerations in X direction.

See Appendix B for the side views of the structure and the side instrumented bracings.

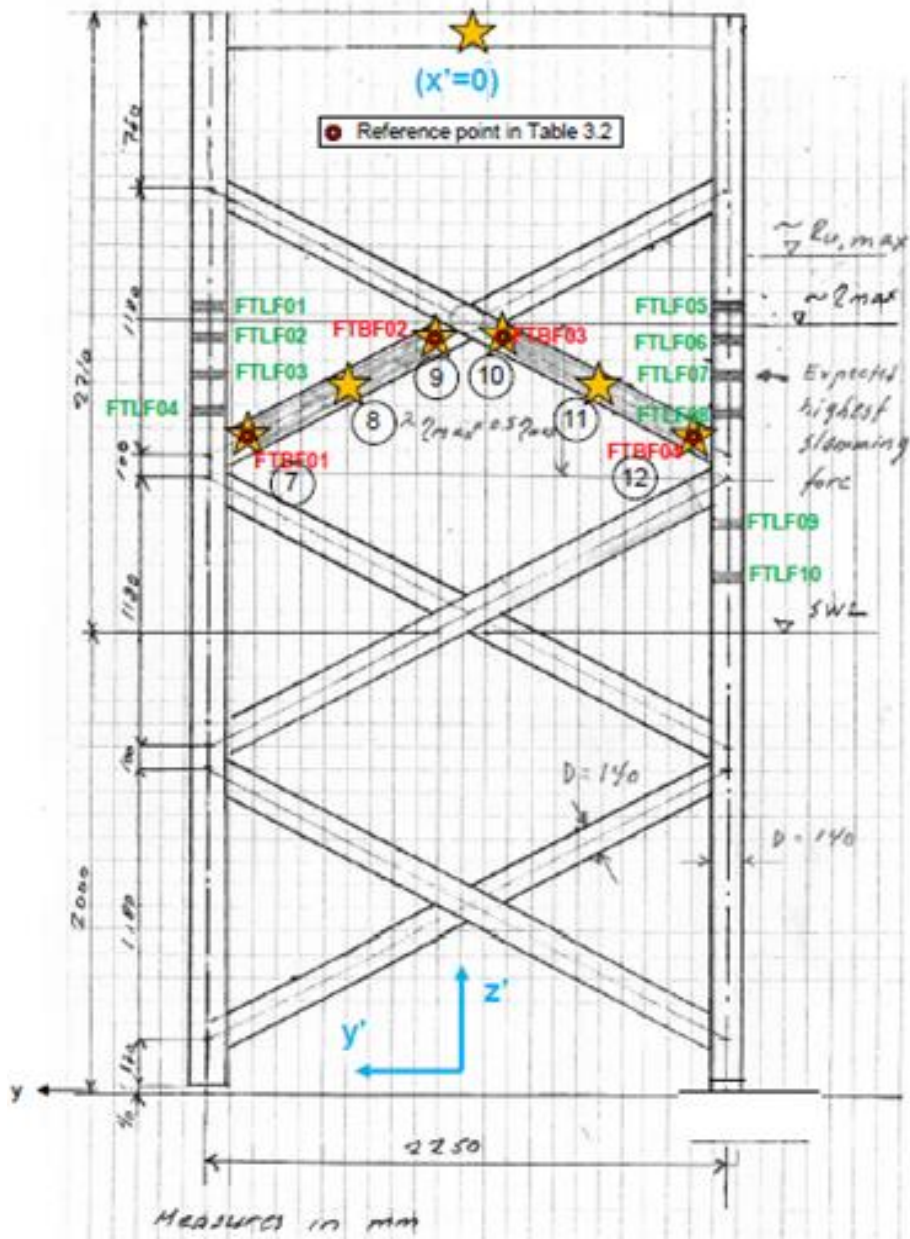



Figure 3.2: Front view of the structure. Location of the transducers on the bracings and columns.

Wave direction comes into the paper plane. The local force measurements on the front bracings are defined by FTBF01, FTBF02, FTBF03 and FTBF04. The local force measurements on the columns are described by: FTLF01, FTLF02, FTLF03, FTLF04 on the left column and FTLF05, FTLF06, FTLF07, FTLF08, FTLF09 and FTLF10 on the right column. The symbol  indicates points where the impulse hammer hit in the horizontal

direction on the front bracings and the numbers in circles are data file reference numbers for the hammer tests.

### 3.2 Definition of the coordinate system

There are two coordinate systems, the global coordinate system (X,Y,Z) is set X=0 at the center of the wave board, Z=0 at the bottom of the channel and Y=0 along the south side of the flume. The X axis is positive in the direction of the wave. The Z axis is positive upwards. The Y axis is positive in the direction normal to the left of the X-axis.

To identify the locations of the force cell transducers a local coordinate system is defined as (x',y',z') with x'=0 corresponding to X=139.8 m and defined in the front side of the structure, y'=0 at the middle of the flume and a positive value in direction normal to the left x'-axis. The x' positive direction is defined in wave direction. The z' axis is located at the end of the front columns, which were located 4 cm above the bottom channel.

Additional information with respect to the location of the sensors can be found in the Excel spreadsheet: *Waveslam channels for DAQ 20130626.xlsx*.

### 3.3 Sampling frequencies

The sampling frequency used in the experiments is different for the force measurements, water gauges and hammer test.

In Table 3.1 is described all the sampling frequencies used during the experiments.

**Table 3.1: Sampling frequencies**

Data	Sampling frequency [Hz]
<b>Force measurements</b>	10000 (Initially 20000)
<b>Water gauge</b>	200
<b>Hammer test</b>	9600

#### 4. ANALYSIS OF THE RESULTS ON THE FRONT BRACINGS

##### 4.1 Introduction

The following report is a study of the response recorded on the bracings under different wave conditions. The aim is to analyze and represent the response and the dynamic forces focusing on the four bracings transducers at the front side: FTBF01, FTBF02, FTBF03, FTBF04. The time delay among all front bracings transducers will be also investigated and to study whether the wave is breaking at the same instant in front of the structure or not, the number of transducers is extended to FTLF04 and FTLF08 which are located in the left and right column. The Table 4.1 indicates the location of them.

**Table 4.1: Location of force cell transducers**

Channel	Description	Channel no.	Location			Location z=0 lower end column		
			X	Y	Z	x'	y'	z'
FTBF01	Bracing west north low	45	198.37	3.310	5.251	0	780	2911
FTBF02	Bracing west north high	47	198.37	2.888	5.472	0	358	3132
FTBF03	Bracing west south high	49	198.37	2.172	5.472	0	-358	3132
FTBF04	Bracing west south low	51	198.37	1.750	5.251	0	-780	2911
FTLF04	Local force column west north	38	198.37	3.655	5.363	0	1125	3023
FTLF08	Local force column west south	42	198.37	1.405	5.363	0	-1125	3023

This analysis has been carried out for a ten different run waves tests corresponding to the days: 13/06/2013 and 14/06/2013. The analysis tries to show the behavior of the bracings along different crest heights hitting the structure. The crest height studied goes from 1.04 to 1.551 m at front of the structure recorded from water gauge, WG S 09.

**Table 4.2: Location of water gauge at the structure.**

Channel	Description	Channel no.	Location			Location z=0 lower end column		
			x	y	z	x'	y'	z'
WG S9	WG front column	19	198.37	0.60	7.00	0	-1930	NA

To get an initial sight about how the bracing reacts in front of an impulse load, the response on the four front bracing transducers is analyzed for three different hammer locations along the bracings

### 4.2 Hammer test analysis

In Figure 4.1 the hammer test is located close to where FTBF01 has been installed so the response is produced without any delay. It can be seen clearly the existence delay for the other bracing transducers.

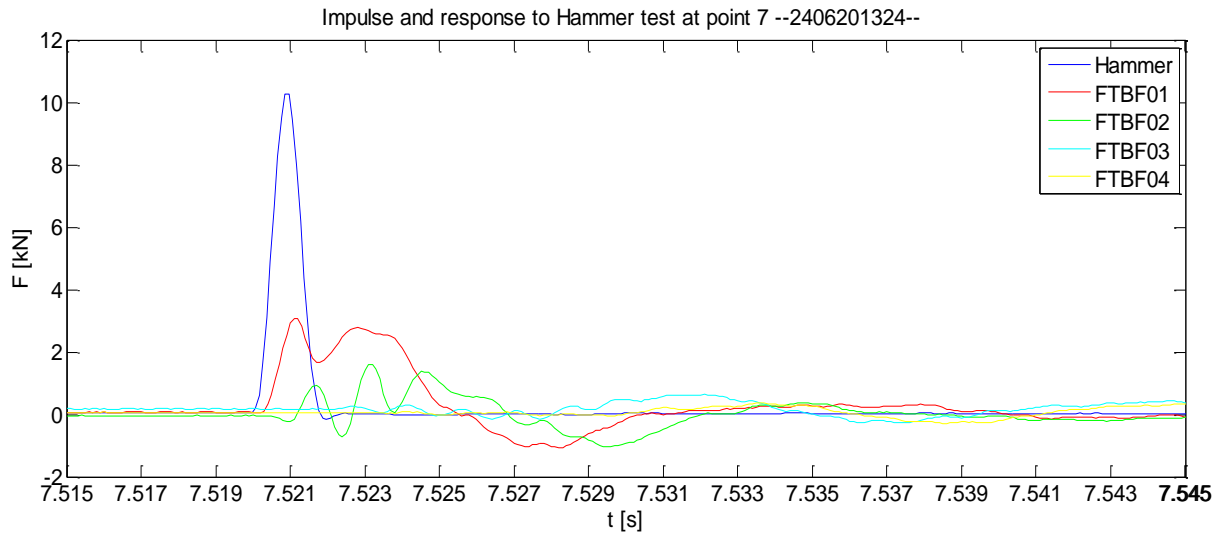


Figure 4.1: Hammer impulse at position 7 and responses recorded at FTBF01-02-03-04

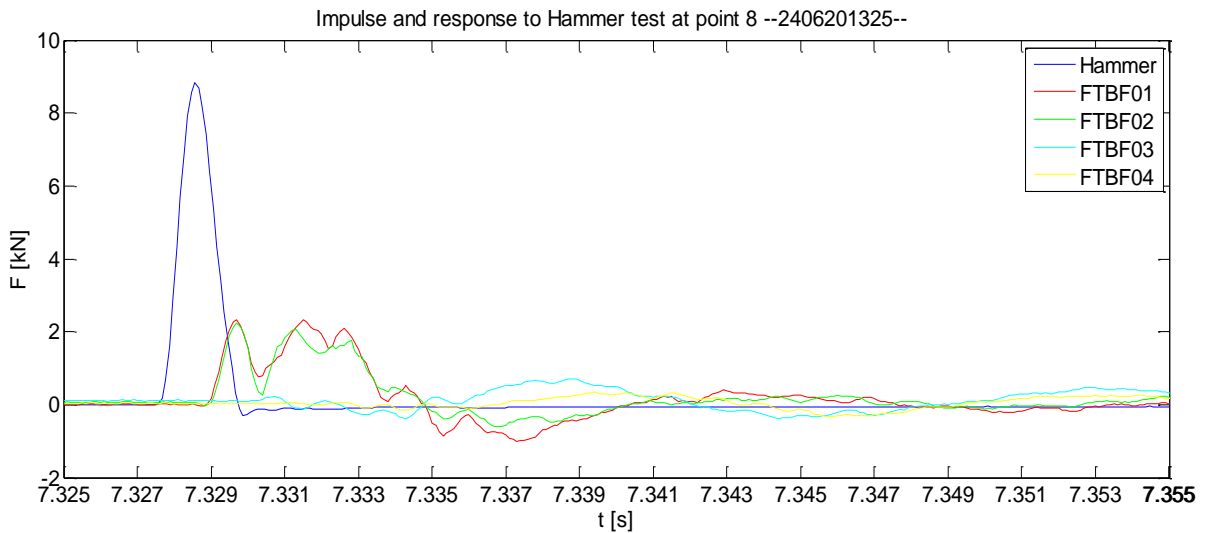
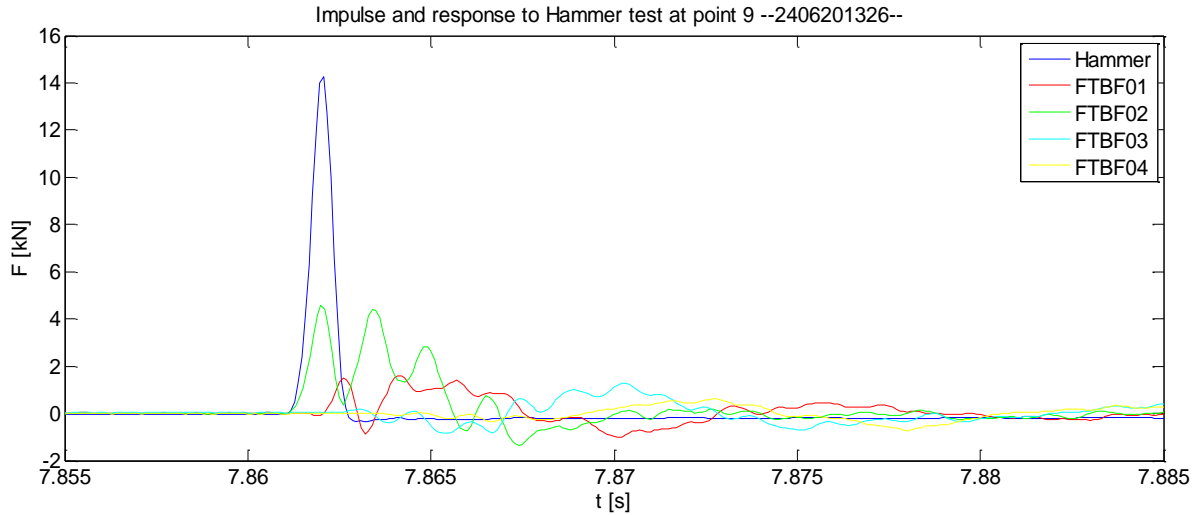


Figure 4.2: Hammer impulse at position 8 and responses recorded at FTBF01-02-03-04

In Figure 4.2 is shown that when the hammer test is applied at the middle point of the left instrumented bracing the results obtained at the ends of the bracing, FTBF01 and FTBF02 respectively, are produced at the same time and with the same intensity.

Table 4.3 describes at what time the maximum response is given in the bracing transducers as well as at what time is produced. The time delay with respect the impulse hammer is defined in Table 4.4.



**Figure 4.3: Hammer impulse at position 9 and responses recorded at FTBF01-02-03-04**

The Figure 4.3 represents the last situation where the hammer test is applied at position n°9. This situation is similar to the first hammer tests analyzed, where the response from FTBF02 is at the same time as the impulse and the others responses show a decay both in response and time.

**Table 4.3: Description of the time delay response and force decay**

	Hammer test [24062013]									
	Hammer Impact		FTBF01-H		FTBF02-H		FTBF03-H		FTBF04-H	
	$D^1$ [s]	Time [s]	Peak value [kN]	Time [s]	Peak value [kN]	Time [s]	Peak value [kN]	Time [s]	Peak value [kN]	Time [s]
-24-Blow 7	0.0018	7.521	3.08	7.521	1.60	7.523	0.63	7.532	0.36	7.534
-25-Blow 8	0.0021	7.322	2.32	7.329	2.24	7.329	0.71	7.338	0.33	7.339
-26-Blow 9	0.0015	7.862	1.61	7.864	4.58	7.862	1.29	7.87	0.60	7.873

<sup>1</sup> It refers to the duration of the impulse.



**Table 4.4: Delay of the maximum positive response**

Hammer test [24062013]				
<i>Delay [s]</i>				
	FTBF01-H	FTBF02-H	FTBF03-H	FTBF04-H
-24-Blow 7	0	0.002	0.011	0.013
-25-Blow 8	0.007	0.007	0.009	0.01
-26-Blow 9	0.002	0	0.008	0.011

The above table shows the time delay between the impact and the maximum response in the different transducers. When the hammer impact is at FTBF01 (Blow 7) or FTBF03 (Blow 9), the response on the other side of the bracer is at around 10 millisecond afterwards. The same behavior is observed when the hammer hits in the middle of the bracing.

These hammer tests studied show us how the bracing reacts in terms of time delay and response intensity. The farther we go from the blow of the hammer test, the lower will be the response and the higher the time reaction.

It is also shown the high existence decay in the response from one bracing to the other with a reduction of around 87-89% in the peak force.

The large and small hammer test will be helpful tools for validating the structure model, issue that will come back in the next chapter of the report.

### 4.3 Analysis of the results

As it was mentioned before, 10 regular waves' tests have been analyzed corresponding to the 13<sup>th</sup> and 14<sup>th</sup> of June. For each test, a total of 20 waves were generated under specific conditions. The analysis has been carried out taking 8 samplings out of 20 for these 10 different tests. That makes a total number of 80 samplings.

For the analysis, the four force transducers on the front bracings have been selected and also two force local transducers located at the same height on the columns, in particular, FTLF08 and FTLF04. The main purpose for that is to see whether the front wave impacts simultaneously or not at the front of the structure.

The criterion for taking 8 samplings out of 20 in each test is mainly about having enough samplings to do statistics. For each test, the maximum response regarding to the six transducers (4 at the bracings + 2 at the columns) is taken, and the other two left are randomly chosen.

The analysis of the dynamic response implies a previous treatment of the signal for taking out the quasi static forces which turns out into a laborious task. The complete analysis for the

20 samplings in each test would make it unaffordable in terms of time for this initial part of the project.

The dynamic response is obtained filtering down the response signal, using a low pass filter with a cutoff frequency ranged between 15 - 25 Hz. The upper limit is the Eigen frequency of the structure in wave direction as it can be seen in Figure 4.6. Using a frequency in between this range allows to remove the quasi static forces from the signal and they are not high enough to significantly disturb the dynamics of the impact. Analyzing the spectrum of the bracings response is seen that the frequency related to the highest peak is around 80-100 Hz. There are several frequencies which contribute to the variance of the response and the main contribution is found in frequencies from 25 to 125 Hz. So it can be concluded that for frequencies below 25 Hz the disturbance produced to the impulse signal is minimized.

Then the dynamic response is the result of subtracting the filtered signal to the response.

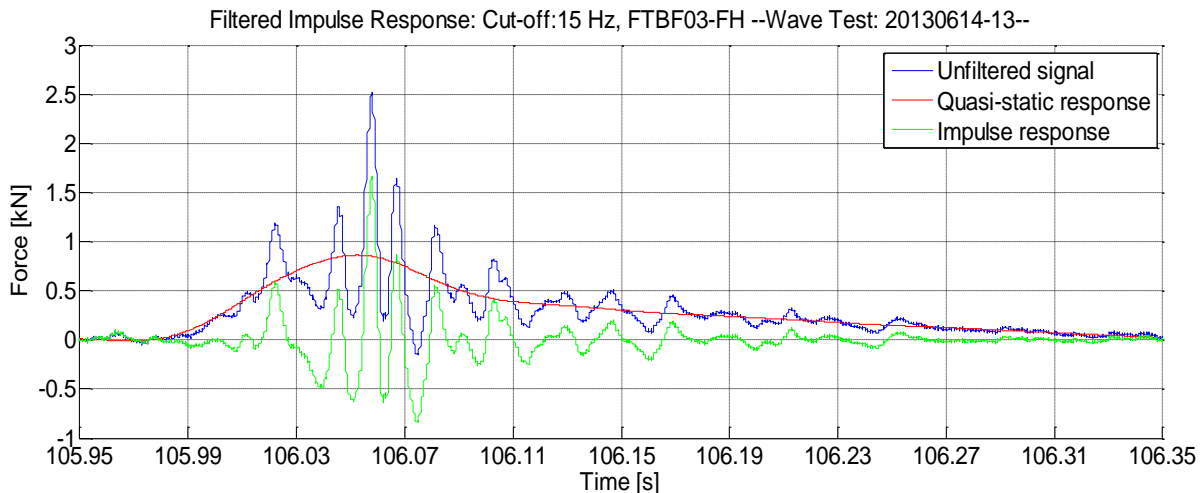


**Figure 4.4: Decomposition of the response Wave Test 20130614-13 [105-106s]**

Once the signal has been filtered down, it is filtered down one more time to take out the noise. In the Figures 4.7-4.9, there is another sampling signal filtered down with different cutoff frequencies. For a cutoff frequency of 50 Hz, frequencies that belong to the impulse are removed. On the other hand, a cutoff frequency of 800 Hz is not taking out any noise. A cutoff frequency of 400 Hz seems reasonable due to a smooth dynamic response is expected. It takes out the noise and does not disturb the response signal.

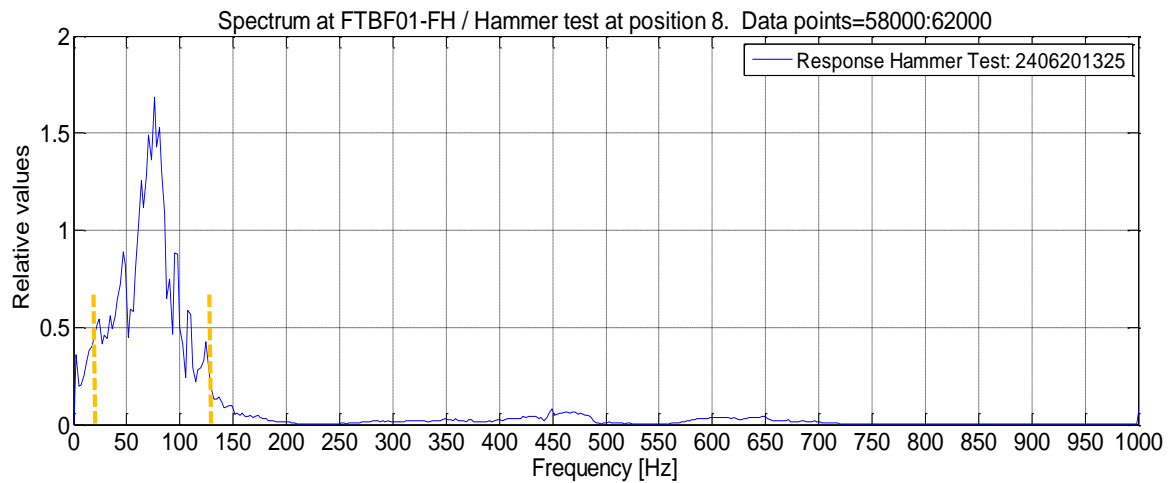


**Figure 4.5: The bracing response spectrum at FTBF01 from a hammer test located at position n°09**

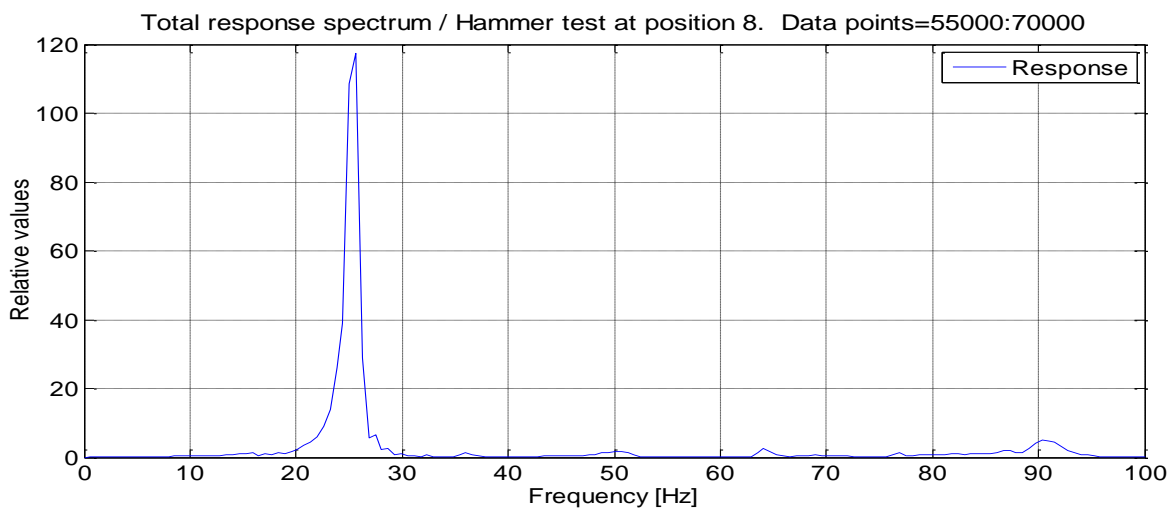


**Figure 4.6: The total response spectrum obtained from a hammer test located at position n°8. Hammer test 2406201325**

Initially the response on the bracings was recorded on a local axis  $x'$  and  $y'$ . The results were transformed to a global axis, H and V in order to avoid problems in further processing of data and make it more understandable. All the analysis have been done for the horizontal plane H.

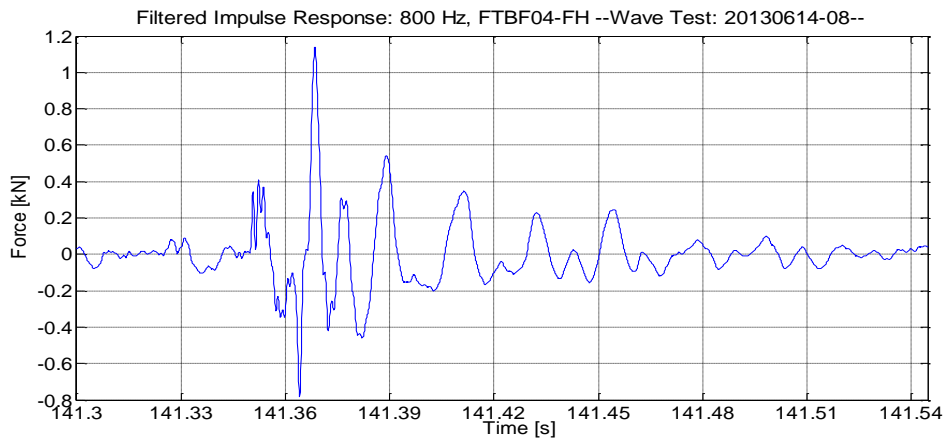


**Figure 4.7: Filtered response for a cut-off frequency of 800 Hz. Wave test: 20130614-08- [140-142s]**

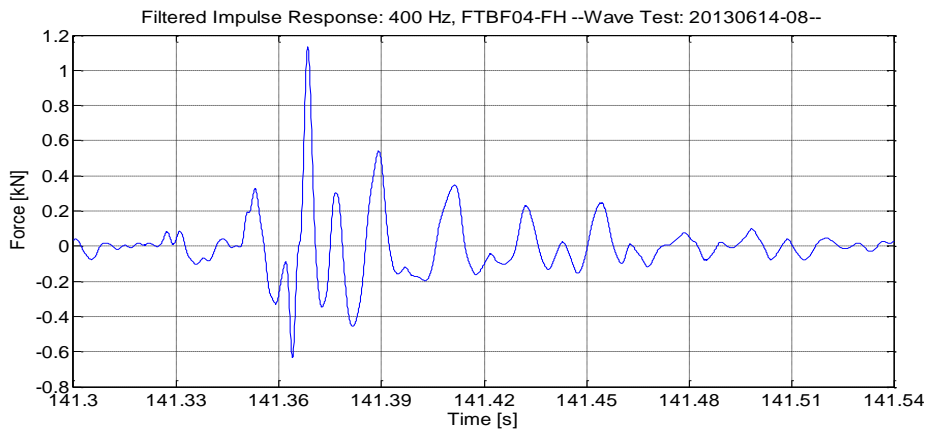


**Figure 4.8: Filtered response for a cut-off frequency of 400 Hz. Wave test: 20130614-08- [140-142]**

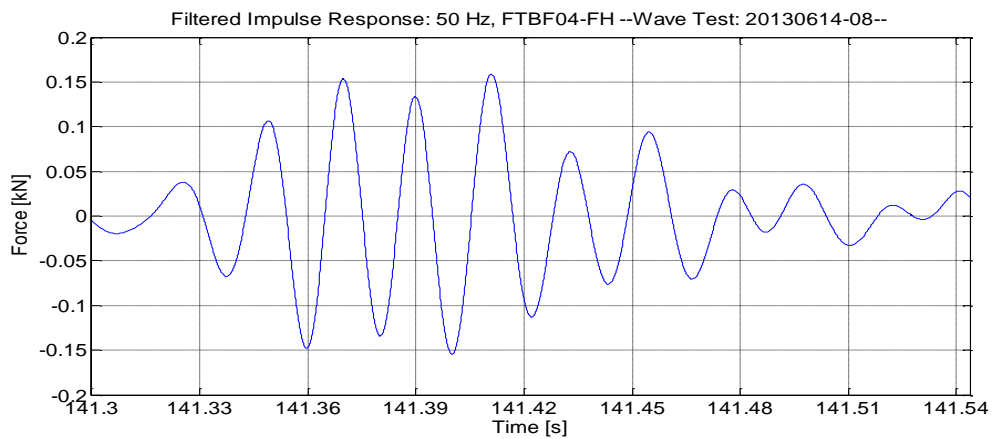


**Figure 4.9: Filtered response for a cut-off frequency of 50 Hz. Wave test: 20130614-08 [140-142s]**

### 4.3.1 Force analysis

The filtering has been done using ‘*low butter filter*’ in Matlab and using ‘*filtfilt*’ function. This function does zero phase filtering by filtering the data in forward and reverse direction. For the order of the filter a sensitive analysis has been done and is described in Table 4.5 and Figure 4.10.

**Table 4.5: Analysis of the degree of filter**

Degree of filter	20130614 - 25 [146-147 s]		20130614 - 24 [67-69 s]	
	Value [kN]	Relative Error <sup>2</sup> [%]	Value [kN]	Relative Error [%]
1	1.172	11.547	3.84	16.047
2	1.275	3.774	4.337	5.181
3	1.306	1.434	4.485	1.946
4	1.32	0.377	4.546	0.612
5	1.325	0.000	4.574	0.000

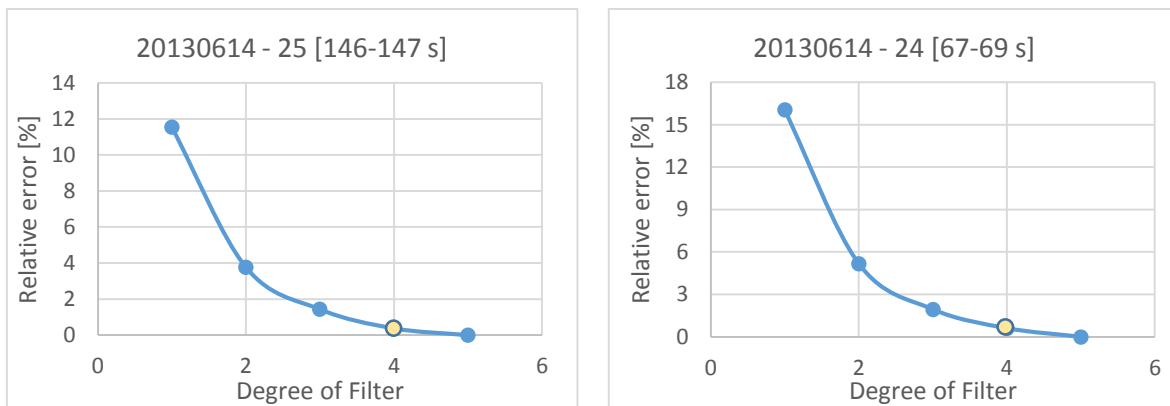


**Figure 4.10: Convergence Analysis of degree's filter**

A higher degree of a filter means a more accurate result and higher computational cost as well. The election for the degree of a filter is a balance upon the computational cost and the desired accuracy.

The accuracy is highly increased rather than using a 2 degree filter. Taking into account both factors, computational cost and desired accuracy, the response is going to be studied with a 4 degree filter, which offers for more than 90% of the study samplings and error lower than 1%.

<sup>2</sup> The relative error is obtained using the result from a 5<sup>th</sup> degree filter as *true value*.

Table 4.6 describes the properties of the waves hitting the structure for the test studied. They have been selected in order to analyze the response form a range of wave heights that goes from 1.55 to 1.7 m above SWL.

**Table 4.6: Properties of the waves analyzed for all 10 tests**

N° Test	Wave height [m]	Height at WGS09 [m]	Wave period [s]	Depth [m]	Run type
13/06 -11 -	1.55	1.63	4	4.3	Regular
13/06 -13 -	1.6	1.677	4	4.3	Regular
14/06 -02 -	1.5	1.723	4.6	4.3	Regular
14/06 -04 -	1.6	1.78	4.6	4.3	Regular
14/06 -08 -	1.75	1.87	4.6	4.3	Regular
14/06 -13 -	1.6	1.883	4.9	4.3	Regular
14/06 -23 -	1.6	2.002	5.55	4.3	Regular
14/06 -16 -	1.8	1.995	4.9	4.3	Regular
14/06 -25 -	1.8	2.078	5.55	4.3	Regular
14/06 -24 -	1.7	2.095	5.55	4.3	Regular

The analysis has been done for both total response and filtered signal. For the 8 samplings recorded the average value has been calculated in Table 4.7. The results are shown in Figure 4.11. See the Appendix C for the full table.

**Table 4.7: Impulse average response of different wave heights along the bracings**

Dynamic Response –Cutoff Frequency 15 Hz - 400 Hz -- Filtered signal					
N° Test	$\bar{H}$ . at structure, $z=SWL$ [m]	$\overline{FTBF01}$ [kN]	$\overline{FTBF02}$ [kN]	$\overline{FTBF03}$ [kN]	$\overline{FTBF04}$ [kN]
13/06 -11	1.0904	0.4976	0.3729	0.6529	0.4218
13/06 -13	1.1510	0.6313	0.3541	0.6137	0.5816
14/06 -02	1.1998	0.6968	1.0963	1.0547	0.7595
14/06 -04	1.2288	1.2319	1.1991	0.9135	0.9864
14/06 -08	1.2560	1.4247	1.1783	1.0811	1.1870
14/06 -13	1.2891	1.2487	1.5008	1.2763	1.4662
14/06 -23	1.4019	0.5377	1.1605	0.8726	0.7419
14/06 -16	1.3970	1.3189	1.5807	1.7790	1.4632
14/06 -25	1.4568	2.6276	1.2776	1.3070	1.9210
14/06 -24	1.4615	2.5646	3.1488	2.4448	1.4035

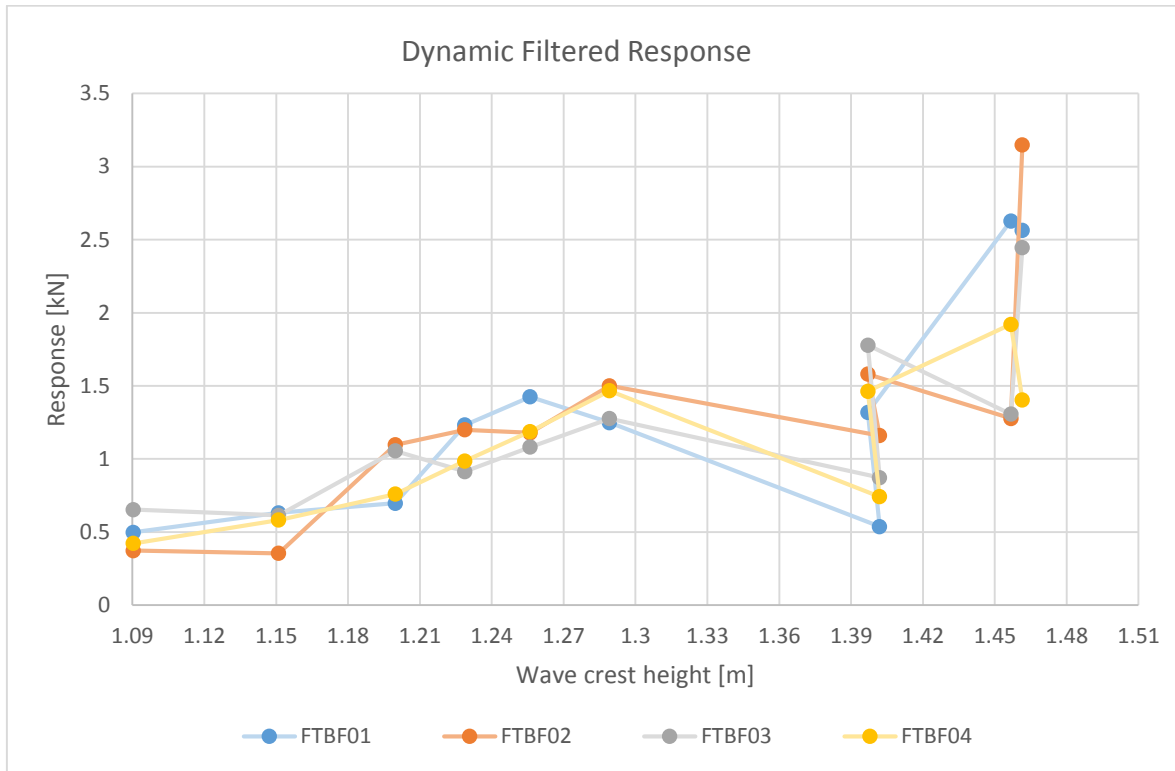


**Figure 4.11: Impulse response along the front bracings for different wave crest height**

The tendency of the results points out that the response on the front bracings becomes larger as the wave crest height increases. This trend is partially broken for heights 1.40 m and 1.45 m, tests 23 and 25 of 14<sup>th</sup> of June respectively where the values are lower. This behavior might be explained because the wave is not breaking in front of the structure but some meters after. Anyway, the tendency of the force response is clearly rising for the bracings when the wave crest becomes larger.

A first analysis shows that for wave crest heights higher than 1.28 m around the 80% of the highest results are found at FTBF02 and FTBF03.

From 1.09 m to 1.18 m the results on FTBF01 and FTBF04 which are located at the same height show average similar results. This behavior is no longer appreciated for higher wave crests on these two transducers and neither for the transducers at the top, FTBF02 and FTBF03.

As it was previously explained this analysis has been carried out for a total of 8 samplings out of 20 for each test. The results from the analysis show a high scattering that can be consulted on Appendix C. If the number of samplings is nearly doubled to 15, the deviation is not significantly reduced.

For instance, for n° test 14/06 -13 with a wave crest height of  $1.28 \pm 0.07$  m the average deviation of the bracing results for 8 samplings is around 50%. If the number of samplings is double the deviation is only reduced until 43%. These details can be found in the Excel spreadsheet “*Data\_Analaysis\_Bracings.xlsx*”.

There are some aspects that might explain all the behaviors described before and they will be further analyzed on the next analysis and fully reported on the final conclusions at the end of the report:

- Possible asymmetry of the breaking wave.
- Existing uncertainties with respect to the breaking wave.
- Correlations between the impact and the response at different points of the bracings.
- Response on the bracings affected by the Eigen frequency and impact duration of the load.

#### 4.3.2 Time delay

For the time delay analysis the instant at what the maximum response was achieved has been recorded. The height of the wave crest at the front of the structure is described as well (SWL taken as reference,  $z=0$ ) in Table 4.8.

In order to plot the average time delay for all the 10 wave tests studied, the reference value (time=0), has been set as the time where the maximum response is produced in each transducers compared to the others. See the Appendix C for the full table.

**Table 4.8: Time delay of the maximum responses along the bracing and columns.**

N° Test	Wave crest [m]	FTBF01 [s]	FTBF02 [s]	FTBF03 [s]	FTBF04 [s]	FTLF04 [s]	FTLF08 [s]
13/06 -11 -	1.0914	0.0197	0.0172	0.0182	0.0147	0.0135	0.0000 <sup>3</sup>
13/06 -13 -	1.1510	0.0225	0.0232	0.0201	0.0185	0.0160	0.0000
14/06 -02 -	1.1996	0.0182	0.0236	0.0250	0.0223	0.0000	0.0029
14/06 -04 -	1.2288	0.0247	0.0261	0.0250	0.0271	0.0000	0.0053
14/06 -08 -	1.2560	0.0349	0.0255	0.0270	0.0405	0.0000	0.0078
14/06 -13 -	1.2891	0.0066	0.0150	0.0173	0.0122	0.0000	0.0011
14/06 -23 -	1.4019	0.0108	0.0276	0.0306	0.0117	0.0035	0.0000
14/06 -16 -	1.3970	0.0100	0.0132	0.0113	0.0096	0.0034	0.0000
14/06 -25 -	1.4568	0.0250	0.0216	0.0177	0.0186	0.0044	0.0000
14/06 -24 -	1.4615	0.0129	0.0127	0.0129	0.0121	0.0005	0.0000

<sup>3</sup> A value of 0 seconds indicates that the maximum response at FTLF08 is first obtained compared to the other maximum 5 responses.



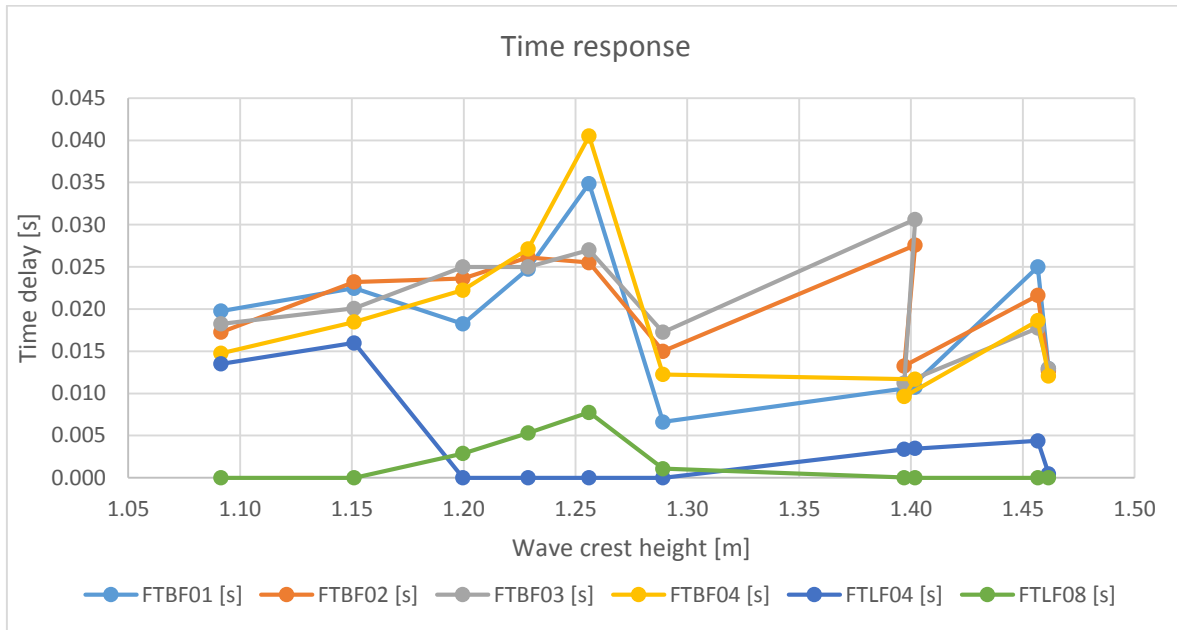


**Figure 4.12: Analysis for the time delay of the maximum response achieved for different wave crest height**

The above graph represents the time delay of the maximum average response, recorded for the different transducers.

For the analysis of the time delay is important to recall the height above the SWL at what the force transducers were installed: FTBF01- FTBF04 (0.951 m), FTBF02-FTBF03 (1.172 m) and FTLF04-08 (1.063 m) are both located at the same height above the SWL respectively.

Even though a moderate time delay between the maximum response on the legs and on the bracings is appreciated, is important to remark that this does not directly represent that the wave is hitting first on the columns. One of the reasons that might explain this behavior is explained below and represented in Figures 4.13 - 4.14.

It is observed in different cases that for instance an initial response on transducers FTBF01-04 is recorded at nearly the same time that in FTLF04-08, but the maximum response is reached afterwards on these transducers when the wave finally hits FTBF02-03. This behavior might be explained because of a first impact of the tongue followed by a higher impact of the crest that hits the upper parts of the front bracings FTBF02-03, or other phenomena as could be run up effects.

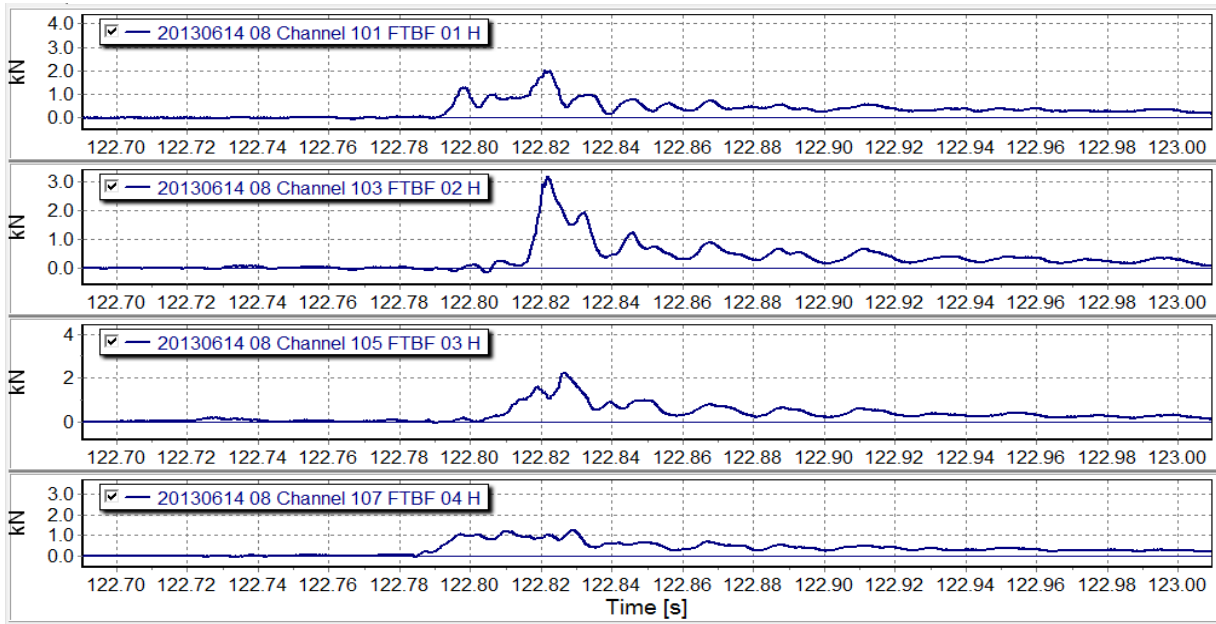


**Figure 4.13: Response for Wave test: 20130614-08 on the bracings.**

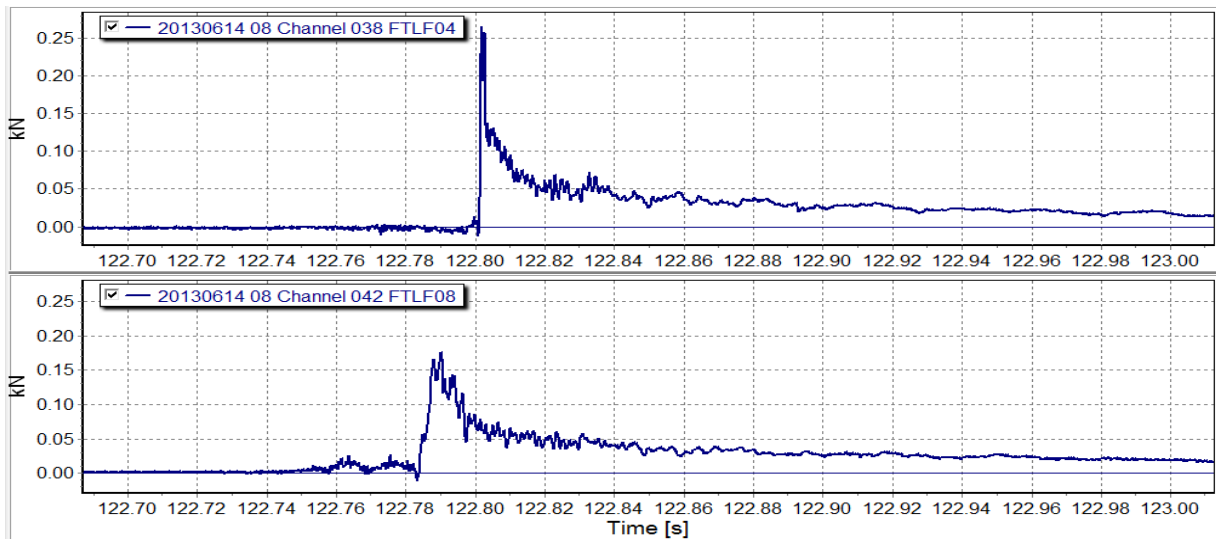


**Figure 4.14: Response for Wave test: 20130614-08 on the columns.**

In the above figures is observed that a first response is obtained in the lower bracing transducers FTBF01-04 and at the columns FTLF04-08 (these four transducers are located nearly at the same height). On the other hand, the maximum response for the legs is produced before than the maximum response on the bracings, even though the impact of the wave reached at the same time the FTLF08 and FTBF04. The reason for that, as was described earlier is that the maximum response on FTBF01-04 is a consequence of the wave impact at the upper part of the bracing, FTBF02-03.

## 5. MODELLING OF THE STRUCTURE IN ANSYS

### 5.1 Introduction

Nowadays, one of the main benefits of computational models is that they allow not only to establish and recreate the conditions under which the structure was tested but, let you to define new and frequently severe conditions. Moreover, the computational modelling offers you a wide variety of different outputs to look at and analyze, and also the response from any part of the structure can be obtained.

So, when a project of this scope is planned and carried out, a computational modelling takes usually a relevant part into the whole project.

All what have been said above are positive aspects but undoubtedly there are still some drawbacks in those models that need to be taken into account. It is crucial to understand how the software works and be sure that what you are modelling corresponds to the real structure tested at the laboratory. That is the reason why the validation of the model plays such an important role.

### 5.2 Finite Element Method and Software used

The software chosen for the modelling is ANSYS 14.5. The module used is a general-purpose structural finite element system with specific features related to offshore and marine structures among many different fields.

The fundamental motion equation for a multiple degree of freedom (MDOF) structure is defined as:

$$M \ddot{u} + C \dot{u} + K u = f(t) \quad (11)$$

where  $\ddot{u}$  is the acceleration vector,  $\dot{u}$  is the velocity vector,  $u$  is the displacement vector,  $M$  is defined as the structural mass matrix,  $C$  is the structural damping matrix and  $K$  is the structural stiffness matrix. Finally  $f(t)$  corresponds to a force vector.

One of the most famous techniques in numerical methods to model any structure is the well-known Finite Element Method (FEM). This method is one of the existing procedures in order to approach the response of a structure with infinite degrees of freedom to another with roughly the same physical and geometric properties, but with finite degrees of freedom. Basically, the equilibrium equations are expressed by an algebraic system of simultaneous equations with a limited number of unknowns.

These equilibrium equations are obtained from the Principle of Virtual Work (PVW). As the lecturer might know, the PVW is necessary and sufficient condition for the equilibrium of any part of the structure or the complete structure.

To make it more comprehensible, a beam of a length  $l$  under a force per unit length  $b(x)$  is considered, and point forces  $X_i$  acting on different points. The forces are acting in the beam axle direction. These forces produce internal stresses  $\sigma(x)$  and strains  $\varepsilon(x) = \frac{du}{dx}$ .

The PVW can be formulated as:

$$\iiint_V \delta_\varepsilon \sigma dV = \int_0^l \delta_u b dx + \sum_{i=1}^p \delta_{u_i} X_i \quad (12)$$

where  $\delta_\varepsilon$  and  $\delta_u$  refers to the strain and virtual displacements at any point of the mean fiber of the beam.  $\delta_{u_i}$  is the virtual movement where the point force acts,  $X_i$ .

It can be proved that in order to obtain the equilibrium configuration of any beam under certain force conditions, is reduced to just obtain the displacements field that fulfills the corresponding PVW. The field displacement can be approached in an easy way as:

$$u(x) = a_0 + a_1 x + a_2 x^2 + \dots + a_n x^n = \sum_{i=1}^n a_i x^i \quad (13)$$

This can be rewritten as:

$$u(x) = \sum_{i=1}^n N_i^{(e)}(x) u_i^{(e)} \quad (14)$$

where  $N_i^{(e)}(x)$  are the interpolation functions defined in the element boundary, also called shape functions.

### 5.3 Theory

The truss structure can be modelled as a solid 3D body. There are many structures which their geometric features, loads and mechanical aspects do not allow simplify calculus. When a body has a uniform cross section and small lateral dimension, it is usually modelled as line body. This way of doing it is specially recommended for beam, frame and truss structures.

The idea behind modelling it as a line body is to create a one dimensional idealization of a 3-D structure. Advantages of using line models over surface models or solid models are

among others: (a) they are computationally more efficient than solid bodies, (b) creating line models is usually easier and (c) the problem size is much smaller.

## 5.4 Geometry

The truss structure model is a recreation of the prototype scaled down 1:8. The experimental model was built and set-up at the Large Wave Flume, in Hannover, Germany in 2013.

This truss structure is mainly composed by steel St-37 for columns and bracings with 139.7 mm of diameter. In Figure 5.1 is shown an isometric view of the structure where the red elements indicates the instrumented bracings and the green ones the instrumented legs. Those parts have been instrumented as follows:

- 10 local force transducers located at the legs, at the front side. They are referred as: FTLF01-...-FTLF10. Four are at the left leg in the front side and the other 6 are at the right leg in the front side as well. All the transducers are placed above the still water level (SWL).
- 12 XY force transducers at the bracings. Four located at front side, other 4 at the bracings in the left side and the rest in the right side. In total, the force on six bracings is measured. They are referred as: FTBF01-...-FTBF12.
- 4 total force transducers that measure the total force on the structure in wave direction. They are located two at the top and two at the bottom. They are referred as: FTTF01-...-FTTF04.

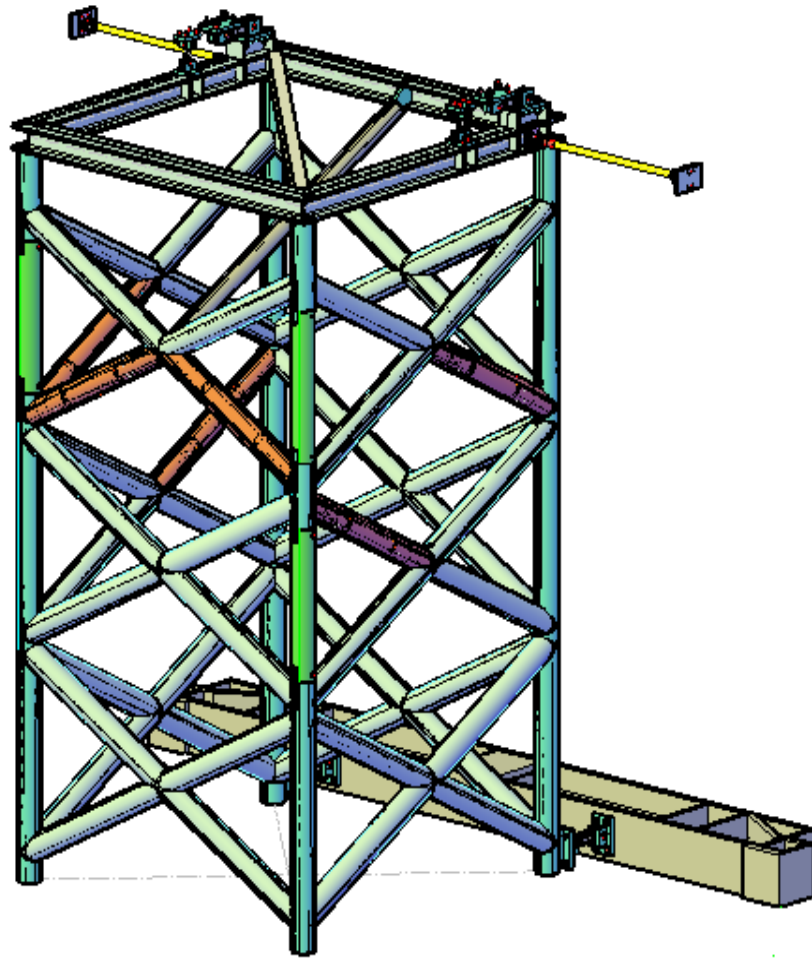


Figure 5.1: Isometric view of the structure.

In Figure 5.2 the waves are coming in the direction normal to the plane, Y direction. Units in mm.

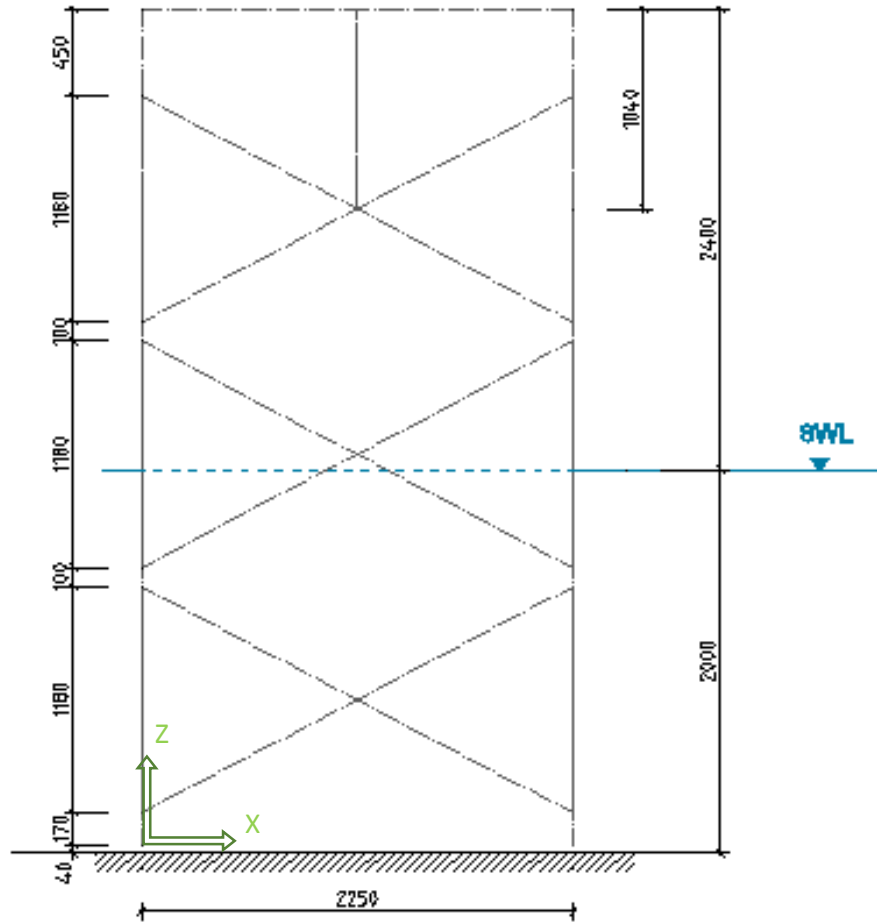


Figure 5.2: Dimensions of the front side of the structure.

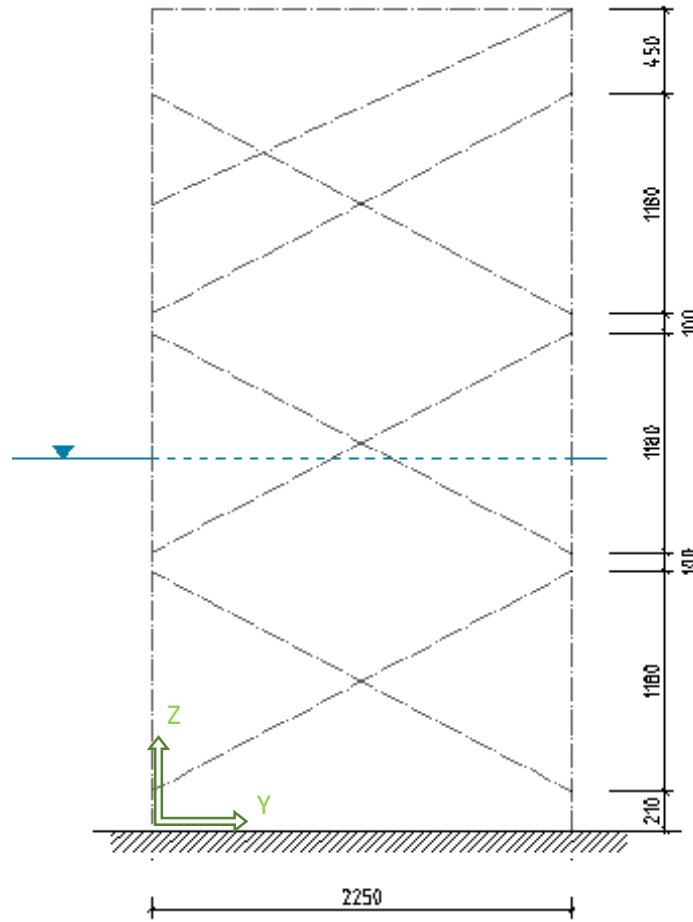


Figure 5.3: Dimensions of the right side of the structure.

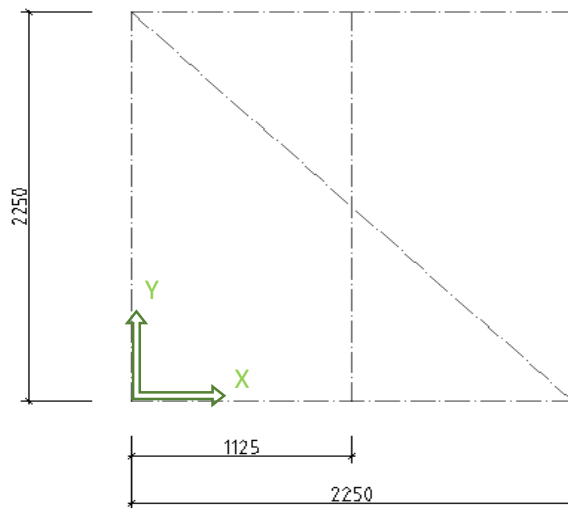


Figure 5.4: View from an upper position.



### 5.4.1 Cross sections

The structure is composed by six different cross sections. The upper part of the structure is formed by 4 HEBI 140 and a diagonal beam. The three instrumented legs were designed as a solid cross section of aluminum with the same outer diameter as the rest of the structure, 139.7 mm. The remaining structure is composed by steel tubes with a wall thickness which varies whether the tube is instrumented or not, from 5 to 4 mm respectively. There is a remaining tube which connects the upper front bracings with the backside of the structure in order to increase the stiffness which has a different geometry. The cross sections are described in Figures 5.5, 5.6 and 5.7. Units in mm. The properties are defined in Table 5.1.



Figure 5.5: Cross section of the normal tubes and instrumented bracings.

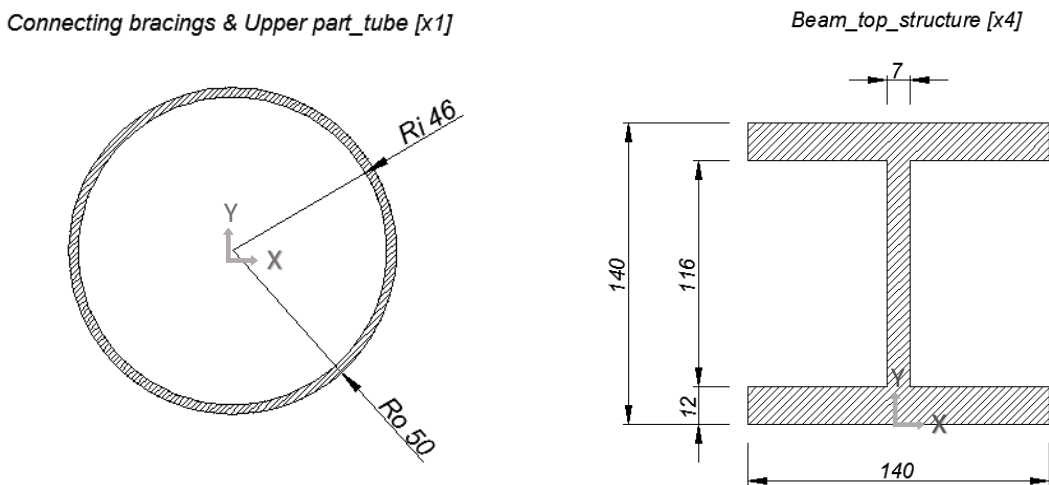
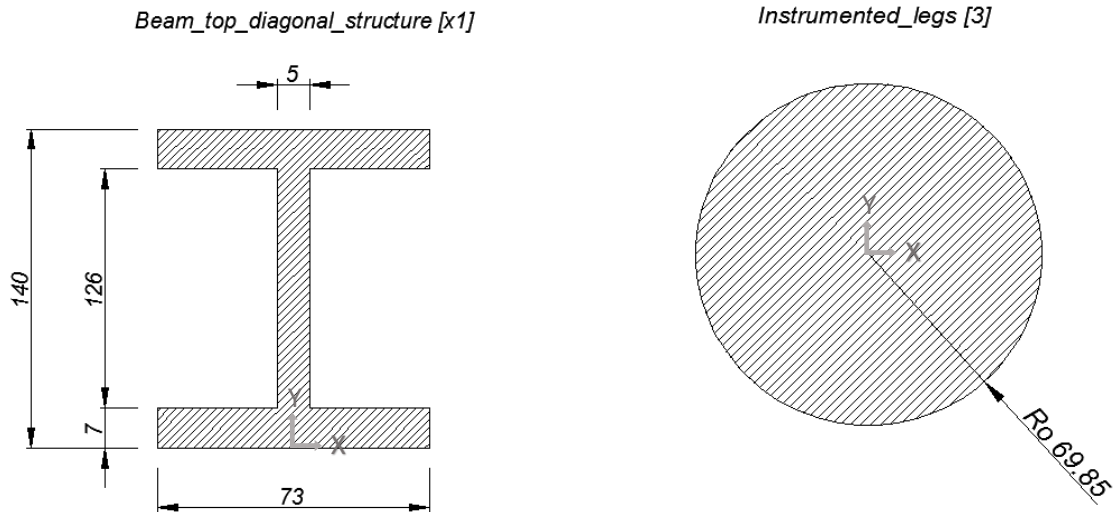


Figure 5.6: Cross section of the tube that connects the upper front bracings to the backside of the structure and the beams at the top of the structure.



**Figure 5.7: Cross section of the diagonal beam located at the top of the structure and cross section for the instrumented columns. Units in mm.**

*Properties of the cross sections*

**Table 5.1: Properties of all the cross sections.**

Cross section	Area [m <sup>2</sup> ]	I <sub>xx</sub> [m <sup>4</sup> ]	I <sub>yy</sub> [m <sup>4</sup> ]	Length [m]
<i>General_tube</i>	0.00170	3.886E-06	3.886E-06	67.600
<i>Instrumented_bracings_tube</i>	0.00211	4.750E-06	4.750E-06	7.377
<i>Connecting bracings &amp; Upper part_tube</i>	0.00120	1.375E-06	1.375E-06	2.056
<i>Beam_top_structure</i>	0.00417	1.471E-05	5.491E-06	8.977
<i>Beam_top_diagonal_struct.</i>	0.00165	5.357E-06	4.552E-07	3.182
<i>Instrumented_legs</i>	0.01533	1.842E-05	1.842E-05	2.700

5.4.2 Connections

Most of the connections between the non-instrumented bracings and tubes in the laboratory model have been welded. All these connections have been defined as rigid connections in the computational model.

The existence connections between the instrumented bracings and legs were not welded but melded with steel plates. This new scenario in these connections will have an influence in the dynamic response.

This can be appreciate in Figures 5.8-5.11. Nevertheless, all the connections have been initially defined as rigid joints in ANSYS.



**Figure 5.8: Front view of the front instrumented bracings and instrumented columns.**

The instrumented bracings<sup>4</sup> (from number 3 and number 6 until the center of the structure, number 9) were not welded to the rest of the structure. The joint can be appreciated from Figure 5.8. The left column where the force cell transducers are installed is called Pole\_1 (from n°1 to n°3). The same element but in the right column (from n° 4 to 6 in the figure) is defined as Pole 2. Pole 3 does not appear on the figure but is located just below Pole\_2. Number 7 and number 8 refers to the non-instrumented front bracings. The green points represents roughly the location of the force bracing transducers, FTBF01-02-03-04 from left to right.

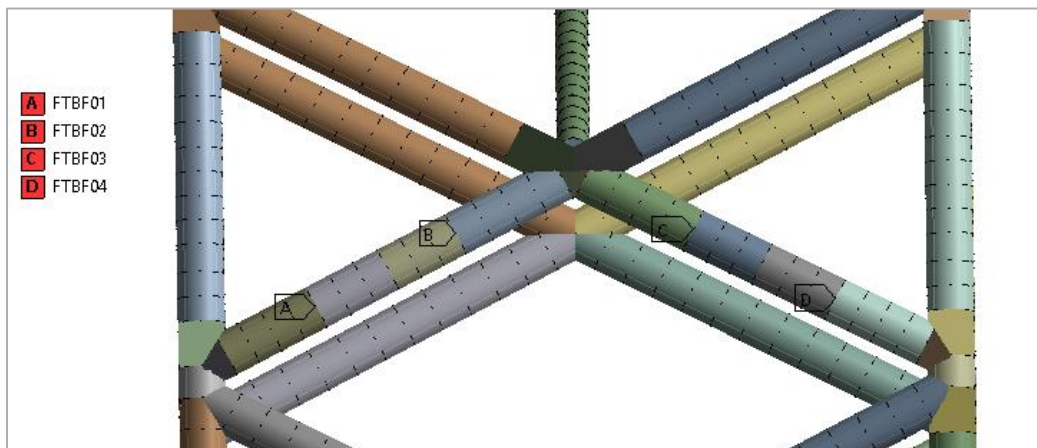


**Figure 5.9. Front view in ANSYS.**

<sup>4</sup> Each instrumented bracing, from 3 to 9, is made by two half shells. For instance one half shell goes from 3 to the first green point. The second half shell goes from the second green point until 9. See Figure 5.8 and 5.10.

In the following figures from CAD is shown the plate between the instrumented front bracings and the rest of the structure.

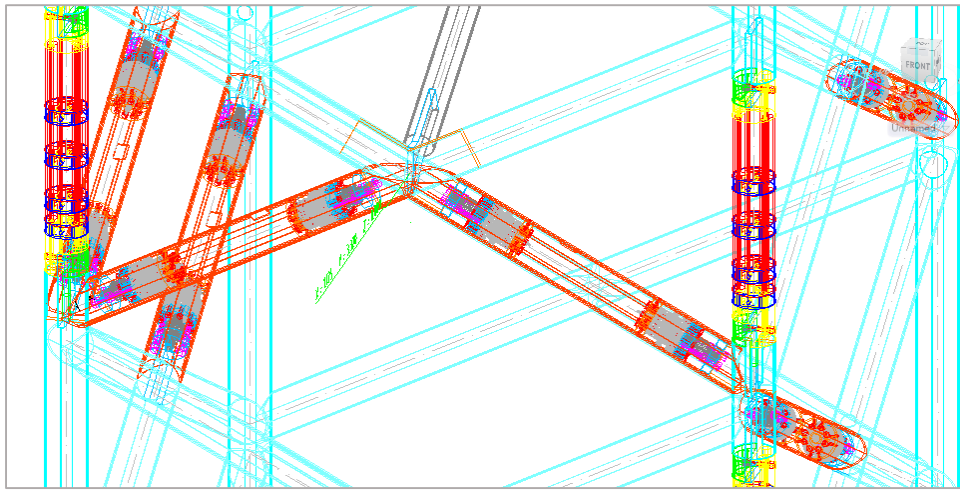


**Figure 5.10: Front view in AUTOCAD showing the bracing and legs transducers.**

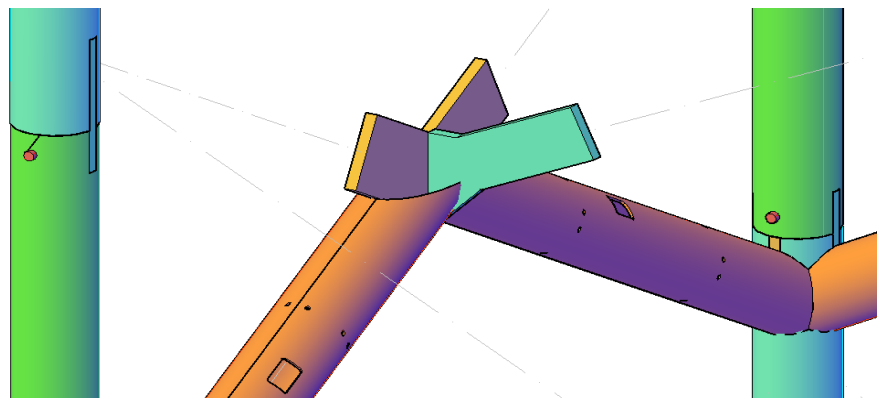


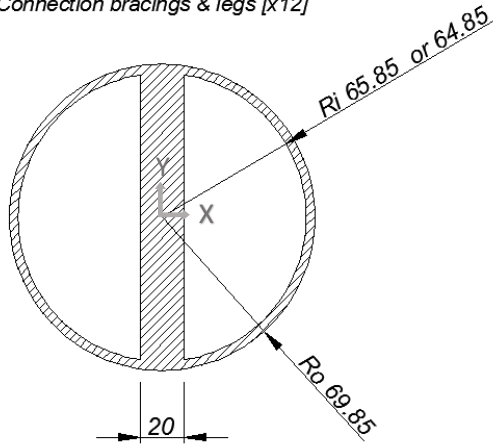
**Figure 5.11: Back view of the front bracings**

Furthermore, in the computational design a recreation in detail of the geometry of those junctions have been done for the instrumented bracings and legs. Although these modifications might not represent large changes on the structure response, their recreation will faithfully depict the junctions of the model tested on the laboratory in terms of mass and inertia.

This singularity in the design has only done for the connections at the front side between the instrumented bracings and the instrumented legs. The Figure 5.12 shows the designed connections.

As it was mentioned before, the connections between the instrumented bracings and columns during the experiments may generate a different structural response than simply defining the joint as rigid as initially was done in ANSYS.

Connection bracings & legs [x12]



Connection tube & bracings / upper part structure [x2]

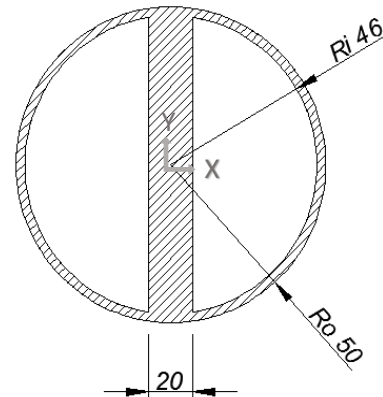


**Figure 5.12: Cross sections of the connections between instrumented front bracings and instrumented legs.**

The internal radius is subject to whether the connection is between and instrumented bracing, 64.85, or it connects an instrumented legs with other part of the structure, 65.85 mm.

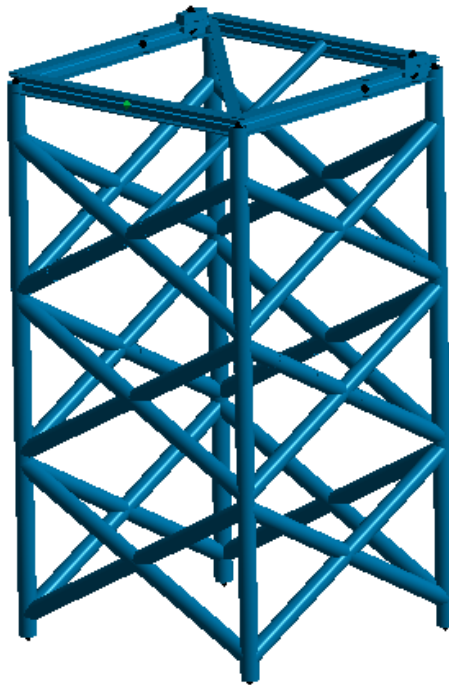


**Figure 5.13: Representation of the structure modelled in ANSYS**

## 5.5 Materials

The predominant material for all the tubes is steel, St-37 with Young's modulus of 210000 N/mm<sup>2</sup>. In particular this material corresponds to 94.89% of the structure. The rest of it is made of aluminum and belongs to the instrumented legs.

As it was shown previously, not the whole structure exhibits homogeneity. There are some specific locations where force cell transducers have been installed, that need to be recalculated in order to consider the increase of density, see Table 5.2-.3. See Figure 5.1-.8 for the location of the instrumented transducers. Each cell transducers weights around 4 -4.5 kg.

**Table 5.2: Instrumented bracings [x1, one cell transducer for every instrumented part]**

Instrumented bracing / Half shell		
<i>Length</i>	0.389	m
<i>Area</i>	0.00215	m <sup>2</sup>
$\rho_i$ (Steel)	7850	kg/m <sup>3</sup>
<i>N° of force cells</i> <sup>5</sup>	1	-
<i>Initial mass</i>	6.58	kg
<i>Extra mass</i>	4	kg
$\rho_f$ (Considering one force cell)	12619.60	kg/m <sup>3</sup>

**Table 5.3: Instrumented legs. Pole 3 is partially submerged below still water level (BSWL).**

Instrumented legs				
	Pole_1 ,2	Pole_3		Pole_3_BSWL
<i>Length</i>	0.9	0.53	m	0.37
<i>Area</i>	0.01533	0.01533	m <sup>2</sup>	0.01533
$\rho_i$ (Aluminum)	2700	2700	kg/m <sup>3</sup>	It will be calculated in the Hydrodynamic added mass section
<i>N° of force cell elements</i>	4	2	-	
<i>Initial mass</i>	37.25	21.93	kg	
<i>Extra mass</i>	16	8		
<i>Total extra mass</i> <sup>6</sup>	9.38	4.7	kg	
$\rho_f$	3379.94	3278.54	kg/m <sup>3</sup>	

<sup>5</sup> Every instrumented bracing is seen as two half shells and each one has equipped with one force cell transducer. This table only indicates the properties of one half shell.

<sup>6</sup> The total extra mass takes into account not only the extra mass from the cell transducers but also the material replaced for the cell transducers. The width for every force cell transducers on the legs is 0.04 m

Even though, the extra weight is not completely uniformly distributed along the tubes in the experiment, the new density,  $\rho_f$ , has been assigned along the entire instrumented tubes.

The structural response has been studied from the hammer tests performed the 24<sup>th</sup> of June, 2013. These tests were done with a water level of 2m. So, all the elements below the SWL have to be recalculated in order to take into account the hydrodynamic effects of the surrounding water along the submerged beams, as well as the buoyancy effects.

A recapitulation about the new densities for the instrumented parts can be found in Table 5.4.

**Table 5.4: Properties of the materials**

Material		
	$\rho$ [Kg/m <sup>3</sup> ]	$E$ [MPa]
<i>Aluminum [Pole 1 &amp; 2]</i>	3380	7.00E+10
<i>Aluminum_2 [Pole 3]</i>	3280	7.00E+10
<i>Aluminum_3 [Pole 3 below SWL]</i>	Defined in section: 5.6 Hydrodynamic added mass	
<i>Bracing_instrum [Side Bracings]</i>	12619	2.10E+11
<i>Bracing_instrum_2 [Front Bracings]</i>	12619	2.10E+11
<i>St-37 [General Structure]</i>	7850	2.10E+11
<i>St-37_BSWL [General Structure below SWL]</i>	Defined in section: 5.6 Hydrodynamic added mass	
<i>Structural_Steel [Material in between instrumented front bracings]<sup>7</sup></i>	7850	2.10E+11
<i>Structural_Steel_2 [Material for the two upper non-instrumented front bracings]<sup>8</sup></i>	7850	2.10E+11
<i>Upper_Beam_Connexion [Tube connection]</i>	7850	2.10E+11
<i>Upper_Beams</i>	7850	2.10E+11

## 5.6 Hydrodynamic added mass

During the application of the most hammer test and throughout wave tests, the still sea water level (SWL) is around 2m height. The fact that 2m of structure is under water level needs to

<sup>7</sup> See Figure 6.12 (A)

<sup>8</sup> See Figure 5.8 for details

be considered and model it properly in the computational model. To consider it the density for the elements located under the SWL has been recalculated.

The additional masses such as: hydrodynamic added mass and water flooded in legs and bracings, play a really important role in the dynamics of the structure. Furthermore, mainly because of the geometry of the cross sections, with very thin wall thickness, the buoyancy effects are not especially large but are taken into consideration as well.

The added mass is a concept from fluid mechanics use it for considering the inertia added to a system, in our case the study of the tubes below the water level, because the movement of the structure involves a movement of the fluid surrounding it. So, the added mass coefficient  $C_A$  (15), needs to be estimated.

The added mass coefficient is the non-dimensional added mass:

$$C_A = \frac{m_a}{\rho A} \quad (15)$$

where  $m_a$  is the added mass per unit length [kg/m],  $A$  is the cross-sectional area [m<sup>2</sup>] and  $\rho$  the density of the fluid [kg/m<sup>3</sup>].

According to DNV-RP-C205 (2010 b), the Added mass coefficient is:

For  $K_C < 3$ ,  $C_A$  can be assumed to be independent of  $K_C$  number and equal to the theoretical value  $C_A=1.0$  for both and smooth cylinders. See Figure 5.13.

The Keulegan – Carpenter number  $K_C$  is defined as:

$$K_C = v_m \frac{T}{D} \quad (16)$$

Where  $D$  is the diameter of the tubes [m],  $T$  is the wave period [s] and  $v_m$  is the maximum velocity [m/s].

Because of the very small velocities of the elements of the structure, the  $K_C$  number presents low values. In that case, where  $K_C \ll 3$ , the added mass coefficient is taken as  $1.0$ .



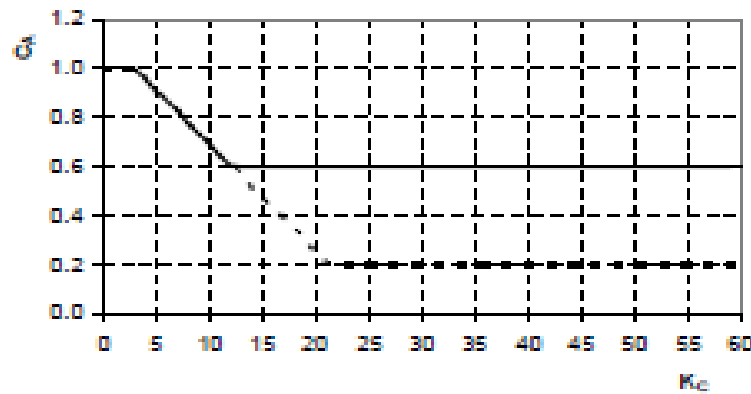


Figure 5.14: Added mass coefficient as function of  $K_c$  number for smooth (solid line) and rough (dotted line) cylinder.

5.6.1 Structure under the water level (St-37 BSWL):

For the structure located below the still water level the effects of the water needs to be considered. In Table 5.5 there is a summary of its properties.

**Table 5.5: Properties of the elements located below the still water level**

Cross section	General_tube (bracings and legs)	
Ri (internal radius)	0.06585	m
Ro (external radius)	0.06985	m
Area_cross section	0.00170	m <sup>2</sup>
Area_ext (Considering it as solid tube)	0.01533	m <sup>2</sup>
Area_int (Area of the hole inside the tube)	0.01362	m <sup>2</sup>

In order to know how much water is displaced, the geometry of the structure under SWL (BSWL) is calculated.

**Table 5.6: Geometry of all the structure below the SWL.**

Geometry structure_BSWL		
Total length BSWL	16.705	m
Volume of the structure BSWL	0.0285	m <sup>3</sup>

$$\text{Volume of the structure BSWL} = \text{Total length BSWL} * \text{Area\_cross section} \quad (17)$$

As it was mentioned before is assumed that all the bracings and legs are water flooded.

In order to obtain the new density for the structure below the water level (BSWL), the mass of the submerged structure before immersing it into water needs to be calculated (Mass in the air). Then the water displaced by the structure will reduce the real mass under the water (Buoyancy effect).

**Table 5.7: Properties of the part of the structure submerged.**

$\rho_{steel}$	7850	kg/m <sup>3</sup>
<i>Mass in the air</i>	223.61	kg
$\rho_w$	1000	kg/m <sup>3</sup>
<i>Buoyancy effect</i>	28.48	kg
<i>Real mass under water</i>	195.12	kg

Secondly, as all the legs and beams BWSL are fill of water, this mass of water inside beams needs to be considered, Table 5.8.

**Table 5.8. Consideration of water flooded structure**

<i>Volume of water inside structure</i>	0.2275	m <sup>3</sup>
<i>Mass of water</i>	227.563	kg

Finally, once the added mass coefficient is found to be 1.0, the added mas per unit length is calculated (18). Then, the total added mas is found multiplying the added mass times the total length under the still water level.

$$C_A = \frac{m_a}{\rho A} \rightarrow m_a = C_A * \rho_w * Area_{ext} = 1.0 * 1000 * 0.0153 = 15.32 \text{ kg/m} \quad (18)$$

$$Total \text{ added mass} = m_a * Total \text{ length under SWL} = 15.32 * 16.70 = 256.04 \text{ kg}$$

So, summing up the three different masses calculated:

$$Total \text{ mass} = 195.12 + 227.56 + 256.04 = 678.74 \text{ kg} (\sim 3.5 \text{ times the initial mass})$$

The new density defined for the whole structure BSWL is:

$$\rho_{s'} = \frac{Total \text{ mass}}{Volume \text{ structure}_{BSWL}} = 23827 \text{ kg/m}^3 \quad (19)$$

### 5.6.2 Instrumented leg, Pole 3

There is one instrumented leg which is partially submerged. It has a length equal to 0.37 m. This instrumented leg is composed by aluminum so its equivalent density has to be calculated.

**Table 5.9: Properties of the partial instrumented leg situated below the still water level.**

Geometry instrumented leg, Pole3, BSWL		
<i>Length BSWL</i>	0.37	m
<b><i>Area<sub>ext</sub></i></b>	0.01532	m <sup>2</sup>
<i>Volume of the structure BSWL</i>	0.00567	m <sup>3</sup>
<b><i>ρ<sub>aluminum</sub></i></b>	2700	kg/m <sup>3</sup>
<i>Mass in the air</i>	15.30	kg
<i>ρ<sub>w</sub></i>	1000	kg/m <sup>3</sup>
<i>Buoyancy effect</i>	5.66	kg
<i>Real mass under water</i>	9.64	kg

The added mass regarding to the part of Pole\_3 that is located below the still water level is:

$$m_a = C_A * \rho_w * Area_{ext} = 1.0 * 1000 * 0.0153 = 15.32 \text{ kg/m}$$

$$Total \text{ added mass} = m_a * Total \text{ length under SWL} = 15.32 * 0.37 = 5.67 \text{ kg}$$

As it has a solid cross sections there is no water to consider inside it. The effect of the added mass is contra rested by the buoyancy effect as is described in Table 5.9.

Finally an overview of the mass properties for each element is presented in Table 5.10.

**Table 5.10: Contribution of the different parts of the structure to the total mass.**

Cross section	Length [m]	Mass [kg]	Total [%]
<i>General_tube</i>	67.600	2015.9	75.2
<i>Instrumented_bracings_tube</i>	7.377	162.2	6.05
<i>Connecting bracings &amp; Upper part_tube</i>	2.056	29.53	1.10
<i>Beam_top_structure</i>	8.977	294.75	11
<i>Beam_top_diagonal_struct.</i>	3.182	41.26	1.54
<i>Instrumented_legs</i>	2.700	136.91	5.11
<i>Total Structure [kg]</i>			2680.55

## 5.7 Boundary conditions

The boundary conditions can be divided into two different groups, the ones regarding to lower part of the structure and the supports located at the upper part.

### 5.7.1 Lower part

The structure is fixed to a special steel beam through two supports located at left and right column. In those supports there are two total force transducers installed. Obviously, they cannot be considered as completely rigid supports, so they are modelled as springs with stiffness defined in the Table 5.11. These supports have constrained the displacement in Y direction and free movement in X and Z

The force transducer at the right leg (seen from wave direction) is named as FTTF01, meanwhile the transducer located at the left leg is defined as FTTF03. The Figures 5.15-5.16 show the details of these supports.

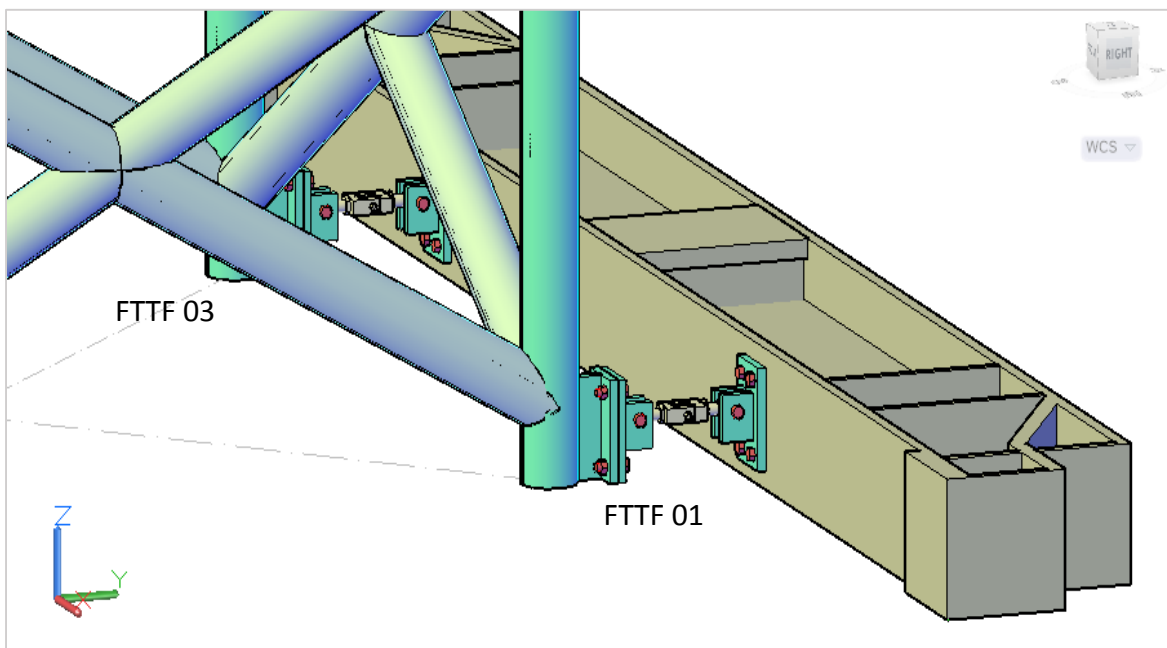


**Figure 5.15: Details of the lower supports on AUTOCAD.**

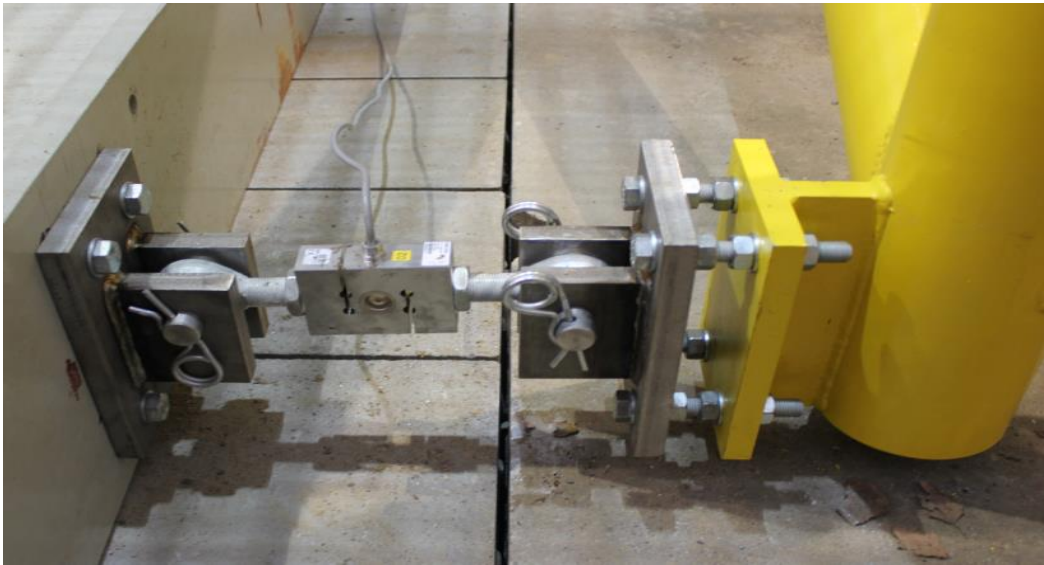


**Figure 5.16: Detail of the FTTF03 in the Large Wave channel in Hannover, Germany**

### 5.7.2 Upper part

The top of the structure is supported by six different supports, three in each side. Each one constrained the displacement in one different direction as can be seen from Figures 5.17-5.18.

The structure is subjected to the two walls of the channel through two slender beams (1). This support constraint the displacement in X direction, whereas the displacement in Y and Z is free.

The other four supports, two at each side, constraints the displacements in Z and Y direction. The support which limits the displacement in Z direction (2), allows the movements in X and Y direction. It is connected to a beam above the structure.

Finally, the last two supports constrained the displacement in Y direction (3), wave direction, and in the same way that in the lower part, in those supports there are two total force transducers installed. They are defined as FTTF02 (right side) and FTTF04 (left side). These force transducers are defined as springs with certain stiffness in Y direction. It is defined in Table 5.11 as well.

It is assumed that all supports are free to rotate in all directions.

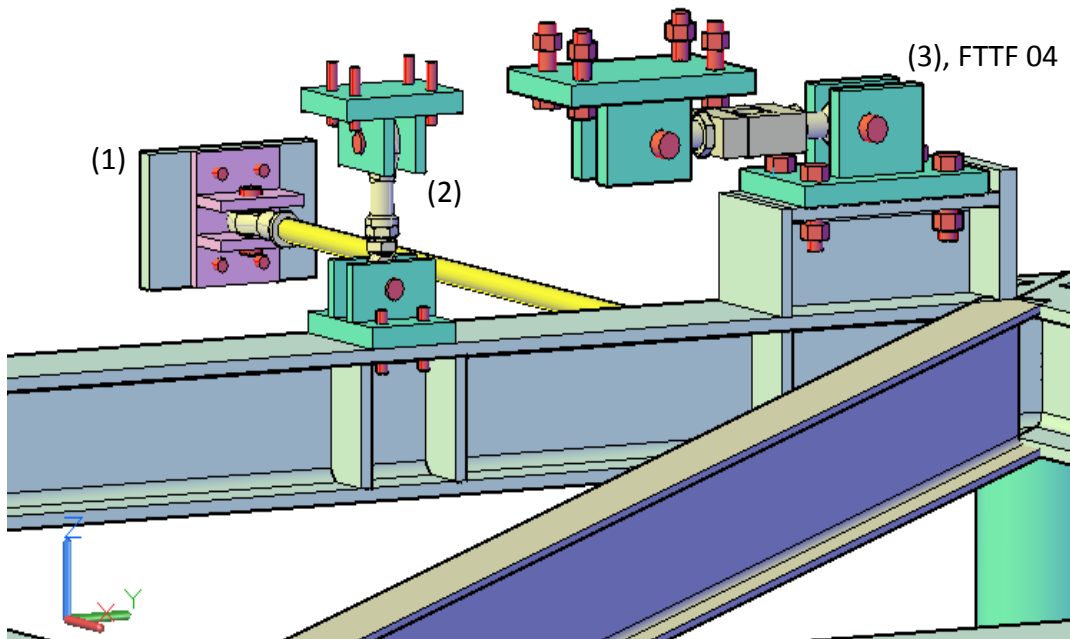


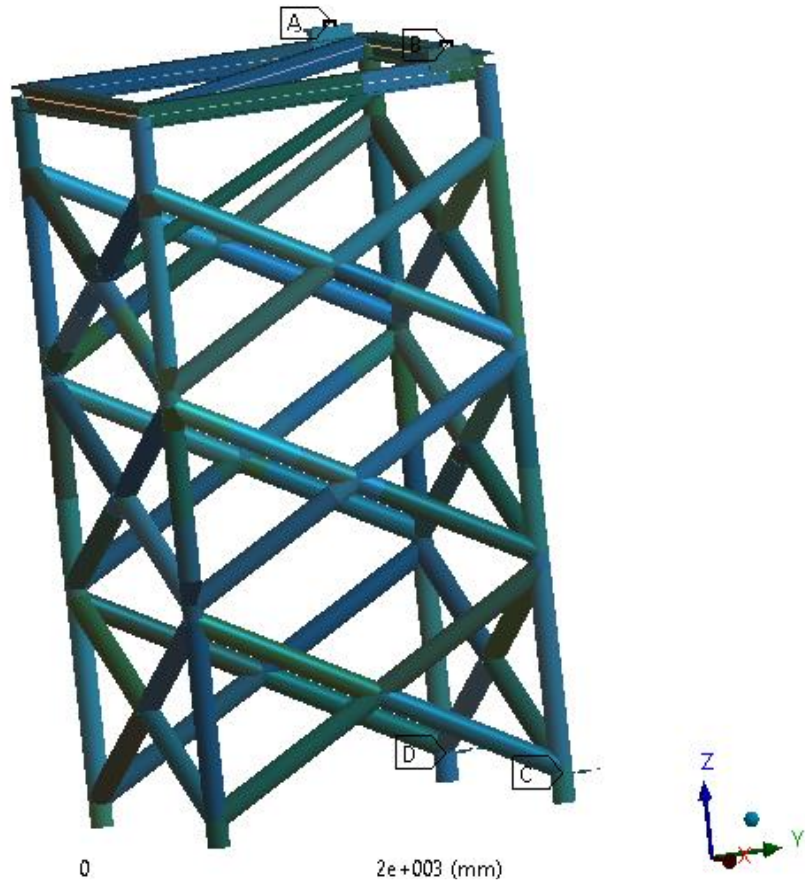
Figure 5.17: Supports (1), (2) and (3) corresponding to the left part of the structure.



Figure 5.18: Real view from the Large Wave Flume.

Longitudinal - FTTF03  
24/04/2014 10:34

- A** Longitudinal - FTTF04
- B** Longitudinal - FTTF02
- C** Longitudinal - FTTF01
- D** Longitudinal - FTTF03



**Figure 5.19: Total Force transducers in ANSYS.**

According to the calibration files the following nominal force transducers were installed:

**Table 5.11: Features of all four total force transducers.**

	Nominal Load [kN]	Nominal displacement [mm]	Stiffness, Y [N/mm]
FTTF01	20	0.2	100000
FTTF02	50	0.4	125000
FTTF03	20	0.2	100000
FTTF04	50	0.4	125000

So, all four total force transducers have been defined in the model as springs with longitudinal stiffness in Y directions defined above. See Figure 5.20 and Table 5.12.

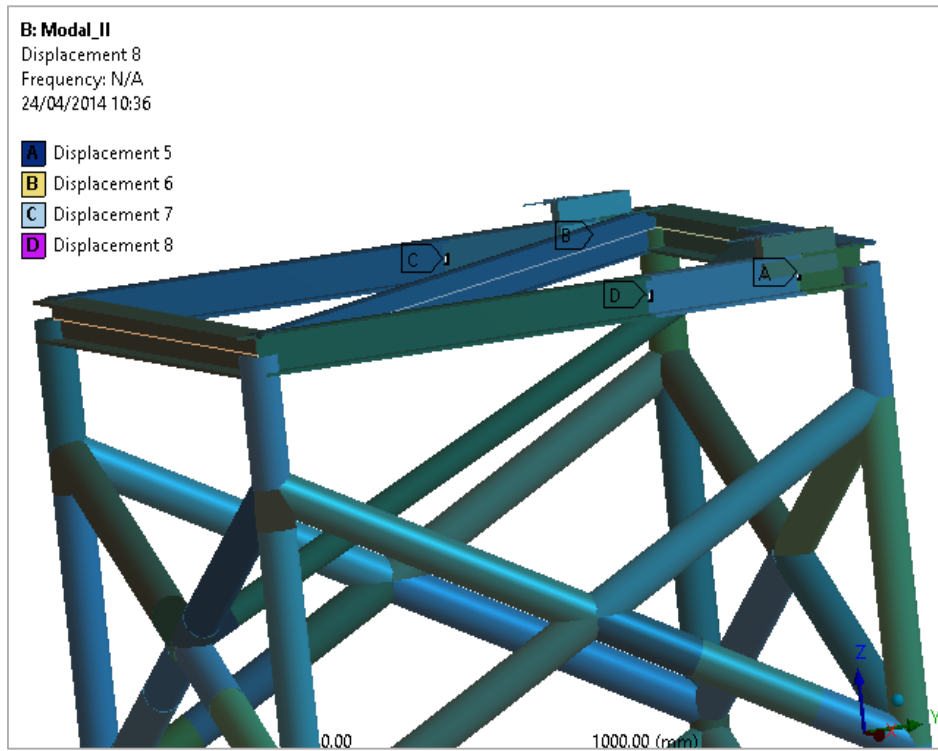


**Figure 5.20: Fixed supports at the top of the structure, ANSYS.**

**Table 5.12: Boundary conditions at each support.**

Support	Constrained displacement [Direction]	Free displacement [Direction]	Rotations
A	X	Y, Z	Free all directions
B	X	Y, Z	Free all directions
C	Z	X, Y	Free all directions
D	Z	X, Y	Free all directions

### 5.8 Mesh

For a 3D line boy, the Workbench in ANSYS 14.5 meshes only with the element BEAM 188. This element is a 3D 2-node first-order beam element. The BEAM 188 element is appropriate for analyzing from slightly thick to slender beam structures. This element is based on Timoshenko beam theory.

Basically, the Timoshenko beam theory maintain the same hypothesis from the Classic beam theory (Euler-Bernoulli), but it establish a new hypothesis where the shear deformation effects are included.

The BEAM188 has six degrees of freedom at each node: 3 translational and 3 rotational degrees of freedom. It is based on linear polynomials, unlike other Hermitian polynomial-



based elements in ANSYS (for example, BEAM4). The refinement of the mesh is really recommended in order to accommodate such loading. This element is strongly computationally efficient and has super-convergence properties with respect to mesh refinement.

In order to define a good mesh is important to perform a convergence analysis, Table 5.13 and Figure 5.21. A load of 1000 kN is applied at the middle of the upper beam and positive in Y direction. The results shown in the following analysis are from the upper left corner at the front side.

**Table 5.13: Evolution of the error varying the mesh size.**

Static Analysis --- Mesh Convergence ---			
Mesh size	Stress (Absolute value) [MPa]	N° Elements	Relative error [%] <sup>9</sup>
25	0.4323	3791	0
50	0.43236	1938	0.0138
100	0.43248	996	0.04163
200	0.43267	547	0.08558
300	0.43282	394	0.12028
500	0.43306	280	0.17580
750	0.4334	214	0.25445
1500	0.4349	157	0.60143

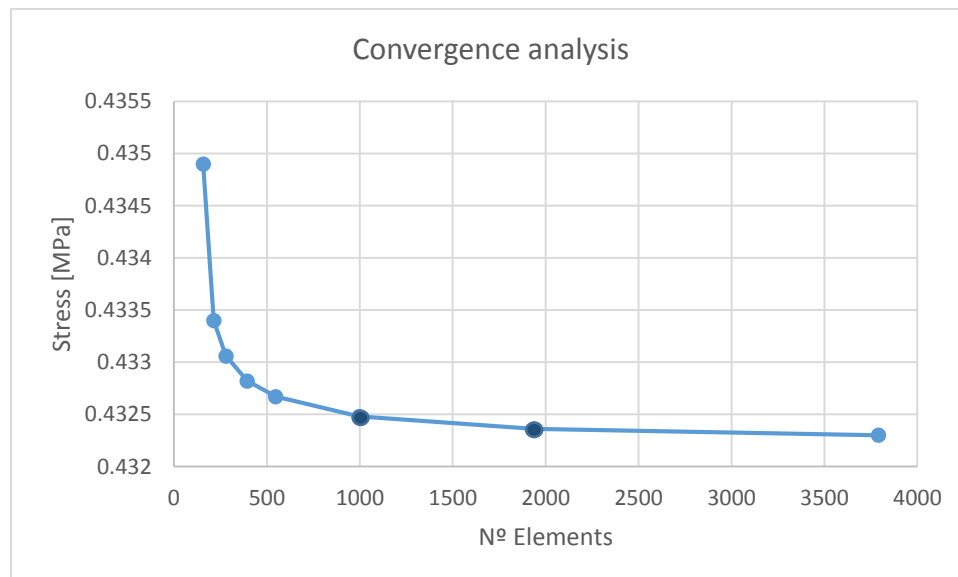


**Figure 5.21: Convergence analysis of different mesh sizes.**

<sup>9</sup> The *true value* to obtain the relative error has been defined as the result of the finer mesh (25)

Although the accuracy of the results are really good for sparse mesh, there is a fast convergence to the true value for n° of elements around 1000 - 2000.

So, from now on the *mesh size* chosen is 50, 1938 elements in the whole structure. A representation of it is shown in Figure 5.22.

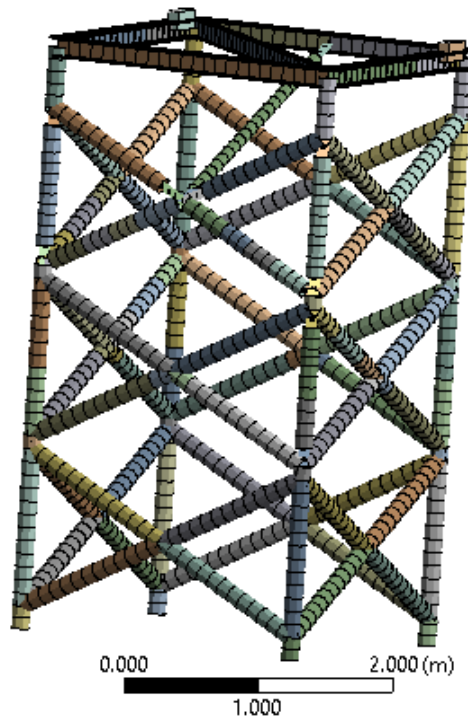


**Figure 5.22:** Representation of the mesh size 50 which has 1938 elements.

### 5.9 Modal Analysis

Usually when a structure is modelled and before carrying out any either static or transient analysis a modal analysis is performed. This analysis is used to calculate which are the natural frequencies and mode shapes of a structure. Those parameters are really important in the design of a structure and in further dynamic simulations. The Table 5.14 and the Figures 5.23 and 5.24 represents the main vibration modes where the mass contribution is larger.

**Table 5.14:** The main mode shapes are defined

Mode	Type	Frequency [Hz]	Direction
1	Global	7.19	X
2	Global	19.68	Z
3	Global	21.28	Torsion X
4	Local	29.43	-
5	Local	31.47	-
6	Global	34.85	Y

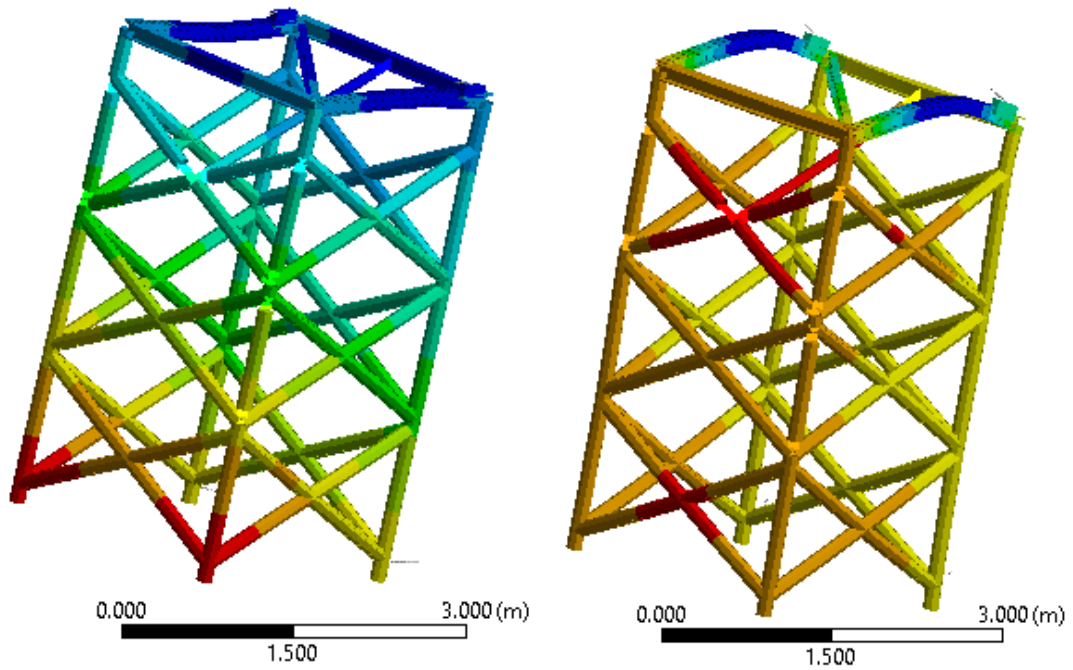


Figure 5.23: Vibration modes 1 and 2 respectively

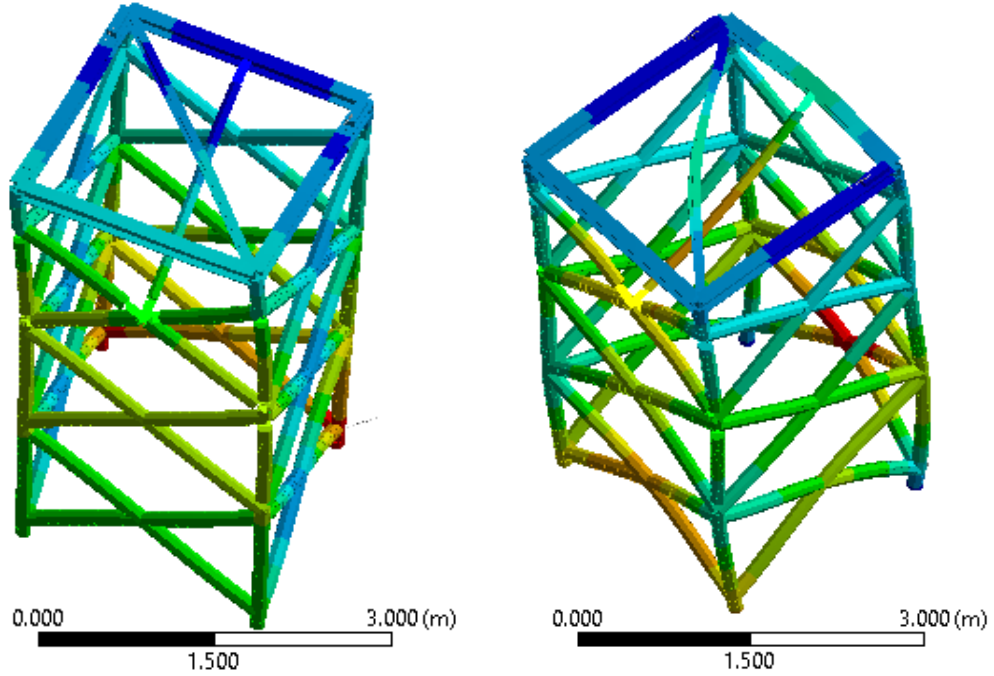


Figure 5.24: Vibration modes 3 and 6 respectively

## 5.10 Damping Ratio

Damping can be defined as dissipation of energy from a vibrating structure, causing the amplitude of free vibration to decay with time. Sometimes is deliberately added for limiting the peak response. This dissipation of energy is used defined as a transformation into another form of energy.

There exist many different types of damping that have an effect on structural dynamics: Coulomb damping (related to dry friction), Radiation damping (for example soils supporting a building, where the support medium is practically limitless), Hysteresis damping (implicit in the material) and Viscous damping.

The force that produces a Viscous damping is proportional to velocity and has been previously presented (11) as  $C \dot{u}$ .

Among all types of damping defined above, the one which is the easiest to be represented in dynamic equations is viscous damping. The damping in structural problems is well defined regarding it as viscous.

One way to represent viscous damping is called proportional damping. See figure 5.25.

### *Proportional damping*

The damping of the structure is studied as Rayleigh Damping in the form of:

$$[C] = \alpha [M] + \beta [K] \quad (20)$$

The above equation (20) says that the global damping matrix is as linear combination of the stiffness and mass matrices. This linear combination depends on two parameter called mass coefficient ( $\alpha$ ) and stiffness coefficient ( $\beta$ ). They can be determined using (22) and (23).

The orthogonal transformation of the damping matrix turns it into:

$$2\xi_i \omega_i = \alpha + \beta \omega_i^2 \rightarrow \xi_i = \frac{\alpha}{2 \omega_i} + \frac{\beta \omega_i}{2} \quad (21)$$

$$\xi = \frac{\beta \omega}{2} \text{ (stiffness proportional)} \quad (22)$$

$$\xi = \frac{\alpha}{2 \omega} \text{ (mass proportional)} \quad (23)$$

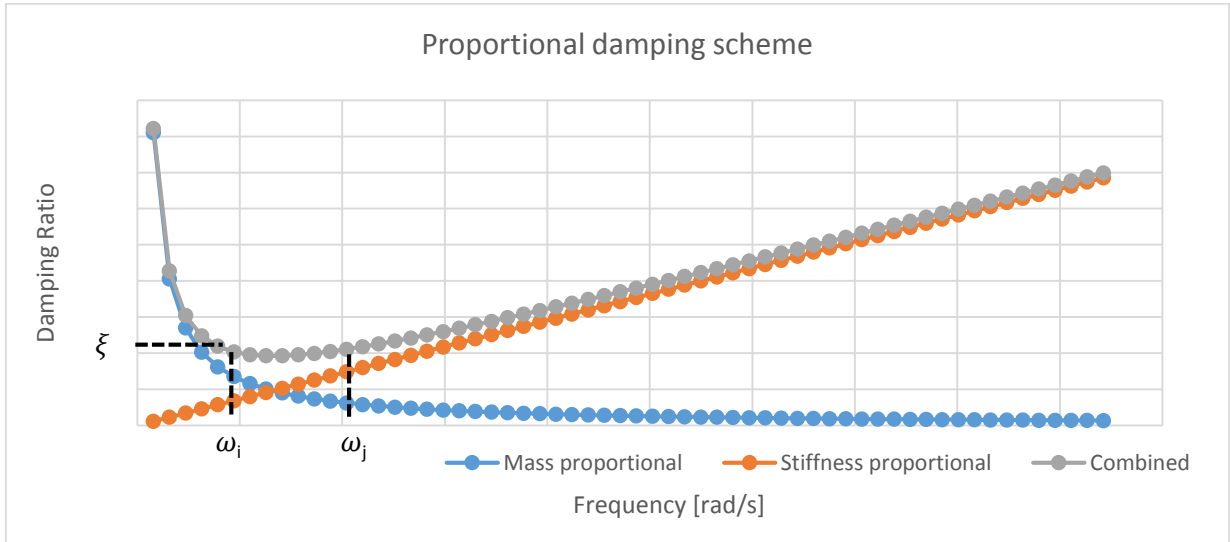


**Figure 5.25: Proportional damping scheme.**

The procedure for determining  $\alpha$  and  $\beta$  has been as follows:

- Define a damping ratio for the first main vibration modes of the structure,  $\xi_i \omega_i$  and  $\xi_j \omega_j$  respectively:

$$\omega_i = \omega_1 = 2 \pi f_1 = 2 \pi 7.2 = 45 \text{ rad/s (1}^{\text{st}} \text{ mode of vibration)} \quad (24)$$

$$\omega_j = \omega_3 = 2 \pi f_3 = 2 \pi 21 = 125 \text{ rad/s (3}^{\text{rd}} \text{ mode of vibration)} \quad (25)$$

- Based on the above equations  $\beta$  is defined as:

$$\beta = \frac{2\xi_j \omega_j - 2\xi_i \omega_i}{\omega_j^2 - \omega_i^2} \quad (26)$$

- Back in (22) and substituting  $\alpha$  is obtained:

$$\alpha = \frac{2\omega_i \omega_j (\xi_i \omega_j - \xi_j \omega_i)}{\omega_j^2 - \omega_i^2} \quad (27)$$

So, to get the damping ratio  $\xi_i$  that defines the structure, an initial method called Half-power bandwidth is used, see Figure 5.26. Even though this method is defined for lightly damped single degree of freedom systems is often used for multi degree of freedom systems as well.

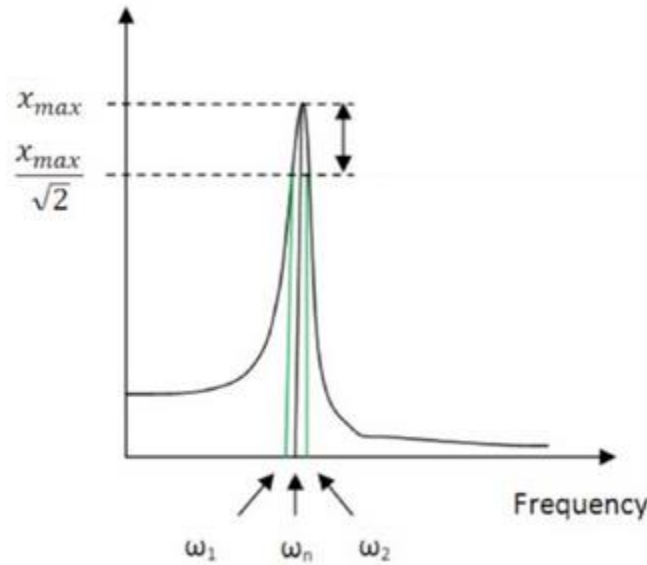


Figure 5.26: Half-power bandwidth method description

The damping ratio is obtained as:

$$\xi = \frac{\omega_2 - \omega_1}{2 \omega_n} \tag{28}$$

The spectrum from the total response in wave direction (sum up of the response at FTTF01-02-03-04) from different hammer test locations (2, 25, 5, 1, 3, 4, 6 and 8) is calculated and an average damping ratio is found. See Appendix B for details in the hammer test locations. The details from the results of each hammer test can be found in Appendix D. The average of these values is found in Table 5.15.

Table 5.15: Average damping ratio found using Half power bandwidth method

Damping Ratio	
$\xi$	0.0155

The structural damping depends mostly on the strain level and deflection. Following the recommended practice *DNV-RP-C205, Environmental conditions and environmental loads, 9.1.9 – Structural damping*; for slender elements in water, the structural damping at moderate deflection is typically 0.005 for pure steel elements.

So, theoretically the average damping ratio found using the Half bandwidth method is 3 times larger. That might suggest that with this damping ratio of 0.015 the signal will be damped out very fast.

In order to clarify that issue, an analysis for different damping ratios is performed for a *Large Hammer Impulse 20132624-18, position tested 02*. In this analysis the only point of interest is the duration of the response and at what time is damped out. Figures 5.27 – 5.28 show the behavior for different damping ratios.

**Table 5.16: Mass and stiffness coefficients for different damping ratios**

Rayleigh Damping			
$W_i$ [rad/s]	45	45	45
$W_j$ [rad/s]	125	125	125
$\xi_i$	0.004	0.008	0.015
$\xi_j$	0.004	0.008	0.015
$\alpha$	0.2424	0.4848	0.9090
$\beta$	4.848E-05	0.0000969	0.000181

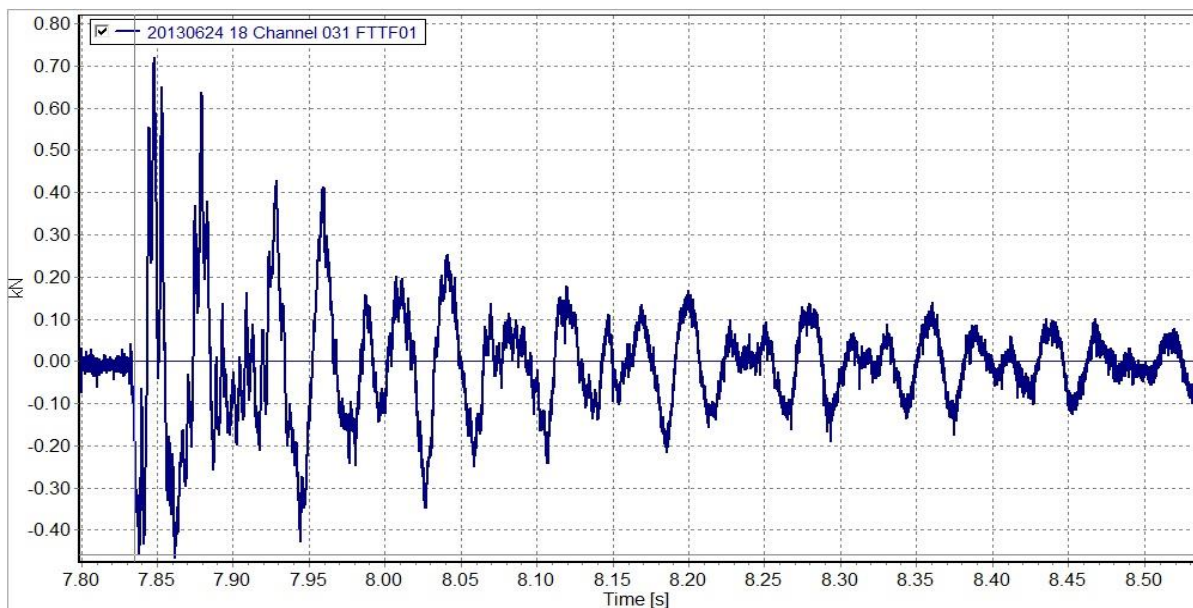


**Figure 5.27: Time force response at FTTF01. Wave Test: 20130624-18**

The response is damped out around 0.6 – 0.7 s.

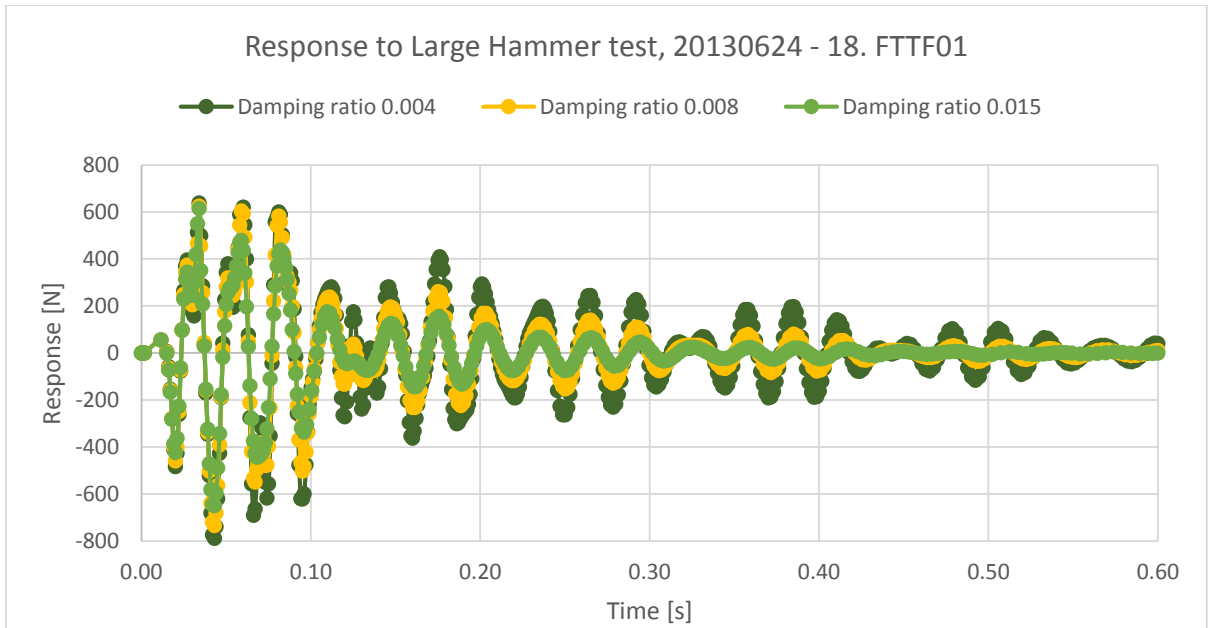


**Figure 5.28: Time force response at FTTF01 in ANSYS for different damping ratios**

For a damping ratio of 0.015 the signal is damped out at 0.35 seconds. This is half length of the theoretical response from the data. Reducing the damping ratio until 0.008 decreases the damping out to 0.5s. For a damping ratio of 0.004 the response is damped out nearly at the same time as the experiment structure does, at around 0.6 seconds.

The damping ratio used for the following analysis is set as 0.004.



## 6. VALIDATION OF THE MODEL

Once the structure has been completely defined in terms of geometry, materials and boundary conditions, the validation of it takes place.

It mainly consists of two different parts. Firstly, the local response on the instrumented bracings is going to be examined. To do that, hammer test n°8 and n°11 are going to be analyzed and the response at FTBF01-FH<sup>10</sup>, FTBF02-FH, FTBF03-FH and FTBF04-FH is going to be studied.

Secondly, a global analysis of the structure is required as well. For this analysis, the response from the total force cell transducers in the horizontal direction (Y direction, wave direction) : FTTF01, FTTF02, FTTF03 and FTTF04 will be examined from the following large hammer tests: n°2, n°3, n°5, n°6 located on the legs; and n°8 and n°11 on the bracings.

For details about the location of the hammer Tests see Figure 3.2 and Appendix B.

During this process the focus of the analysis is defined in the initial response of the element studied.

An initial goal is defined as:

- To get a good fit in magnitude for the first two peaks of the force response analyzed both for global and local response. Furthermore, a fit in time response for those peaks is also important.

### 6.1 The impulse hammer test

The hammer tests were carried out in order to know the response of the structure to a certain impulse load. A study in the frequency domain of the impulse and response load will give us what is called as a Transfer function. This function provides a way for obtaining different element properties of the structure studied. Even though the analysis in the frequency domain it was not initially planned in this project, it might be useful to study it in the next section of the thesis, *Characterization of wave slamming forces*.

The application of the impulse hammer for the model in GWK was as follows:

- Study of the whole structure response. Points from 1 to 6 with. Large Impulse hammer of 1.5 kg. See Appendix B.
- Response of the bracings. Points from 7 to 12, see Figure 3.2. Large and small impulse hammer of 1.5 kg and 0.1 kg were applied.

---

<sup>10</sup> FH refers to the force response in the horizontal plane

So these hammer test are going to be the validation tools for comparing and check the response from the experiment in GWK and the response in the ANSYS model.

## 6.2 Transient Analysis

The loads applied on the structure such as hammer impulse loads or wave loads are defined by rapid force changes compared to the quasi-static loads. They are usually high magnitude forces within a short interval of time. Therefore these kind of loads implies the performance of a transient dynamic analysis.

The setup for the transient analysis requires to define the number of time steps in which the load will be characterized among other aspects. Two time steps are defined, one for where the impulse load is applied and the other going from the end of the load time until the end of the analysis described in Table 6.1. Using two time steps allow the possibility to define different initial, minimum and maximum time steps within each one and optimize the time needed every time an impulse load is applied. See figure 6.3 to see the two time steps defined for a hammer load in ANSYS model.

**Table 6.1: Values for the Transient Analysis**

Step controls - Transient Analysis -		
Step n°	1	2
Initial time <sup>11</sup> [s]	Start impulse load	End impulse load
Final time [s]	End impulse load	End simulation
Initial time step [s]	0.000104	0.0005
Minimum time step [s]	0.00008	0.00006
Maximum time step [s]	0.0003	0.0008

The final time for the step n°2 is defined as 0.015 seconds. If a study of the complete response was required, the simulation time should be set for 0.6-0.7 seconds that is the time in which the response is completely damped out. Considering this initial 0.015 seconds, every simulation takes around 15-20 minutes. Some simulations of the entire response were computed and the total time needed for each complete simulation was around 1h 10 minutes.

## 6.3 Local response analysis of the instrumented front bracings

To carry out the local response analysis on the bracings the hammer test applied on the middle of them will be studied. That is hammer test at position n°8 and n°11.

<sup>11</sup> The start of the impulse load is defined as time 0s.

The analysis of the side bracings are out of scope in this project.

### 6.3.1 Definition of hammer test studied on bracings

The hammer test studied at position n° 8, on the upper left front bracing corresponds to: *Large-hammer-test 2013\_06\_24\_18\_53\_47* and is defined in Figure 6.1.

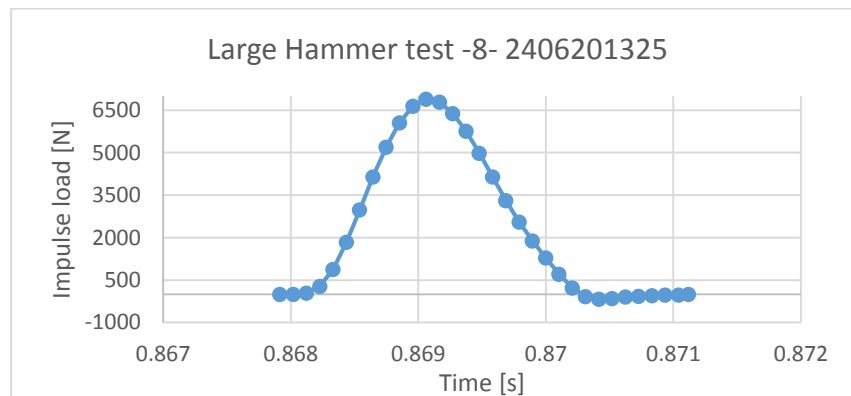


**Figure 6.1: Hammer test 2406201325 at position n°8**

The other hammer test studied at position n° 11 on the upper right front bracing corresponds to: *Large-hammer-test 2013\_06\_24\_18\_59\_19*, defined in Figure 6.2.

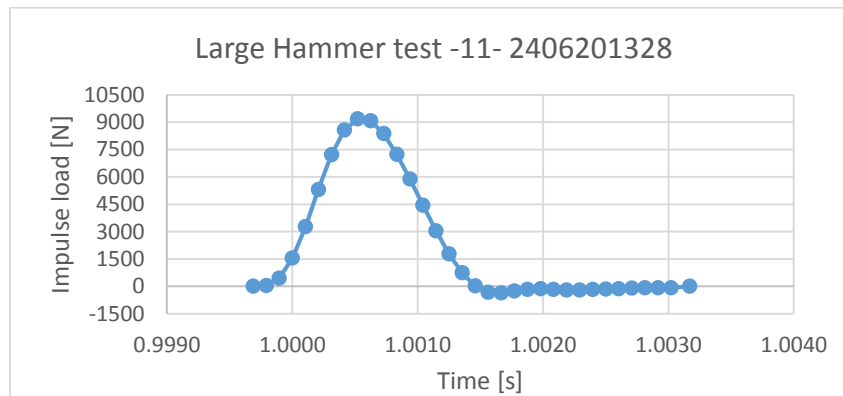


**Figure 6.2: Hammer test 2406201328 at position n°11**

### 6.3.2 Analysis of the results on the bracings

The analysis of the results is going to focus on the response in Y direction (wave direction) at FTBF01-FH, FTBF02-FH, FTBF03-FH and FTBF04-FH. See Figure 3.2 for location details.

At this point it is important to recall that initially the responses on the bracing transducers were recorded in local axis FX and FY. In order to make it easier and more comprehensible,

the responses in the local axis were transformed to global axis, FH and FV, horizontal and vertical plane respectively. So, since the ultimate goal is to characterize the wave slamming forces and they are acting mainly normal to the beams, the validation process only considers the response in wave direction, FH (Global Y direction).

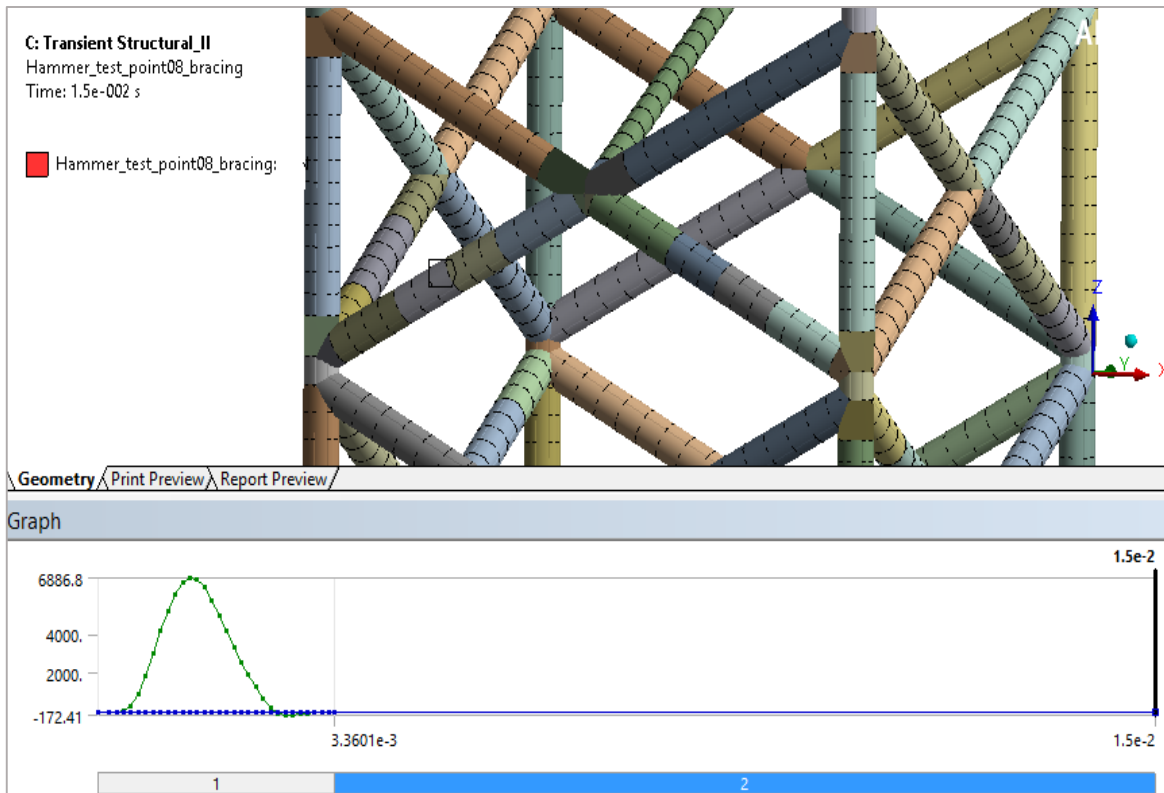


**Figure 6.3: Description of hammer test 8 in ANSYS**

*Response from hammer test -8-*

The following figures show the response in the force bracings transducers 01, 02, 03 and 04 for a hammer impulse at the middle of the left front instrumented bracing, which corresponds to position n°8.

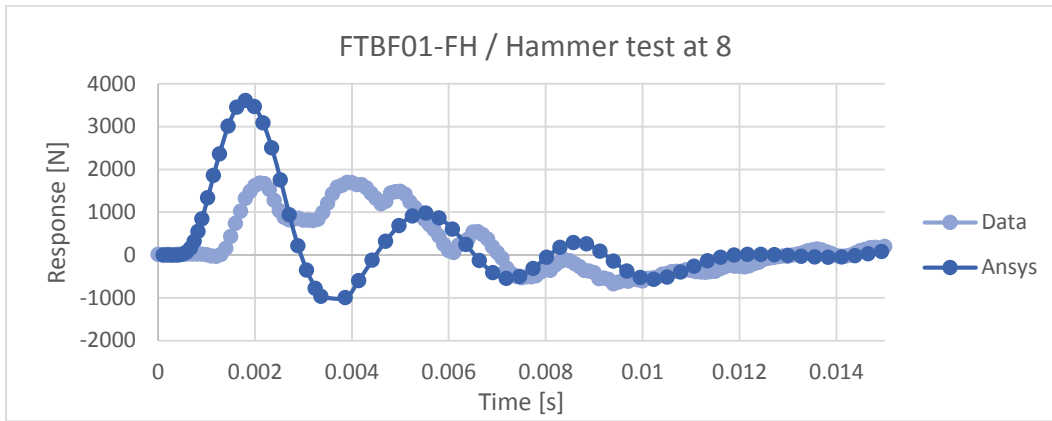


Figure 6.4: Comparison between data and ANSYS response at FTBF01 for hammer test 8.

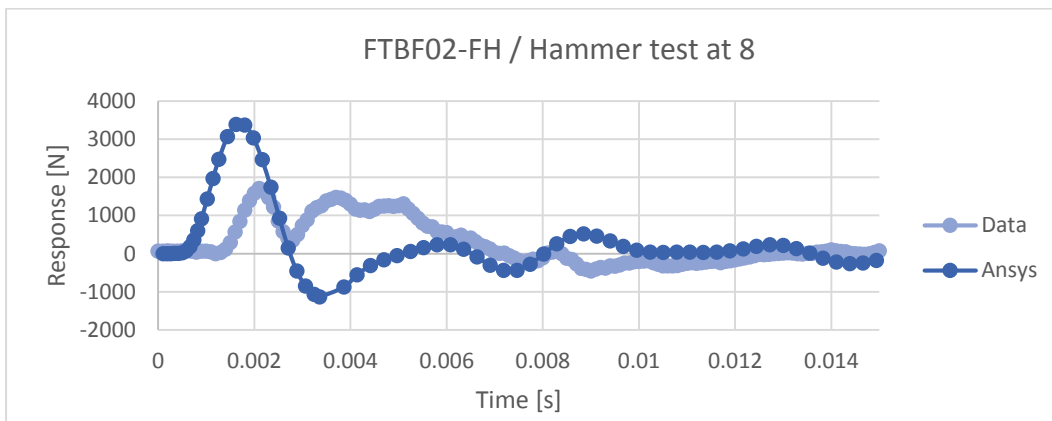


Figure 6.5: Comparison between data and ANSYS response at FTBF02 for hammer test 8.

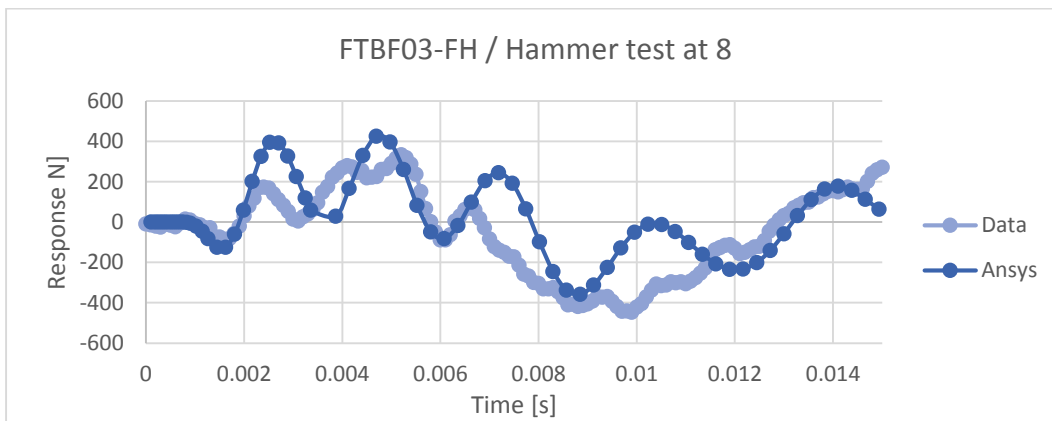


Figure 6.6: Comparison between data and ANSYS response at FTBF03 for hammer test 8.

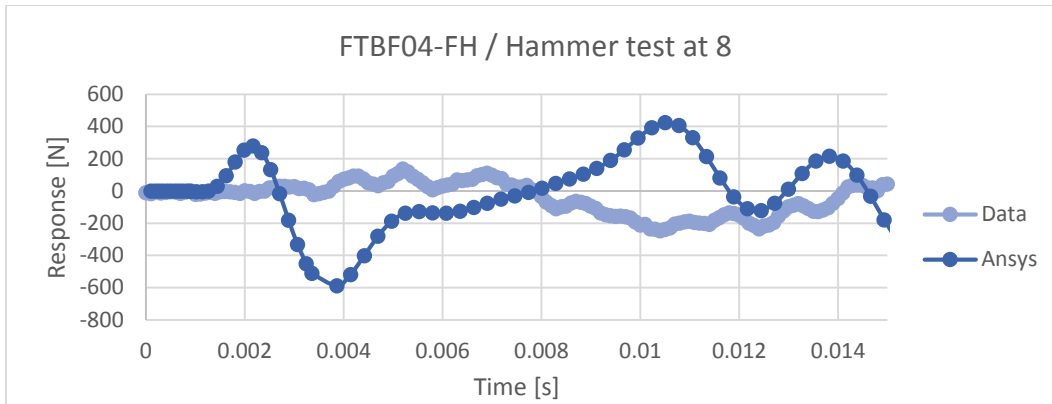


Figure 6.7: Comparison between data and ANSYS response at FTBF04 for hammer test 8.

At a first glance there is a high deviation in the magnitude of the peaks and at what time they are produced. The responses FTBF03-04 have been represented in order to see that there is a time delay in the response in ANSYS as it was expected. The response at these force cell transducers are influenced not only by the local response of the bracings but also by the global dynamics of the structure.

From now on the analysis is going to focus only on the response at the same bracing where the hammer test was applied, e.g., the response at FTBF01-02 for hammer test located at position n°8, and FTBF03-04 from hammer test located at position n°11.

The complete response is described in Figure 6.8 from where a spectrum analysis is going to carry out.

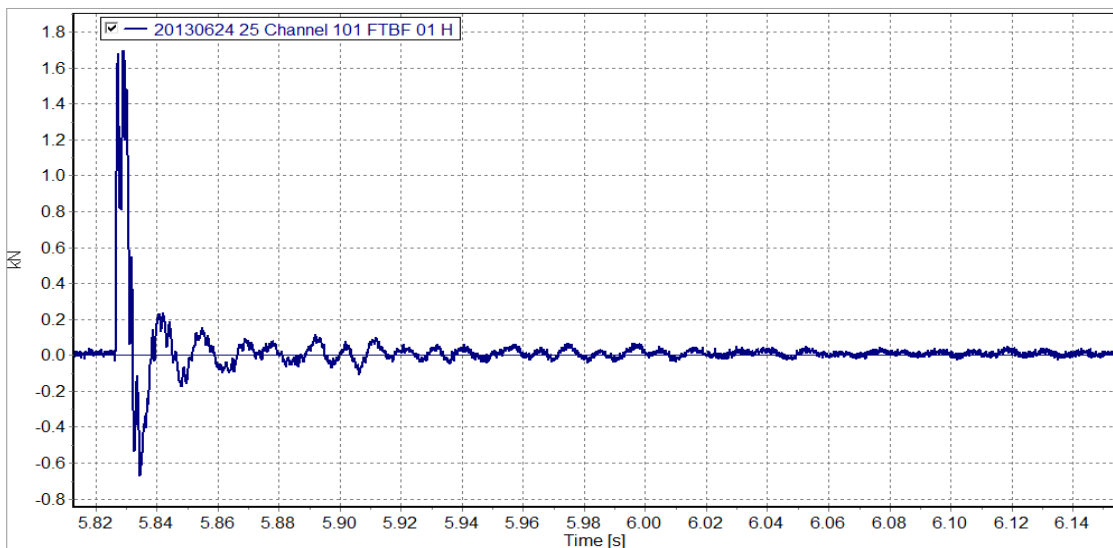
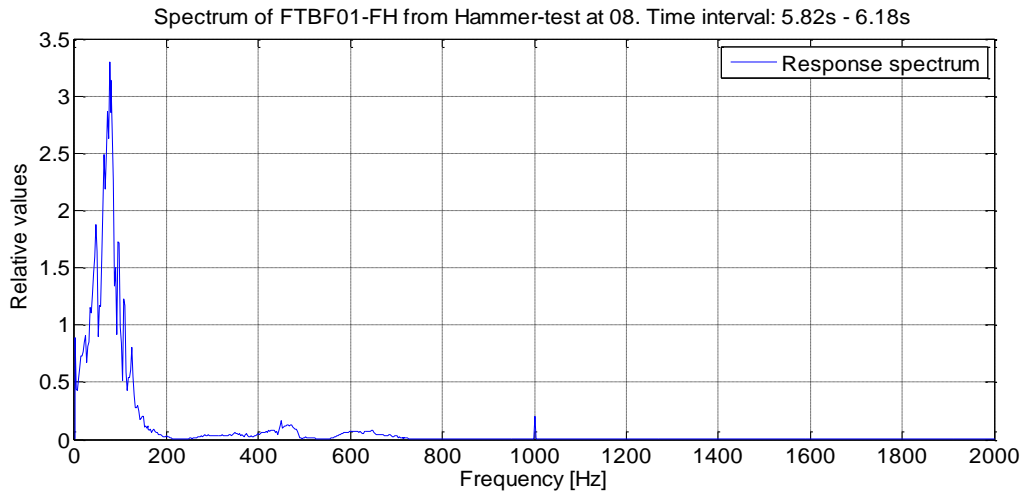


Figure 6.8: Time response at FTBF01-FH from the hammer test n° 08.

A first analysis of the hammer response spectrum on the bracings shows a highest peak at around 80-100 Hz. This means that the Eigen frequency of the bracing is around this value. Higher peaks at around 700 Hz and 1000 Hz are probably noise or might also be related to the Eigen frequency of the cell transducer itself. It is described in Figure 6.9.



**Figure 6.9: Spectrum at FTBF01 of the response hammer test located at position n°8**

Doing a preliminary analysis of the response in ANSYS, equations (29) and (30), is found that the frequencies of the bracings are around 270-310 Hz.

A modal analysis of the bracings is carried out in ANSYS and Figures 6.10-6.11 show that the Eigen frequency for the instrumented front bracings in the wave direction (Y direction) is around 274 Hz.

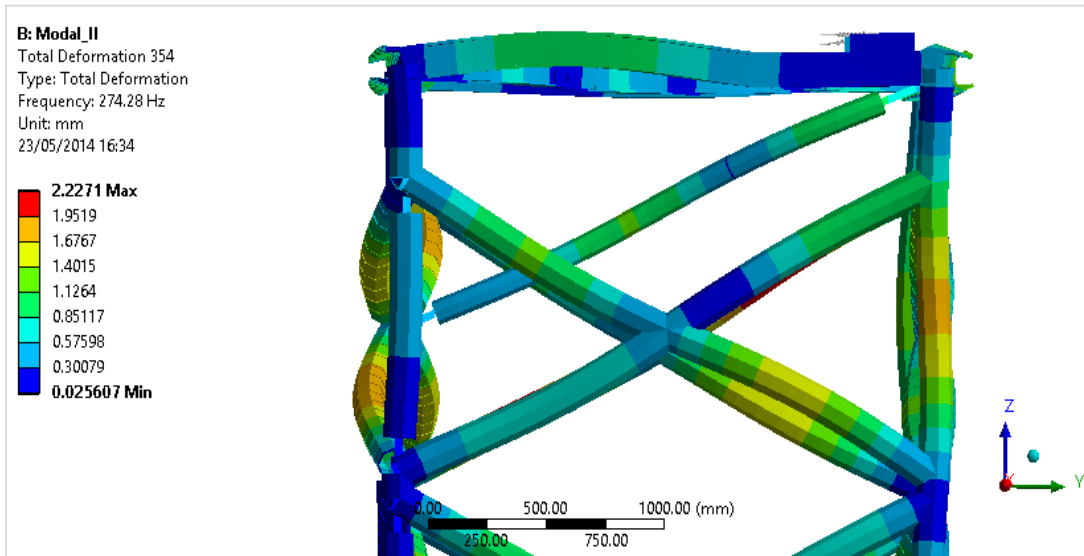


**Figure 6.10: Frequency of the front bracings from a modal analysis in ANSYS (1)**

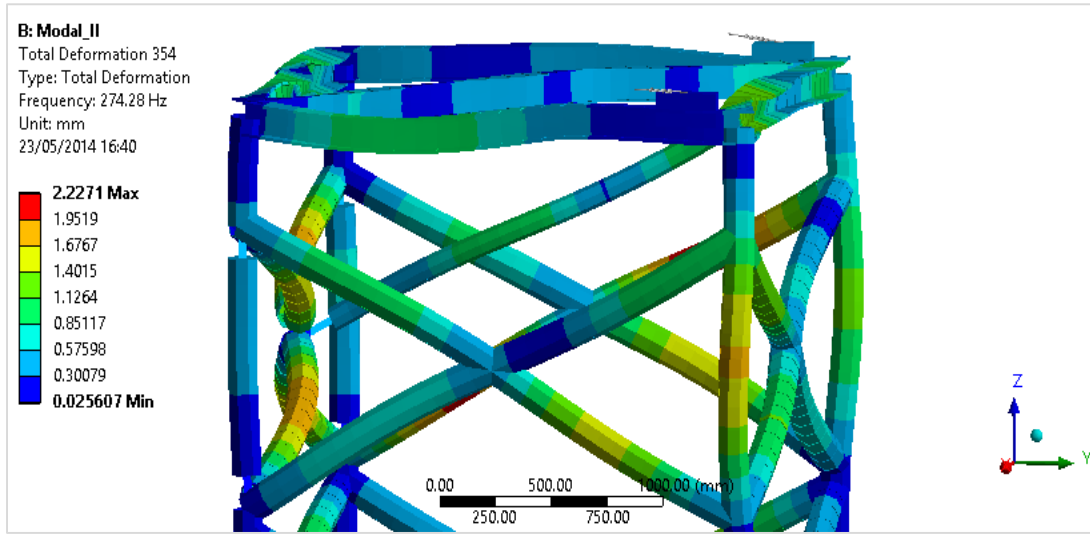


**Figure 6.11: Frequency of the front bracings from a modal analysis in ANSYS (2)**

Some of the peaks from the response in ANSYS are analyzed when the hammer Impulse is at the middle of the bracing, see Figures 6.4-6.5. The frequency found is at around 280-310 Hz.

$$f_{FTBF01-FH} = \frac{1}{0.0084964 - 0.0053119} = 314 \text{ Hz} \quad (29)$$

$$f_{FTBF02-FH} = \frac{1}{0.0120156 - 0.0084964} = 284.1 \text{ Hz} \quad (30)$$

Those initial values point out that the instrumented bracing modelled in ANSYS seems much more rigid than what it was in the experiment.

As it can be observed from the Figures 6.1-6.2, if it is assumed that the impulse load (hammer test) can be described as a triangular load with an impact duration  $t_*$ , the dynamic response becomes lower when the natural period of oscillation is larger, that means a smaller frequency of bracing's oscillation. This behavior is represented in Figure 6.12. This figure gives the maximum dynamic response,  $U_{max}$  for different values of impact duration and Eigen frequency of the element, where  $T_D$  is the period associated to this frequency.

**Table 6.2: Properties of the impulse load and the Eigen frequency of the bracings for the model tested and ANSYS**

Instrumented front bracings	$t_*/T_d$	
Hammer Impulse duration [ms] [s]	0.002	
GWK frequency [Hz]	100	0.2
ANSYS frequency [Hz]	274	0.548



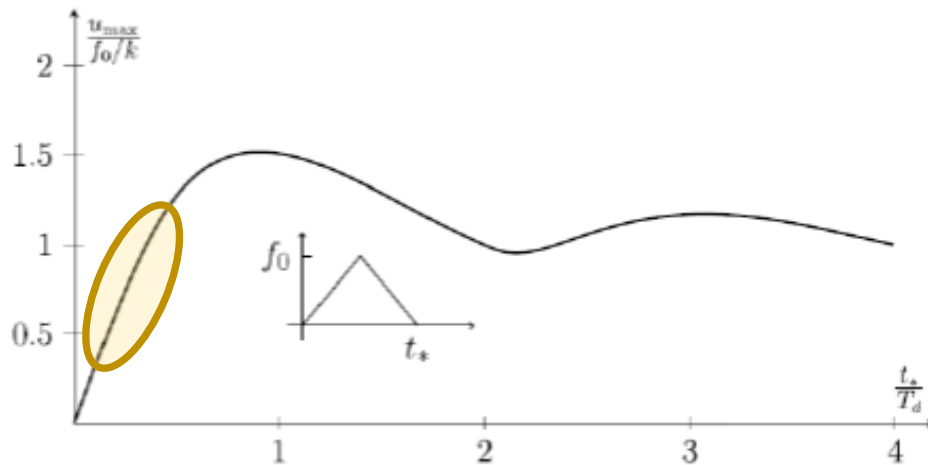


**Figure 6.12: Value of the dynamic response compare to the static for different ratios of impact duration and Eigen frequency of any element. (Naess, 2011).**

The Figures 5.8-5.9 showed that the connection between the bracings and the structure is melded with steel plates and not welded. Another aspect is that the beam has been clamped at where the bracing transducers were installed. Those details have been considered at a certain point throughout the modelling process and the final bracing designed has, as can be seen in Figure 6.13, three different parts.

(A) The middle part of the bracings in between the instrumented parts with an external diameter of 139.7 mm and 5 mm of wall thickness. It is defined in ANSYS as *Structural Steel 2*. (B) The two instrumented parts which have the same geometry as the middle part but with a higher density because of the instrumentation. They are defined in ANSYS as *Bracing\_instrum2*. (C) The junctions between the bracing and the rest of the structure have been independently designed as it has been defined before in the *connection* section.

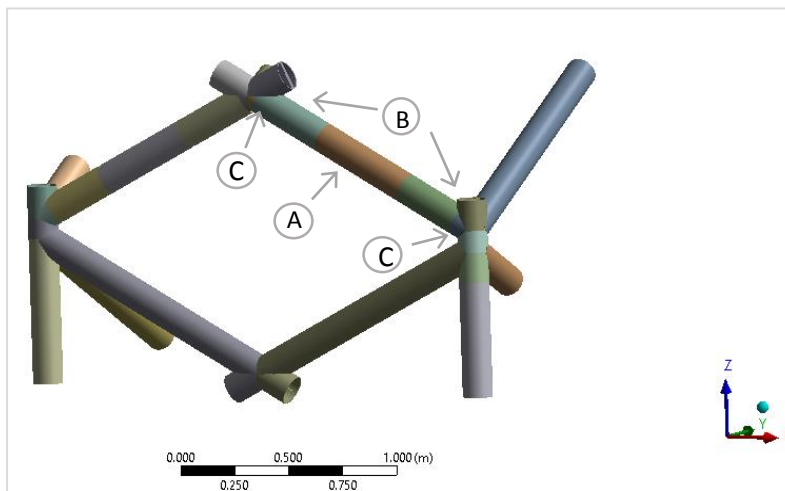


**Figure 6.13: Details of the instrumented bracings designed in ANSYS.**

The Eigen frequency for a beam depends on different parameters such as: supports, mass, length, Inertia and Young Modulus. As the values for the mass, length, density, inertia and Young Modulus are all known, the focus is set on the boundary conditions. Different types of boundary conditions are described in Figure 6.14.

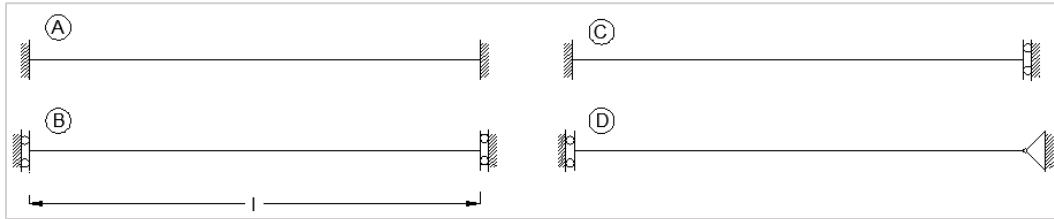


**Figure 6.14: Boundary conditions for a beam.**

Where the Eigen frequency is:

$$W_n = \bar{W}_n \sqrt{\frac{E I}{m l^4}} \quad [rad/s] \quad (31)$$

And  $\bar{W}_n$  depends on the boundary conditions.

For different boundary conditions the frequency of the bracing is going to be calculated as the Young Modulus, inertia, mass and length are well defined. See Table 6.3.

**Table 6.3: Eigen frequency of the front bracings for different boundary conditions**

Case	$W_n$ (n=1)	E [MPa]	I [m <sup>4</sup> ]	M [kg/m]	L [m]	W [rad/s]	f [Hz]
A	22.37	2.10E+11	4.75E-06	26.167	1.2703	2706.57	430.76
B	9.872	2.10E+11	4.75E-06	26.167	1.2703	1194.42	190.10
C	5.593	2.10E+11	4.75E-06	26.167	1.2703	676.70	107.70
D	2.468	2.10E+11	4.75E-06	26.167	1.2703	298.60	47.52

From the previous table and considering the results from the spectrum analysis, it seems that in the experiment in the Large Wave Flume the boundary conditions for the bracings behaved as somewhere in between the cases B and C.

From equation (31) is observed that there are 5 parameters that can be tuned up in order to reduce the Eigen frequency and get smaller peak values as it was seen from Figure 6.12

The Figure 6.12 shows that for these hammer impulse loads the dynamic response of the bracings are in this initial part of the graph. Therefore, a reduction of the bracing frequency would reduce the dynamic response.

Firstly, it was considered to vary the boundary conditions in the ANSYS model. This possibility would imply to introduce at the ends of the bracings springs connections. Then, a

torsional stiffness should be defined and tune up until it behaves as it did in the laboratory. One of the main drawback for this option is the difficulty of dealing with these torsional springs because unfortunately they are in a beta version for Workbench version on ANSYS 14.5. Therefore, the stiffness properties should be coded.

From the other 4 parameters to modify, the Young's Modulus and the density are the ones which are more straightforward to adjust them. Finally, the choice has been to start tuning up the Young's modulus of the material. Once a new Young modulus will be defined and yields a better response, the optimization process for the density will take place.

The Table 6.2 indicates that to get closer to the real frequency oscillation of the bracing the following ratio needs to be reduced:

$$\frac{t_*}{Td} = 0.548 \rightarrow 0.2 \quad (32)$$

That means to reduce nearly 3 times the frequency of the bracings.

$$W_i = 2 \pi 300 = \bar{W}_n \sqrt{\frac{E_i I_i}{m_i l_i^4}} \rightarrow W_f = 2 \pi 100 = \bar{W}_n \sqrt{\frac{E_f I_f}{m_f l_f^4}} \quad (33)$$

$$E_i = 2.1 E11 \text{ MPa}$$

$E_f$ , Young's modulus to be determined

$m_i = m_f$ , Mass of the bracing per unit of length

$I_i = I_f$ , Inertia of the section

$$0.3 \sqrt{E_i} = \sqrt{E_f} \rightarrow E_f = 2.1 E10 \text{ MPa}$$

Defining this new Young's Modulus the results are the following:

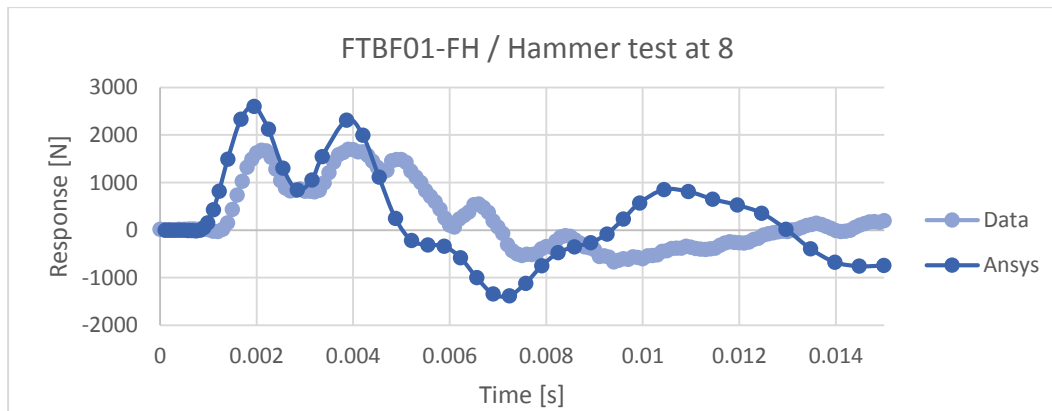


**Figure 6.15: Comparison between the data and ANSYS response at FTBF01-FH from hammer test at 8. Sensitivity analysis I.**

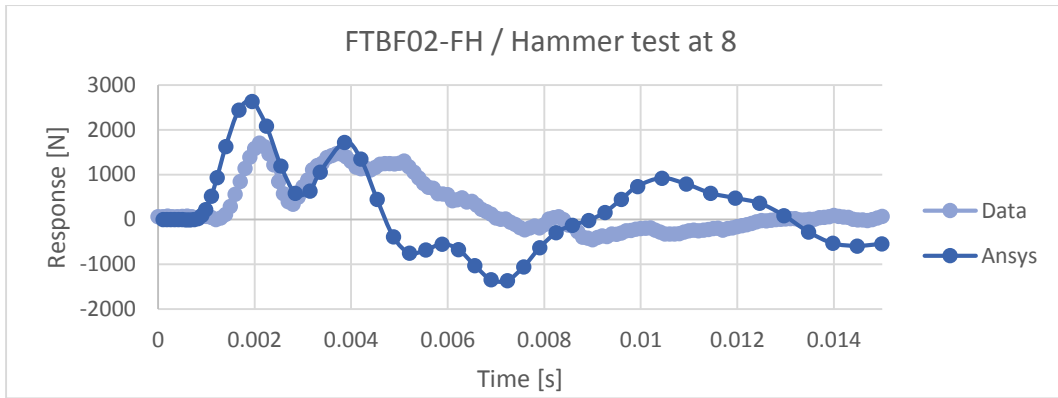


**Figure 6.16:** Comparison between the data and ANSYS response at FTBF02-FH from hammer test at 8. Sensitivity analysis I.

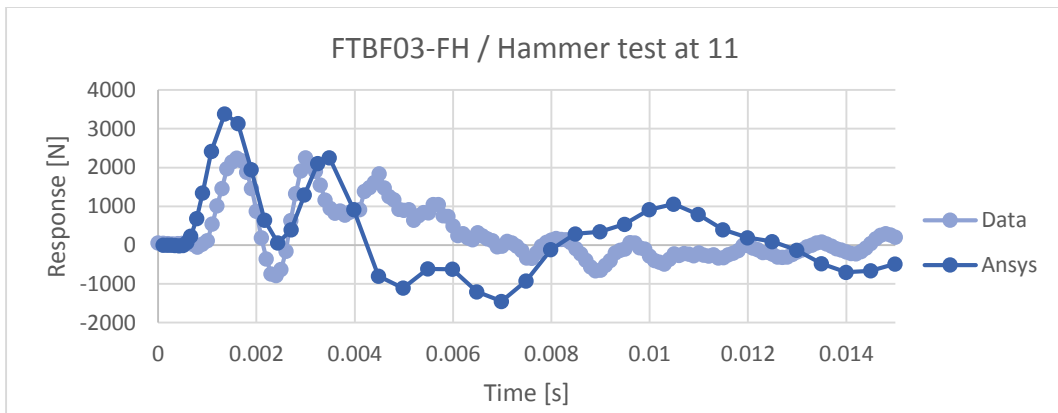


**Figure 6.17:** Comparison between the data and ANSYS response at FTBF03-FH from hammer test at 11. Sensitivity analysis I.

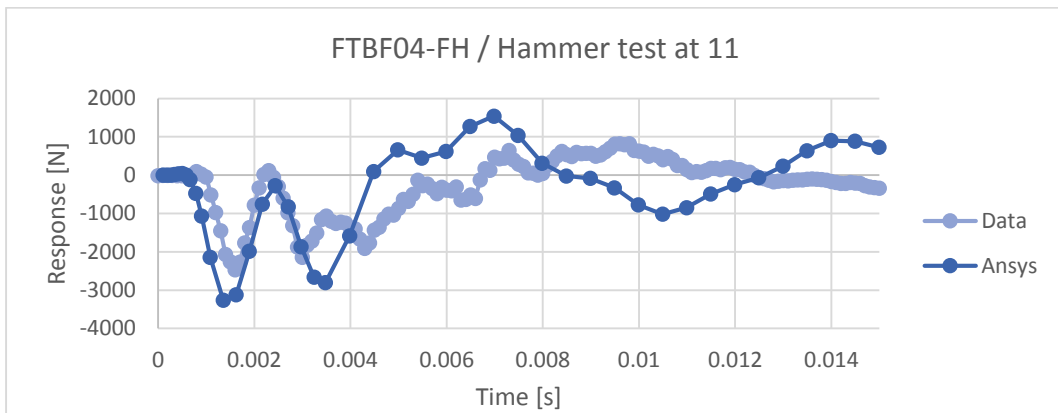


**Figure 6.18:** Comparison between the data and ANSYS response at FTBF04-FH from hammer test at 11. Sensitivity analysis I.

For every test a sensitivity analysis is performed showing a comparison between the first peaks and at what time they have been produced. In that analysis the focus, as it was already mentioned, is centered on the response at the force bracing transducers located in the same bracing as where the hammer test is applied.

A wider study might should consider the necessity of a validation not only for the first milliseconds of the response but a longer time history as well as not only the front instrumented bracings. In this case of study the calibration of the entire response and the side bracings is out of the scope.

**Table 6.4: First sensitivity analysis for the local response on the instrumented bracings.**

Sensitivity Analysis -I-							
Material	Calibrating Parameters						
	$E$ [MPa]	$\rho$ [Kg/m <sup>3</sup> ]					
Bracing_instrum 2	2.10E+10	12700					
Struct. Steel 2	2.10E+10	7850					
		Peak Force-1- [N]	Time -1- [s]	Peak Force-2- [N]	Time -2- [s]	Force deviation, $\overline{Df}$ [%] <sup>12</sup>	Time deviation, $\overline{Dt}$ [%] <sup>13</sup>
Hammer test 8	FTBF01 /L <sup>14</sup>	1682.10	0.0021	1698.90	0.0039		
	FTBF01 /A <sup>15</sup>	2598.80	0.00195	2313.20	0.00386		
	Deviation [%]	54.50	7.14	36.16	1.03	45.33	4.08
	FTBF02 /L	1706.00	0.0021	1469.80	0.0037		
	FTBF02 /A	2630.00	0.00195	1720.00	0.00386		
	Deviation [%]	54.16	7.14	17.02	4.32	35.59	5.73
Hammer test 11	FTBF03 /L	2241.61	0.0016	2248.00	0.003		
	FTBF03 /A	3387.00	0.00136	2254.00	0.00348		
	Deviation [%]	51.10	15	0.27	16	25.68	15.50
	FTBF04 /L	2469.14	0.0016	2146.30	0.003		
	FTBF04 /A	3260.50	0.00136	2801.40	0.00348		
	Deviation [%]	32.05	15	30.52	16	31.29	15.50

$\overline{Df}_f$ [%]	$\overline{Dt}_f$ [%]
34.47	10.20

The first approach for the Young's Modulus seems promising since the peaks are significantly reduced and the time delay among the first peaks is reduced. Even though this is quite good improvement, the average deviation for the peaks is still around 34%.

<sup>12</sup> Force deviation  $\overline{Df}$  refers to the average deviation of the two first peaks: Peak force -1- and Peak force -2-.

<sup>13</sup> Time deviation  $\overline{Dt}$  refers to the average deviation of the time at what the first two peaks are produced

<sup>14</sup> FTBF01 /L refers to the results from the Laboratory in Hannover

<sup>15</sup> FTBF01/A refers to the results from ANSYS.

Another sensitivity analysis is performed with new Young's modulus of  $6.00E+10$  MPa defined for the front bracings.

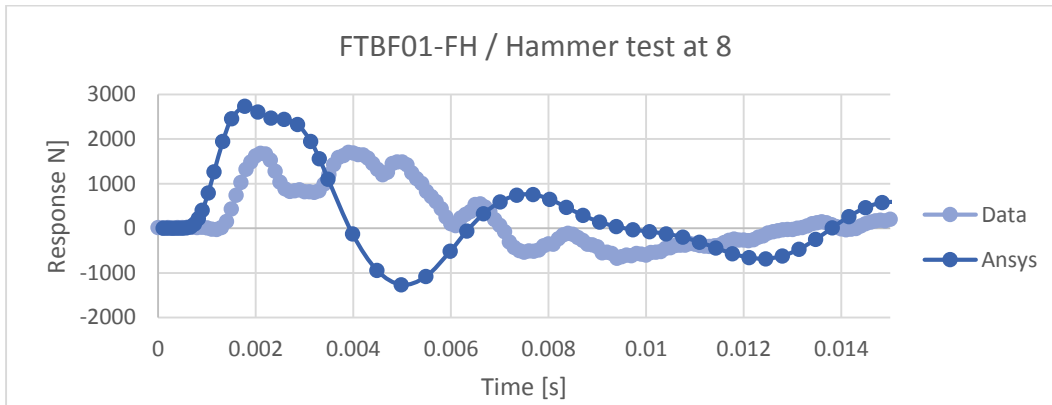


**Figure 6.19:** Comparison between the data and ANSYS response at FTBF01-FH from hammer test at 8. Sensitivity analysis II.

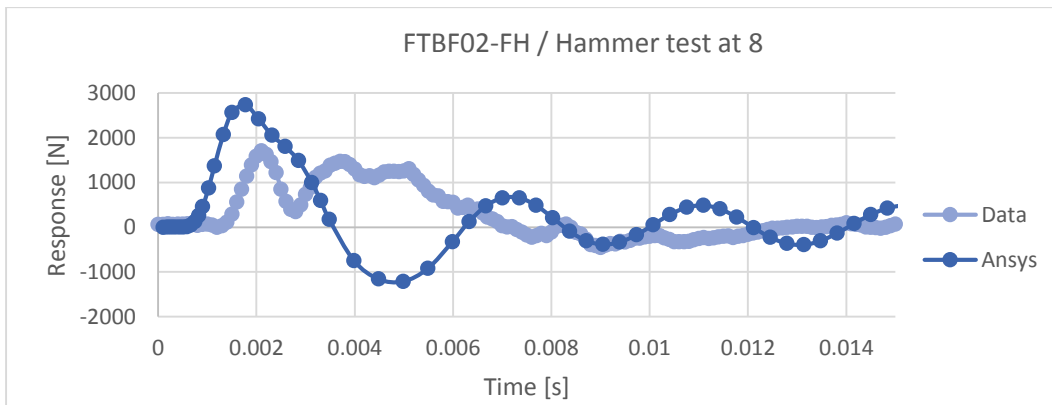


**Figure 6.20:** Comparison between the data and ANSYS response at FTBF02-FH from hammer test at 8. Sensitivity analysis II.

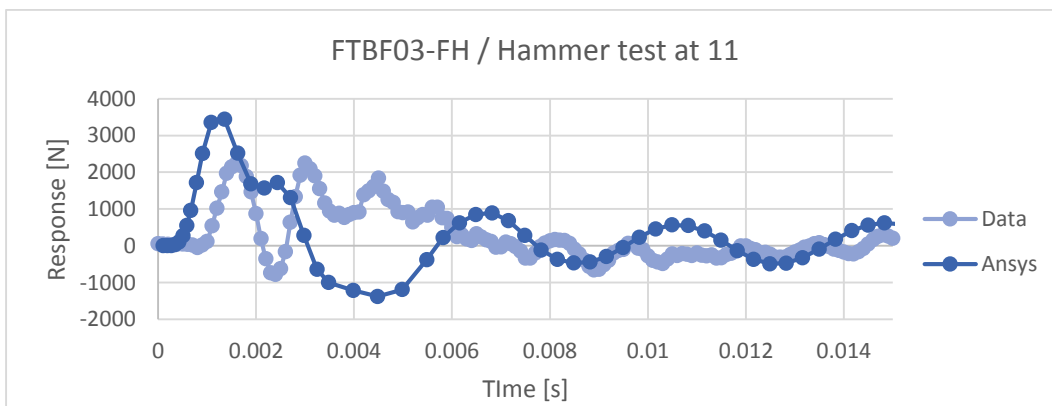


**Figure 6.21:** Comparison between the data and ANSYS response at FTBF03-FH from hammer test at 11. Sensitivity analysis II.

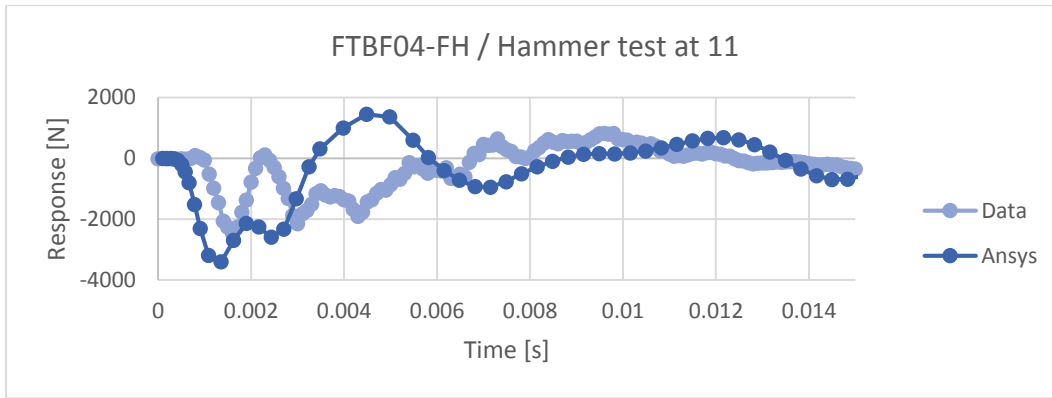


**Figure 6.22: Comparison between the data and ANSYS response at FTBF04-FH from hammer test at 11. Sensitivity analysis II.**

As expected the peak values present slightly higher values than for a Young Modulus,  $E=2.1E10$  MPa. The response presents a higher frequency and in overall the behavior of the model is worse.

**Table 6.5: Second sensitivity analysis for the local response on the instrumented bracings.**

Sensitivity Analysis -II-							
Material	Parameters to tune up						
	E [MPa]	$\rho$ [Kg/m <sup>3</sup> ]					
Bracing_2	6.00E+10	12700					
Struct_2	6.00E+10	7850					
		Peak Force-1- [N]	Time -1- [s]	Peak Force-2- [N]	Time -2- [s]	Force deviation, $\overline{Df_f}$ [%]	Time deviation, $\overline{Dt_f}$ [%]
Hammer test 8	FTBF01 /L	1682.10	0.0021	1698.90	0.0039		
	FTBF01 /A	2732.00	0.00178	756.43	0.00769		
	Deviation [%]	62.42	15.24	55.48	97.18	58.95	56.21
	FTBF02 /L	1706.00	0.0021	1469.80	0.0037		
	FTBF02 /A	2730.00	0.00178	658.00	0.00735		
	Deviation [%]	60.02	15.24	55.23	98.65	57.63	56.94
Hammer test 11	FTBF03 /L	2241.61	0.0016	2248.00	0.003		
	FTBF03 /A	3443.40	0.00136	1716.80	0.00244		
	Deviation [%]	53.61	15.00	23.63	18.67	38.62	16.83
	FTBF04 /L	2469.14	0.0016	2146.30	0.003		
	FTBF04 /A	3400.00	0.00136	2593.40	0.00244		
	Deviation [%]	37.70	15.00	20.83	18.67	29.27	16.83

$\overline{Df_f}$ [%]	$\overline{Dt_f}$ [%]
46.12	36.70



In that case the deviation in the force response has increased 1.33 times the previous one. The deviation in the time response for the peaks is around 3.6 times worse than in the case before with a Young modulus equal to  $2.1E+10$ .

These new results reasserts the first approach. From now on the Young Modulus is going to be slightly reduced from  $2.1E+10$  to  $1.1E+10$  MPa, which should offers better results. In order to keep improving the response the density of the instrumented bracings starts to be tuned up.

Even though all the densities defined until now represent real values, different simplifications were carried out in terms of connections, density uniformly increased along the instrumented bracing and some other uncertainties about how was exactly the instrumented part fixed to the rest of the bracings, etc; which generate the necessity of some changes from the initial defined density of the instrumented bracings in order to get a better fit.

Several sensitivity analysis were carried out varying the density of the front bracings and the closest response to the data is described below .All the other simulations can be found on the Excel spreadsheet “*Ansysis\_analysis\_HammerTest\_8(Final\_v).xlsx*”).

The remaining structure keep the same properties that were defined initially and the last analysis is presented varying the densities of the front bracings. The following figures corresponds to the sensitivity analysis III.

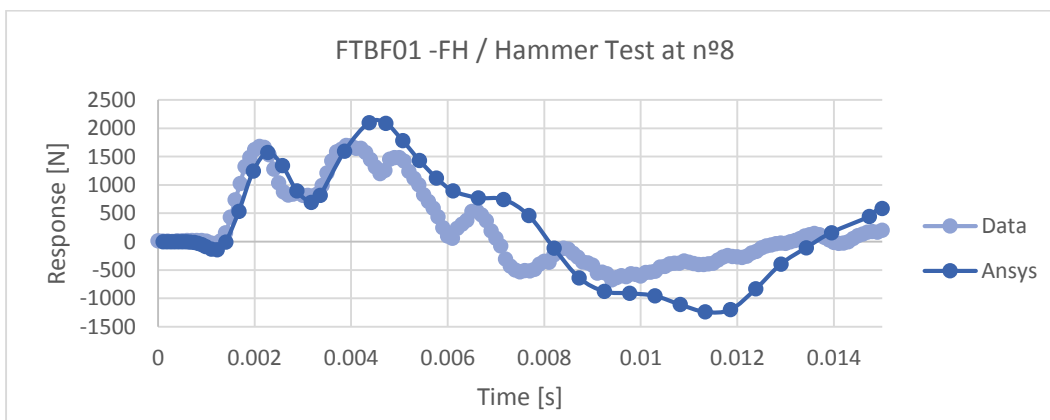


**Figure 6.23: Comparison between the data and ANSYS response at FTBF01-FH from hammer test at 8. Sensitivity analysis III.**

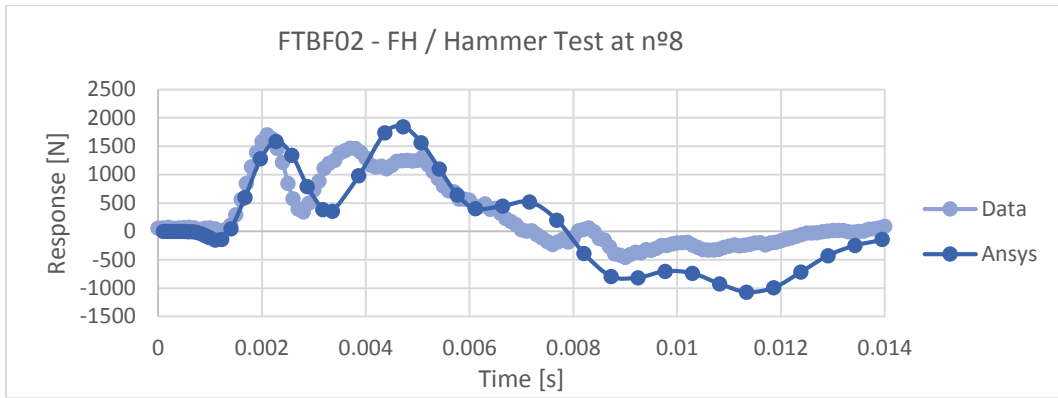


**Figure 6.24: Comparison between the data and ANSYS response at FTBF2-FH from hammer test at 8. Sensitivity analysis III.**

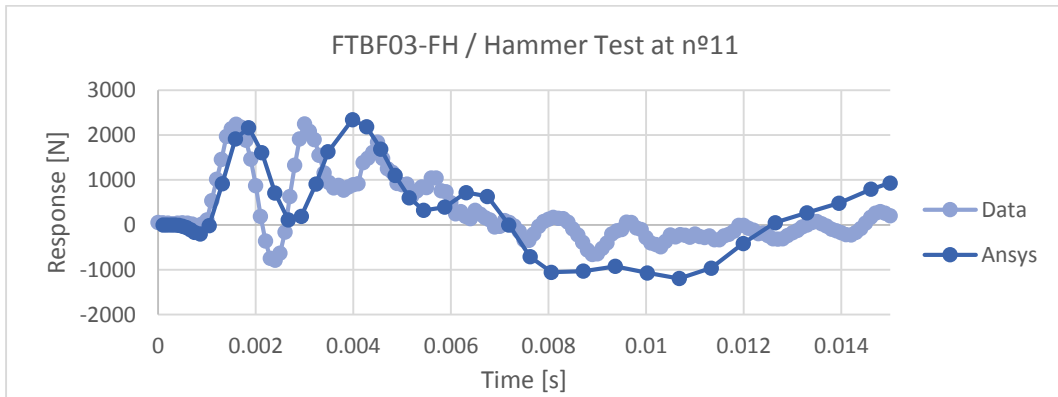


**Figure 6.25: Comparison between the data and ANSYS response at FTBF3-FH from hammer test at 11. Sensitivity analysis III.**

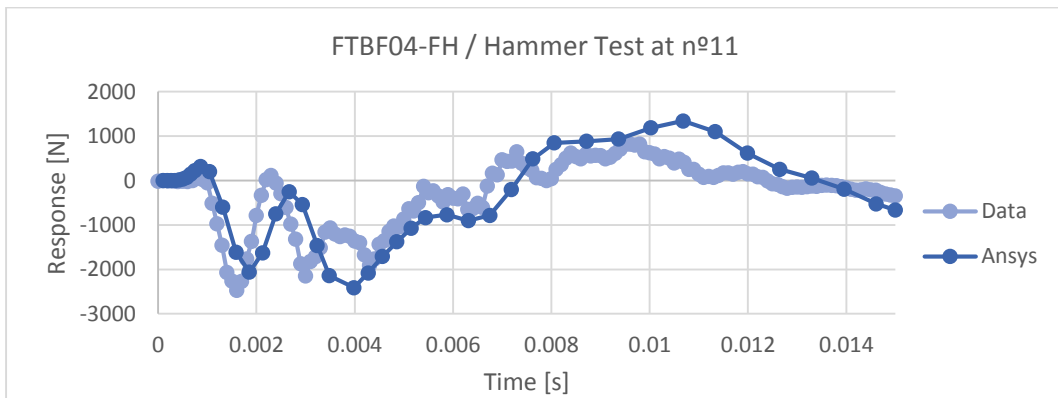


**Figure 6.26: Comparison between the data and ANSYS response at FTBF4-FH from hammer test at 11. Sensitivity analysis III.**

**Table 6.6: Third sensitivity analysis for the local response on the instrumented bracings**

Sensitivity Analysis - III -							
Material	Parameters to tune up						
	E [MPa]	$\rho$ [Kg/m <sup>3</sup> ]					
Bracing_2	1.10E+10	7000					
Struct_2	1.10E+10	16000					
		Peak Force-1- [N]	Time -1- [s]	Peak Force-2- [N]	Time -2- [s]	Force deviation, $\overline{Df}$ [%]	Time deviation, $\overline{Dt}$ [%]
Hammer test 8	FTBF01 /L	1682.10	0.0021	1698.90	0.0039		
	FTBF01 /A	1572.20	0.00228	2098.80	0.0044		
	<i>Deviation [%]</i>	6.53	8.57	23.54	12.05	15.04	10.31
	FTBF02 /L	1706.00	0.0021	1469.80	0.0037		
	FTBF02 /A	1586.00	0.00228	1844.00	0.0047		
	<i>Deviation [%]</i>	7.034	8.571	25.459	27.027	16.25	17.80
Hammer test 11	FTBF03 /L	2241.61	0.0016	2248.00	0.003		
	FTBF03 /A	2165.10	0.00186	2343.30	0.0034		
	<i>Deviation [%]</i>	3.41	16.25	4.24	32.67	3.83	24.46
	FTBF04 /L	2469.14	0.0016	2146.30	0.003		
	FTBF04 /A	2064.10	0.00186	2411.00	0.0034		
	<i>Deviation [%]</i>	16.40	16.25	12.33	32.67	14.37	24.46

$\overline{Df}_f$ [%]	$\overline{Dt}_f$ [%]
12.37	19.26

The results for this last set-up represents a quite improvement and a good approach with an average deviation for the two initial peak force of around 12%. The response with respect to time is slightly lower than 20 % of deviation.

As it is shown in Figure 6.27, after applying all the changes in the properties of the bracings such as Young Modulus and density, the new Eigen frequency from modal analysis in ANSYS is around 80 Hz. That is nearly equal to the frequency of the peak value in the spectrum analysis done for the front bracings, see Figure 6.9.

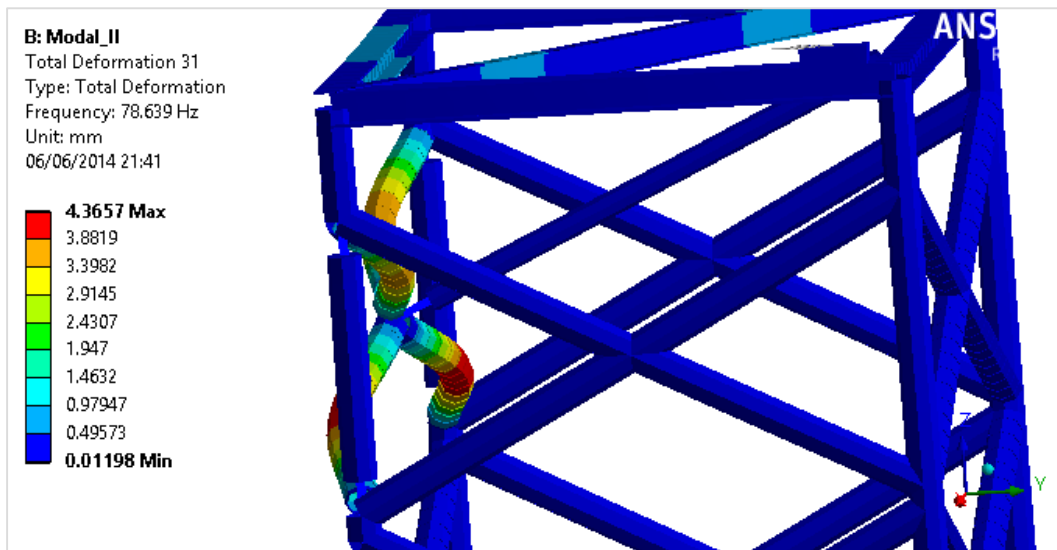


Figure 6.27: Eigen frequency of the front bracings after validation of the local response.

#### 6.4 Global response of the structure

Not only the local response of the bracings needs to be validated but also the global response is an important requirement for the robustness of the model.

The changes applied to the instrumented bracings regarding the Young Modulus and the density might either have a large influence or not in the global response.

When the validation of a structure takes place is quite common to perform first the global analysis and later a local evaluation. As you may notice here the process is just the opposite. The main reason for that is to not present the results twice, because it has been observed that local changes did in the bracings have a much larger effect on the global response than the other way around.

For the present global validation the response at the four total force transducers: FTTF01, FTTF02, FTTF03 and FTTF04 is going to be discussed. These transducers measure the force in the wave direction (Y direction).

A complete analysis of the global structure is given by the analysis of the response to six hammer tests. Those six hammer points include two hammer tests in the left column: n° 02 and n° 03, two at the same height but in the right column: n° 05 and n° 06; and the last two are applied in the middle of the front instrumented bracings: n° 08 and n° 11.

### 6.4.1 Definition of Hammer test studied

The hammer test studied at position n° 2, on the left leg corresponds to: *Large-hammer-test 2013\_06\_24\_18\_42\_58* in the MGC file.

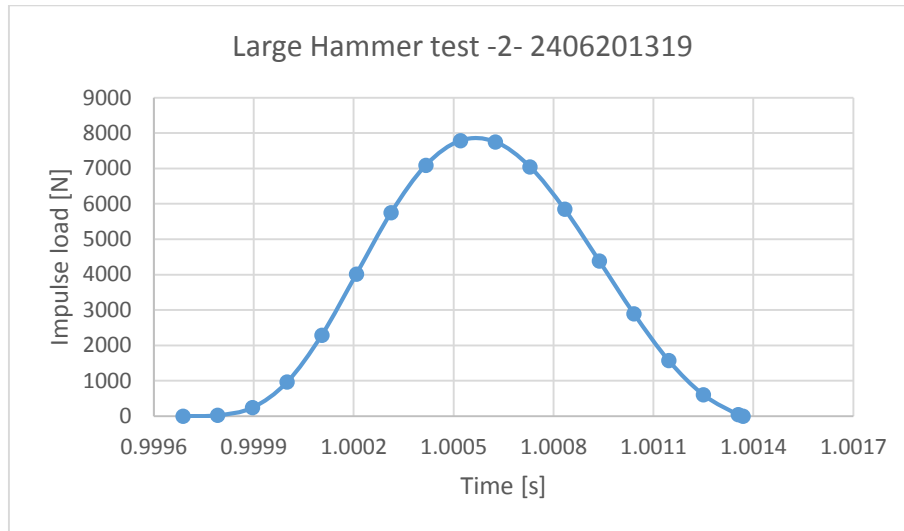


**Figure 6.28: Hammer test at position number 2**

The other hammer test located at the same height in the right leg, n°5 is named as: *Large-hammer-test 2013\_06\_24\_19\_10\_53* in the MGC file.

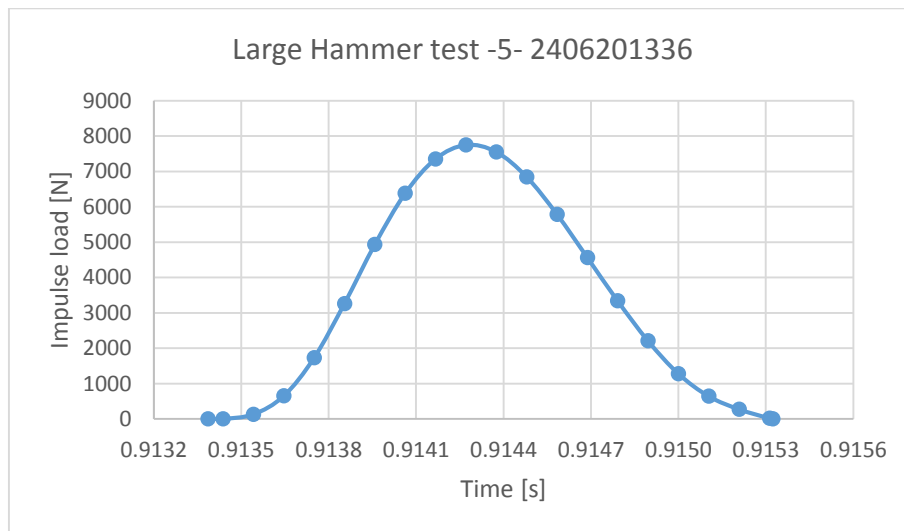


**Figure 6.29: Hammer test at position number 5**

The impulse load corresponding to Large Hammer test n°3: *2013\_06\_24\_18\_47\_29*, and n°6: *2013\_06\_24\_19\_14\_34* can be found in the Excel sheet:

“*Ansys\_analysis\_set\_up\_transient\_analysis.xlsx*”.

The other two hammer test applied on the bracings are the same than the ones used for the analysis of the local response on the front bracings. They have been defined in Figures. 6.1-6.2.

#### 6.4.2 Analysis of the global response

The total duration of the response until damps completely out is around 0.6-0.7 s. The main interest is far from get a perfect fit for the entire response but to focus on acquiring a good approach for the first two peaks. That turns into 0.02 s the time frame of study for all the responses.

An initial study on the responses from hammer test n°2 and n°5 is going to be presented. Those hitting positions are placed at 1.260 m above the SWL, both at the same height in the right and left front columns, respectively.

Then, the initial global response is going to be checked for hammer positions n°8 and n°11 corresponding to the middle point of the front instrumented bracings.

The response for the other two hammer tests, n°3 and n°6 which are located in the left and right column slightly below from n°2 and n°5 are not going to be discussed in this report but they can be found in the Excel spreadsheet: “*Ansys\_analysis\_HammerTest\_02-3(III).xlsx*” The main reason for not appearing in this final report is because they do not offer any new relevant information that what it has already seen on hammer test n°2 and n°5.

After all the changes analyzed and discussed regarding to the material properties for the instrumented bracings the new setup is defined:

**Table 6.7: Material properties set-up after local validation on the instrumented bracings.**

Material		
	Density [Kg/m <sup>3</sup> ]	Young's Modulus [MPa]
<i>Aluminum [Pole1 &amp; 2]</i>	3380	7.00E+10
<i>Aluminum_2 [Pole 3]</i>	3280	7.00E+10
<i>Aluminum_3 [Pole 3 below SWL]</i>	3000	7.00E+10
<i>Bracing_instrum [Side Bracings]</i>	12700	2.10E+11
<i>Bracing_instrum_2 [Front Bracings]</i>	7000	1.1E+10
<i>St-37 [General Structure]</i>	7850	2.10E+11
<i>St-37_BSWL [General Structure below SWL]</i>	23827	2.10E+11
<i>Structural_Steel [Material in between instrumented side bracings]</i>	7850	2.10E+11
<i>Structural_Steel_2 [Material in between the instrumented front bracings]</i>	16000	1.1E+10
<i>Upper_Beam_Connexion [Tube connection]</i>	7850	2.10E+11

*Hammer test n°2 and n°5*

Considering the material properties defined above, the following global response is obtained from hammer test n°5 and n°2.

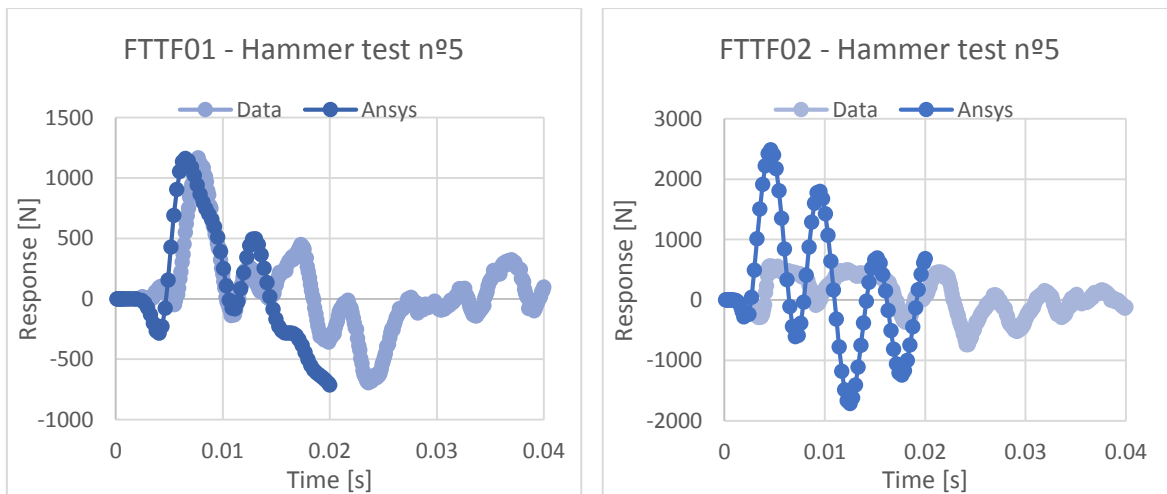


**Figure 6.30: Comparison between data and ANSYS global response at FTTF01-02 from hammer test n°5. Initial set-up.**

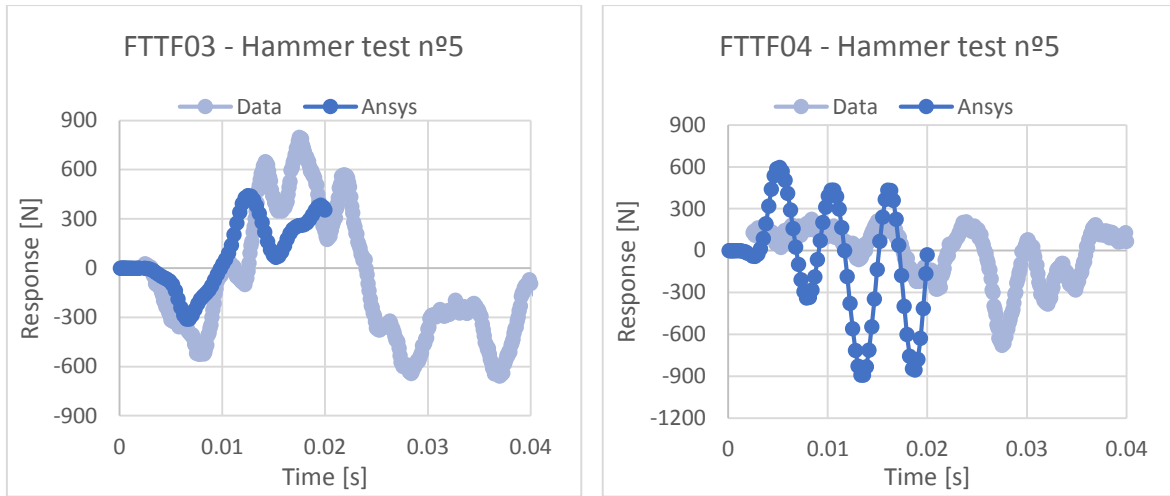


**Figure 6.31: Comparison between data and ANSYS global response at FTTF03-04 from hammer test n°5. Sensitivity analysis I.**

Total force transducer 01 and 03 corresponds to the transducers located at the bottom, whereas total force transducer 02 and 04 are located at the top of the structure. Details can be seen in Figures 5.15- 5.17

For the two at the bottom the initial response from ANSYS roughly follows the Data from the experiments. Otherwise, the response from the transducers at the top exhibits a weird behavior.

The response on the data seems limited around 500 N for FTTF02 and 300 N for FTTF04, for a maximum impulse load 7.7 kN. The response from ANSYS clearly follows the same initial path but is not restricted at any point and reaches peak values around 2500 N and 600 N respectively.

It is quite surprising that even though the Large Hammer test n°5 is located at around 1.10 m from the top of the structure and 3.26 m from the lowest part of the structure; the response achieved in FTTF01 that corresponds to the bottom right column has a response of 2 times the maximum positive response in FTTF02.

This strange limitation in the response is also seen for other different hammer test locations.

Such limitations in the top total transducers response are not presented during the large loads when waves are breaking on the structure. This is the reason why it is believed that during the experiments there were some restraints that produced this limited response if the impulse load is low as it is from the hammer tests.

Moreover, although the hammer test studied and described here were carried out the 24<sup>th</sup> of June, 2013; other hammer tests were performed on the 11<sup>th</sup> of June. The difference between these two tests it that on the 11<sup>th</sup> the channel was empty of water. These tests were also



studied and it is found a restriction now at around 700 N and 800 N for FTTF02 and FTTF04 respectively, for a maximum impulse load of 3.0 kN. On the 11<sup>th</sup> such limits are observed in the opposite direction of the hitting direction.

All these issues were notified to the people in charge of the WaveSlam experiments and they found some inconsistencies on that and this was fixed. The result from this is that the sign of the force for hammer test carried on the 11<sup>th</sup> was reversed.

So far, no reason has been found for such limitations at the upper part of the structure. If this was the real response from the structure it could have been modelled in ANSYS as longitudinal springs with non-uniform stiffness. Having a linear behavior at the beginning and then an infinite stiffness should be define. This situation will introduce nonlinearities in the response.

Other previous researches done by Aashamar, M. (2012) does show a larger response at the top of the structure compared with the bottom, when an impulse load is applied at around this position. Moreover, as said before there is no such limitation when larger loads hits the structure as wave loads does.

Because all of this it is considered that all the global responses at FTTF02-04 are not reliable and they are rejected for the global validation.

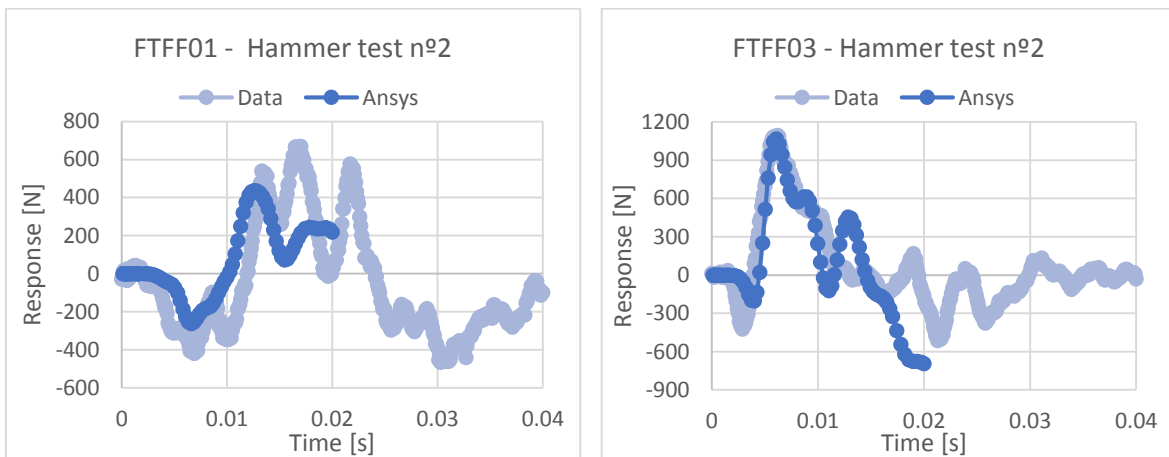


**Figure 6.32: Comparison between data and ANSYS global response at FTTF01-02 from hammer test n°2. Sensitivity analysis I**

**Table 6.8: First sensitivity analysis for the global response on the structure**

Sensitivity Analysis - I -							
Material	Parameters to tune up						
	E [MPa]	$\rho$ [Kg/m <sup>3</sup> ]					
Alum <sup>16</sup> 1	7.00E+10	3380					
Alum 2	7.00E+10	3280					
Alum 3	7.00E+10	3528					
		Peak Force-1- [N]	Time-1- [s]	Peak Force-2- [N]	Time-2- [s]	Force Deviation, $\overline{Df_f}$ [%]	Time Deviation, $\overline{Dt_f}$ [%]
Hammer test 5	FTTF01 /L	-49.49	0.0055	1167.37	0.0077		
	FTTF01 /A	-285.00	0.0041	1160.00	0.0065		
	<i>Deviation [%]</i>	475.87	26.00	0.63	15.58	238.25	20.79
	FTTF03 /L	-522.48	0.0077	648.74	0.0142		
	FTTF03 /A	-310.00	0.0065	443.00	0.0125		
	<i>Deviation [%]</i>	40.67	15.32	31.71	11.97	36.19	13.65
Hammer test 2	FTTF01 /L	-418.62	0.0069	539.48	0.0133		
	FTTF01 /A	-263.00	0.0061	437.00	0.0126		
	<i>Deviation [%]</i>	37.17	11.59	19.00	5.26	28.09	8.43
	FTTF03 /L	-422.87	0.0029	1095.45	0.0062		
	FTTF03 /A	-202.00	0.004	1070.00	0.0061		
	<i>Deviation [%]</i>	52.23	37.93	2.32	1.77	27.28	19.85

$\overline{Df_f}$ [%]	$\overline{Dt_f}$ [%]
82.45	15.68

This initial approach with the materials previously defined raises an average deviation in the first two peak force values of around 82%. The error corresponding to at what time these peaks are produced is much less, about 11%.

In order to improve these values some modifications are introduced. Local changes in the Young Modulus of the instrumented legs might be a good approach as it has already seen for the instrumented bracings.

In this second trial the Young Modulus is reduced for the three instrumented parts of the columns from 7E+10 MPa until 1E+10 MPa.

<sup>16</sup> Alum refers to Aluminium

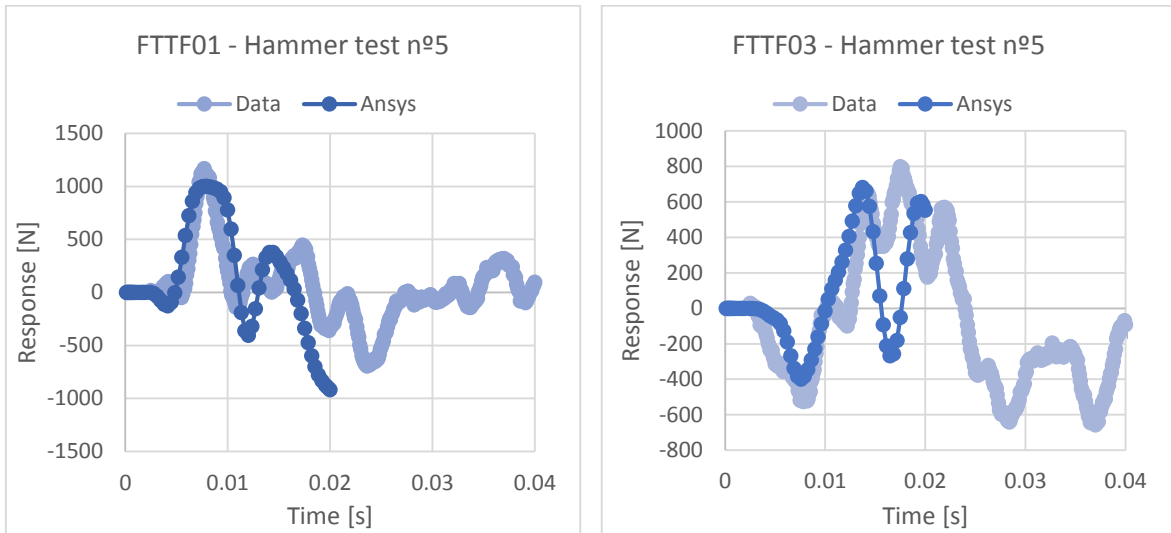


**Figure 6.33: Comparison between data and ANSYS global response at FTTF01-03 from hammer test n°5. Sensitivity analysis II.**

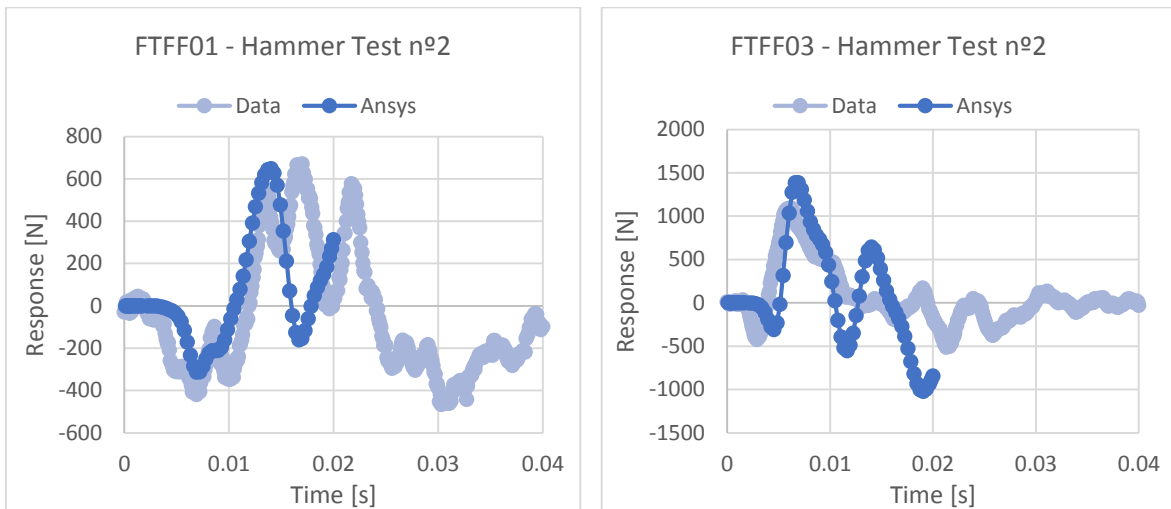


**Figure 6.34: Comparison between data and ANSYS global response at FTTF01-03 from hammer test n°2. Sensitivity analysis II.**

**Table 6.9: Second sensitivity analysis for the global response on the structure**

Sensitivity Analysis - II -							
Material	Parameters to tune up						
	E [MPa]	$\rho$ [Kg/m <sup>3</sup> ]					
Alum 1	1.00E+10	3380					
Alum 2	1.00E+10	3280					
Alum 3	1.00E+10	3528					
		Peak Force-1- [N]	Time-1- [s]	Peak Force-2- [N]	Time-2- [s]	Force Deviation, $\overline{Df}$ [%]	Time Deviation, $\overline{Dt}$ [%]
Hammer test 5	FTTF01 /L	-49.49	0.0055	1167.37	0.0077		
	FTTF01 /A	-126.00	0.0041	1000.00	0.0079		
	Deviation [%]	154.60	24.55	14.34	2.86	84.47	13.70
	FTTF03 /L	-522.48	0.0077	648.74	0.014		
	FTTF03 /A	-398.00	0.0076	682.00	0.014		
	Deviation [%]	23.82	1.56	5.13	3.52	14.48	2.54
Hammer test 2	FTTF01 /L	-418.62	0.0069	539.48	0.013		
	FTTF01 /A	-313.00	0.0062	648.00	0.014		
	Deviation [%]	25.23	10.29	20.12	5.26	22.67	7.78
	FTTF03 /L	-422.87	0.0029	1095.45	0.0062		
	FTTF03 /A	-308.00	0.0045	1390.00	0.0069		
	Deviation [%]	27.16	56.55	26.89	11.45	27.03	34.00

$\overline{Df}_f$ [%]	$\overline{Dt}_f$ [%]
37.16	14.50

The results are far improved from the previous test. The errors in the peak forces are now around 37% and the deviation in the timing is around 14%.

A last set-up is presented with a Young Modulus for the instrumented legs of 3E+10 MPa.

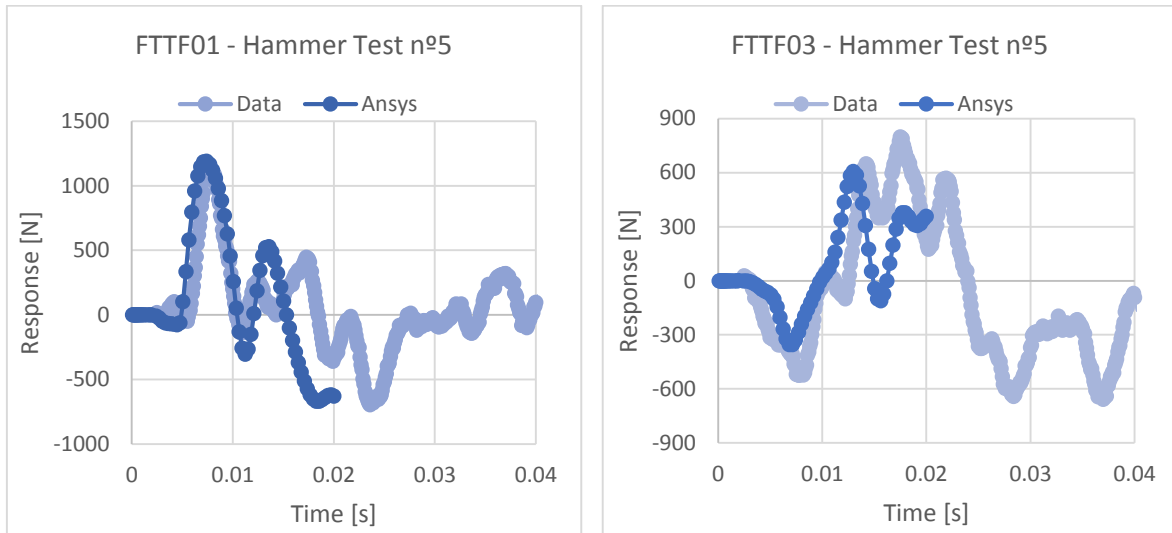


**Figure 6.35: Comparison between data and ANSYS global response at FTF01-03 from hammer test n°5. Sensitivity analysis III.**

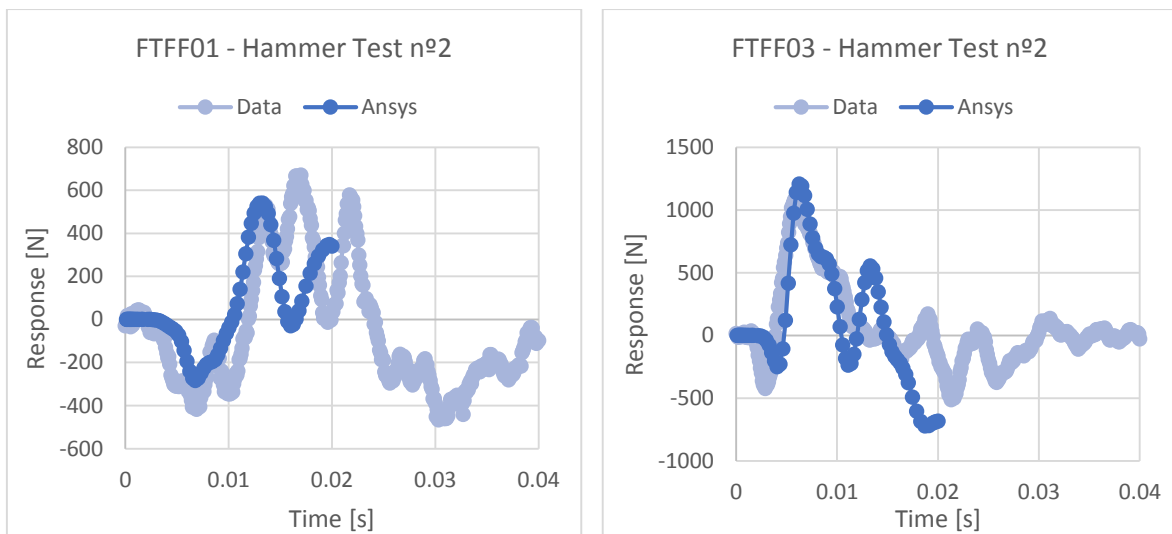


**Figure 6.36: Comparison between data and ANSYS global response at FTF01-03 from hammer test n°2. Sensitivity analysis III.**

**Table 6.10: Third sensitivity analysis for the global response on the structure**

Sensitivity Analysis -III-							
Material	Parameters to tune up						
	E [MPa]	$\rho$ [Kg/m <sup>3</sup> ]					
Alum 1	3.00E+10	3380					
Alum 2	3.00E+10	3280					
Alum 3	3.00E+10	3528					
		Peak Force-1- [N]	Time-1- [s]	Peak Force-2- [N]	Time-2- [s]	Force Deviation, $\overline{Df}$ [%]	Time Deviation, $\overline{Dt}$ [%]
Hammer test 5	FTTF01 /L	-49.49	0.0055	1167.37	0.0077		
	FTTF01 /A	-75.33	0.0045	1190.00	0.0074		
	<i>Deviation [%]</i>	52.20	18.36	1.94	3.64	27.07	11.00
	FTTF03 /L	-522.48	0.0077	648.74	0.014		
	FTTF03 /A	-355.00	0.0071	607.00	0.013		
	<i>Deviation [%]</i>	32.05	7.40	6.43	8.45	19.24	7.93
Hammer test 2	FTTF01 /L	-418.62	0.0069	539.48	0.013		
	FTTF01 /A	-264.50	0.0061	425.14	0.0129		
	<i>Deviation [%]</i>	36.82	11.59	21.19	3.01	29.01	7.30
	FTTF03 /L	-422.87	0.0029	1095.45	0.0062		
	FTTF03 /A	-289.12	0.004	1067.20	0.0061		
	<i>Deviation [%]</i>	31.63	37.93	2.58	1.77	17.10	19.85

$\overline{Df}_f$ [%]	$\overline{Dt}_f$ [%]
23.11	11.52

So, after carrying different analysis this new set-up for the instrumented legs offers far better results for the initial response than using the initial values.

The choice for instrumented legs as being the elements tuned up is basically defined by two factors.

Firstly, the initial response does not show a very different behavior from the Data results. It is only the first peak of the response at FTTF01 which has a large deviation. Considering only the second peak the deviation in the force results are around 8%. So, the overall response is quite good for the set-up previously defined and only small modifications need to be done.

Secondly, accomplishing modifications for other parts of the structure as it could be the properties for the material above SWL composed by St-37 or the properties for the

submerged structure will induce larger changes in the global response that is likely to worsen the results.

There is still one element which has a relevant importance in both global and local response. This element is the beam which connects the upper instrumented front bracings with the back top side of the structure.

It has been previously defined as *Upper\_beam\_connection* in the chapter relevant to material properties and was initially tuned up when the local validation of the bracings was done. In a bid to avoid confusion to the reader and make the validation process as much comprehensible as possible it was not originally mentioned there. Another reason why this decision has been omitted in the bracing analysis is that the material properties of this beam does not have a direct influence on the first response peaks analyzed.

Otherwise, when the Large Hammer Test is applied at position n°8 and n°11 (at the middle of the bracings), the global response is clearly affected by this connecting beam.

The following figures are obtained from the final set-up but now considering the *Up\_beam\_connection* as how it was initially defined. Table 6.11 contains an overview of the final set-up.

**Table 6.11: Material properties of the Final set-up**

Final_Set-up / Material		
	$\rho$ [Kg/m <sup>3</sup> ]	E [MPa]
<i>Aluminum [Pole 1 &amp; 2]</i>	3380	3.00E+10
<i>Aluminum_2 [Pole 3]</i>	3280	3.00E+10
<i>Aluminum_3 [Pole 3 below SWL]</i>	3528	3.00E+10
<i>Bracing_instrum [Side Bracings]</i>	12700	2.10E+11
<i>Bracing_instrum_2 [Front Bracings]</i>	7000	1.10E+10
<i>St-37 [General Structure]</i>	7850	2.10E+11
<i>St-37_BSWL [General Structure below SWL]</i>	23827	2.10E+11
<i>Structural_Steel [Material in between instrumented side bracings]</i>	7850	2.10E+11
<i>Structural_Steel_2 [Material in between the instrumented front bracings]</i>	16000	1.10E+10
<i>Upper_Beam_Connexion [Tube connection]</i>	7850	2.10E+11

A brief analysis is going to be detailed in the next figures:

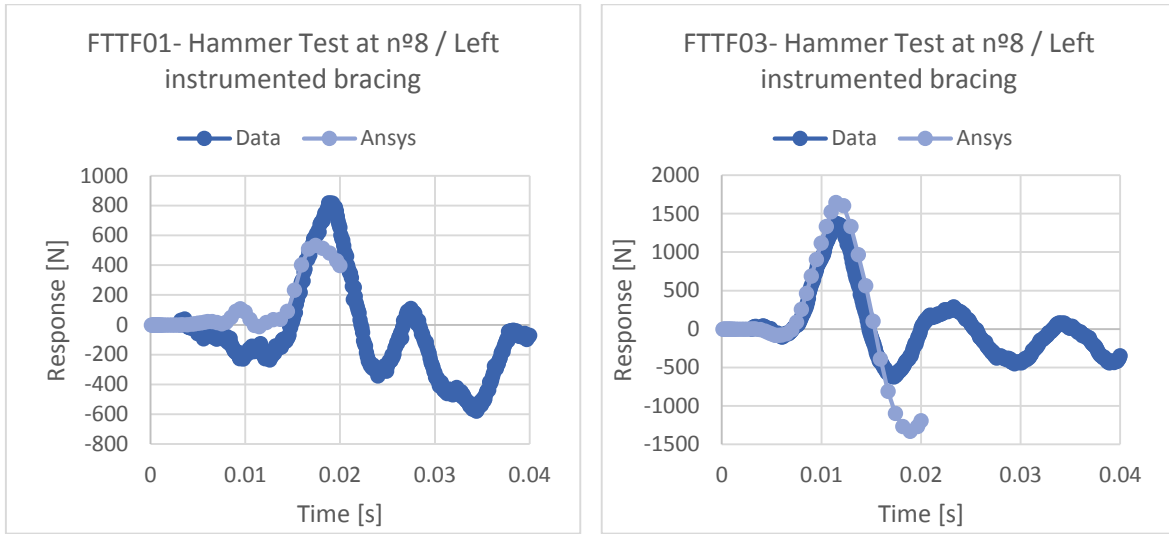


**Figure 6.37: Comparison between data and ANSYS global response at FTTF01-03 from hammer test n°8. Final set-up.**

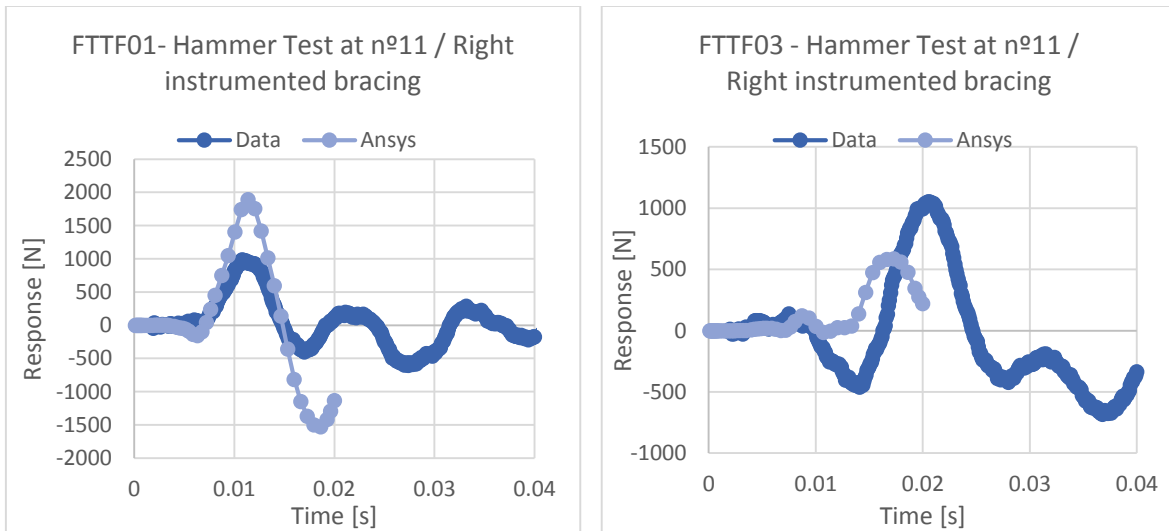


**Figure 6.38: Comparison between data and ANSYS global response at FTTF01-03 from hammer test n°11. Final set up.**

The above figures show that the higher peak values from ANSYS are far from the Data especially in the instrumented right bracing and not giving good enough response for left bracing.

The global response when hitting at the bracings is mostly governed by the beam that connect them to the back to side of the structure. This beam was designed in order to provide higher stiffness to the upper bracings.



The analysis shows an average deviation of the peak force values around 85% and the time deviation is around 13.6 %.

So, some analysis were carried out varying the properties of this specific beam to see how the global response is modified and a brief summary showing the results is described below. This brief overview tries to reflex the final result and other different combinations can be found in the Excel documents attached to this report.

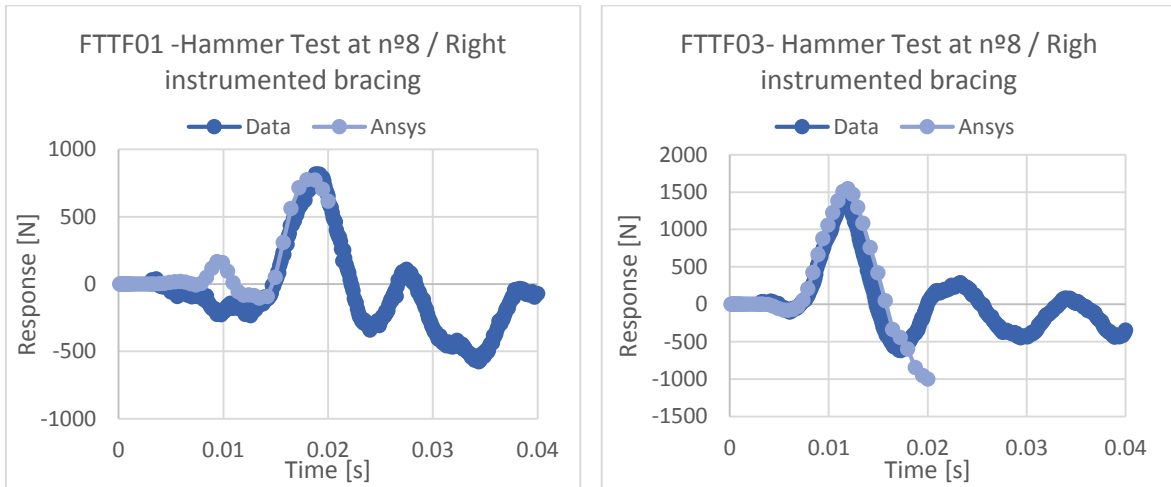


**Figure 6.39: Comparison between data and ANSYS global response at FTTF01-03 from hammer test n°8. Modifications at the upper beam.**

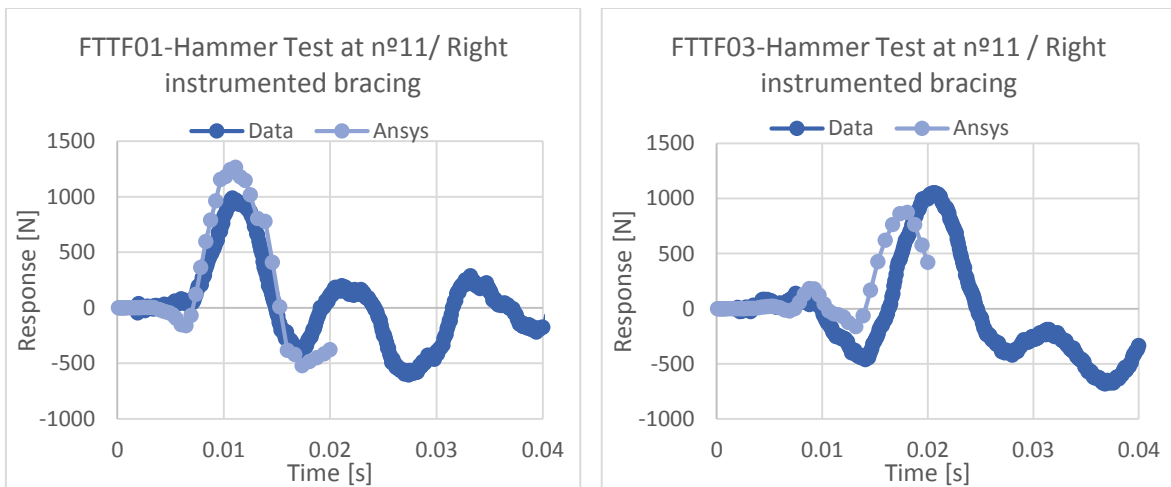


**Figure 6.40: Comparison between data and ANSYS global response at FTTF01-03 from hammer test n°8. Modifications at the upper beam.**

Modifications in the Young Modulus of the Upper\_beam\_connexion lead results with a deviation of around 29% on the peaks force, which is a drastic reduction from the initial 85 %, and regarding the fit for the timing, it is reduced as well and gives an average deviation value of 8.55 %. The results are shown in Table 6.12.

**Table 6.12: Sensitivity analysis for the global response on the structure for hammer test 8 and 11**

Sensitivity Analysis							
Material	Parameters to tune up						
	E [MPa]	$\rho$ [Kg/m3]					
Alum 1	3.00E+10	3380					
Alum 2	3.00E+10	3280					
Alum 3	3.00E+10	3528					
Upper-beam_connex	8.00E+10	7850					
		Peak Force-1- [N]	Time-1- [s]	Peak Force-2- [N]	Time-2- [s]	Force Deviation, $\overline{Df_f}$ [%]	Time Deviation, $\overline{Dt_f}$ [%]
Hammer test 8	FTTF01 /L	-228.29	0.0098	818.91	0.0188		
	FTTF01 /A	-104.42	0.0134	775.76	0.018		
	<i>Deviation [%]</i>	54.26	36.73	5.27	4.26	29.76	20.50
	FTTF03 /L	-100.92	0.0061	1365.54	0.0114		
	FTTF03 /A	-80.97	0.0058	1541.60	0.0119		
	<i>Deviation [%]</i>	19.77	4.92	12.89	4.39	16.33	4.65
Hammer test 11	FTTF01 /L	972.04	0.011	-399.83	0.017		
	FTTF01 /A	1265.36	0.011	-521.36	0.017		
	<i>Deviation [%]</i>	30.18	0.00	30.39	0.00	30.29	0.00
	FTTF03 /L	-461.76	0.0141	1050.51	0.0205		
	FTTF03 /A	-164.76	0.0132	871.73	0.0181		
	<i>Deviation [%]</i>	64.32	6.38	17.02	11.71	40.67	9.05

$\overline{Df_f}$ [%]	$\overline{Dt_f}$ [%]
29.26	8.55

As it is said, this reduction on the Young Modulus is the result of an iterative process where not only the Young Modulus but the density of the material has been modified in order to appreciate and observe how the global response is affected by those changes.

Even this deviation on the peak force is still not too low, it has been considered valid and no further analysis is going to be done, since is not going to be a key aspect in the characterization of the wave slamming forces in the bracings. The reason for that is that to characterize the wave loads the focus of the analysis is going to be defined for the initial response of the bracing.

## 7. CHARACTERIZATION OF THE DYNAMIC WAVE FORCES ACTING ON THE BRACINGS

### 7.1 Introduction

For offshore structures, the most adverse load at which they are exposed is the horizontal force given when the wave breaks in front of the structure. This situation leads to a really high and rapid force acting along the different elements where the impact is produced.

As it was described at the beginning of the report in the *Literature review part*, the slamming force  $F_S$  on a cylindrical member due to effect of breaking wave is:

$$F_S(t) = \lambda \eta_b \rho_w C_s R C_b^2 \quad (34)$$

The characterization of the wave loads on the bracings has as ultimate goal to find the slamming factor  $C_s$  occurring at the beginning of the impact  $t = 0$  on the bracings.

Once determined the slamming force, the slamming coefficient can be obtained directly as:

$$C_s = \frac{F_S}{\rho_w R C_b^2 \lambda \eta_b} \quad (35)$$

### 7.2 Case of study: Wave test 2013061414

The wave test selected for the analysis is the test run n°14 performed the 14<sup>th</sup> of June. In this test as in all the others a total number of 20 waves were generated. The main properties of this wave test are defined in Table 7.1 and Figure 7.1.

**Table 7.1: Wave parameters corresponding to 2013061414 run test**

Wave test 2013061414							
Test Run	Nº of waves	Wave height [m]	H. at structure [m]	T [s]	Depth [m]	Run type	Breaking
14	20	1.7	1.972	4.9	4.3	Regular	Yes

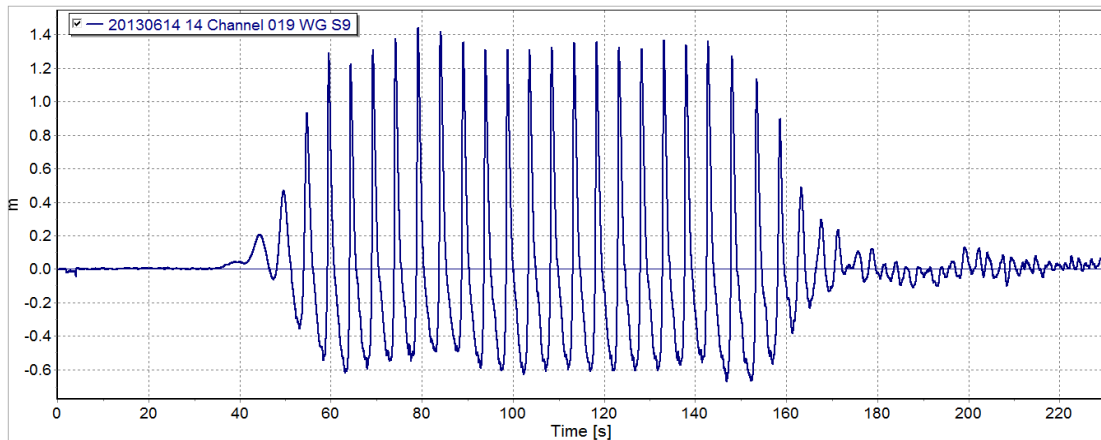


**Figure 7.1: Representation of the wave height at water gauge WG S9 located at the front of the structure.**

The dynamic forces generated by the wave at time 132-135 s are going to be analyzed. The main reason for selecting this specific wave among all the others is because the hitting time for the lowest part and the upper part of the front bracing is enough spaced in time that allows a better analysis as it will be shown in Figure 7.4.

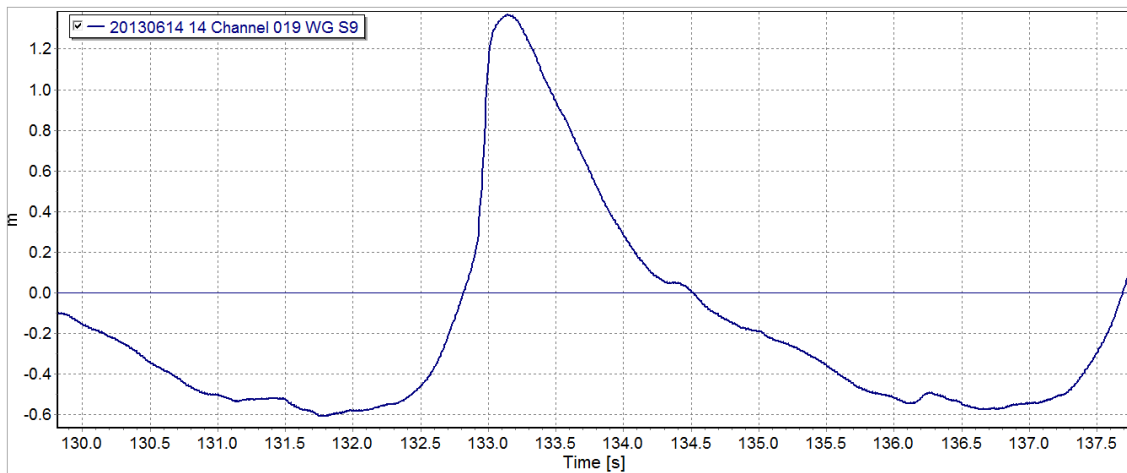


**Figure 7.2: Wave at the structure of Wave Test: 20130614-14 [132-135s]**

The corresponding wave height is:

$$H_{at\ structure} = A_c + A_t = 1.371 + 0.601 = 1.972\ m \quad (36)$$

Taking into account that the water depth at this point  $d$  is 2.0 m and the front of the structure is held 4 cm above the ground, the final height taking as reference level  $z = 0$  as the ground of the channel is given in equation (37). The impact area of this specific wave is represented in Figure 7.3.

$$z = 1.371 + 2.0 = 3.71 \text{ m} \quad (37)$$

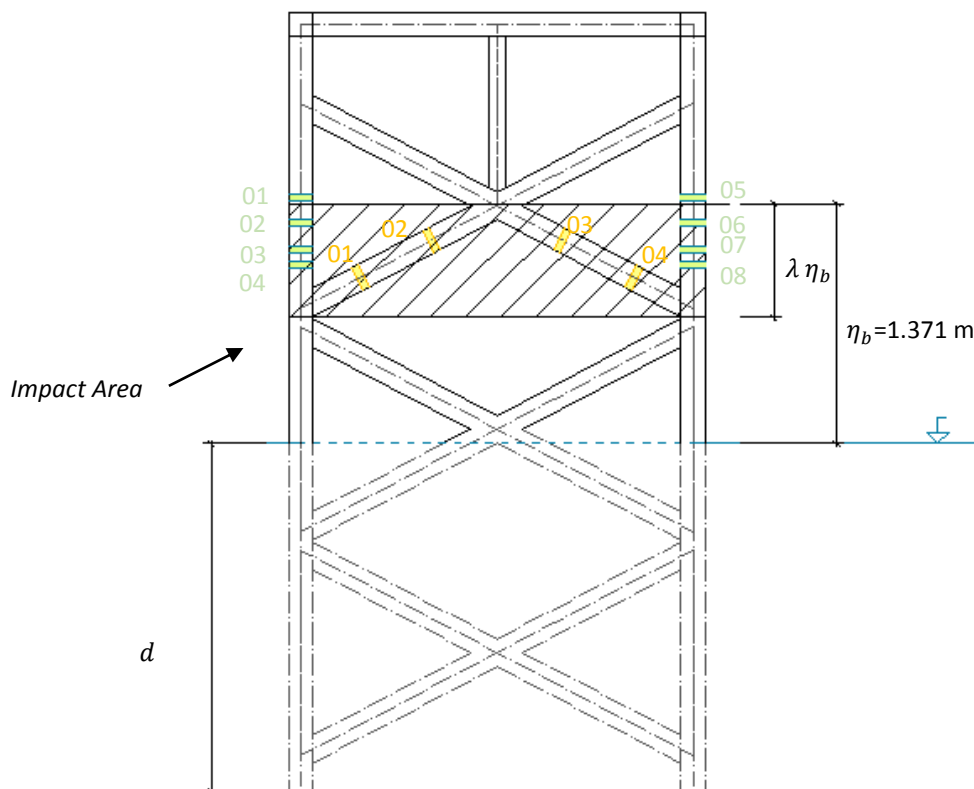


Figure 7.3: Front view of the wave impact area.

The response on the instrumented bracings FTBF01-FH, FTBF02-FH, FTBF03-FH and FTBF04-FH is:

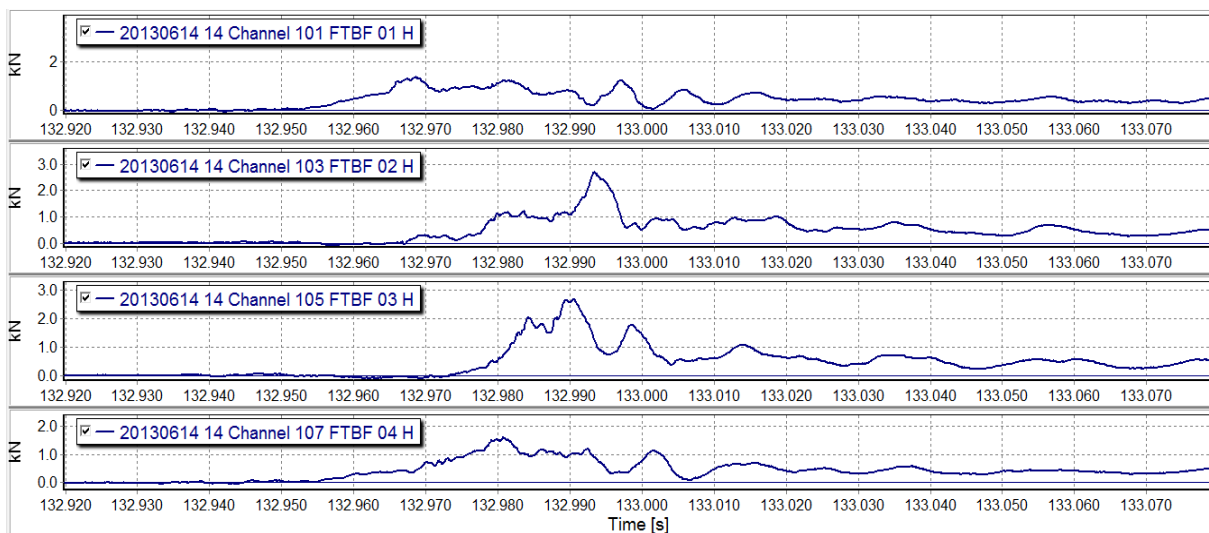
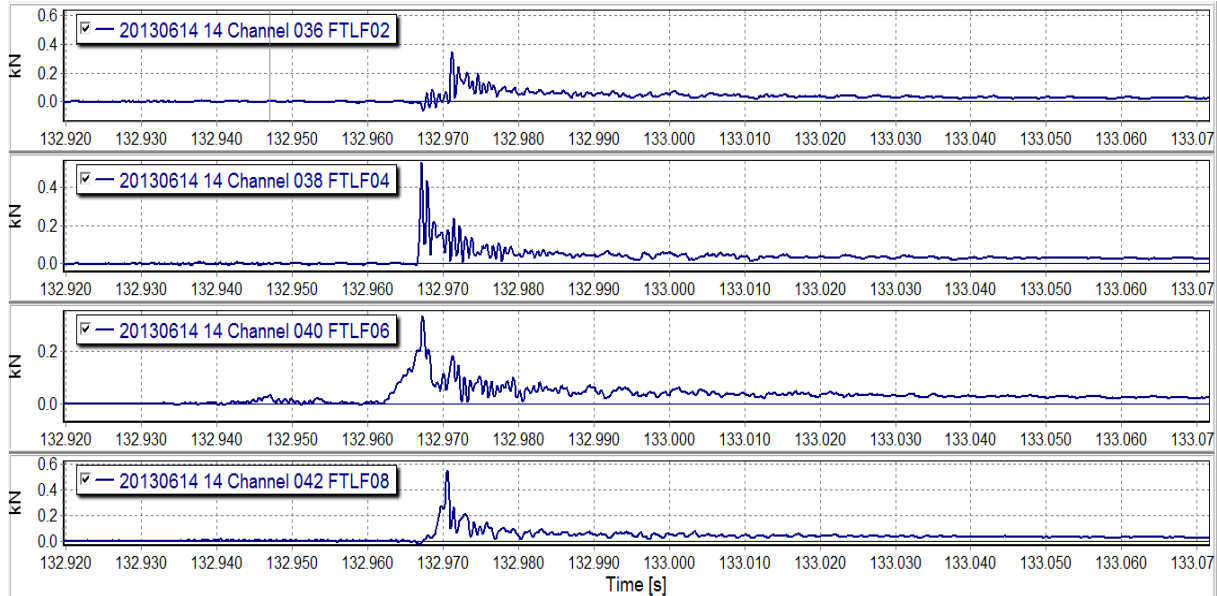


Figure 7.4: Force-time response for the front bracings.

Initially in the defined area of impact part the right and left column are within this area. The Figure 7.3 indicates that local force cell transducer FTLF02, 03, 04 and 06,07,08 are located within the impact area of study.



**Figure 7.5: Force time response for the instrumented columns**

The response on the left and right column as is shown in Figure 7.5 is considerable lower than the results in the instrumented bracings.

In order to obtain the wave loads acting on the instrumented bracings it was decided to discard the wave loads acting on the columns. The different reasons for that are: Firstly, as can be seen from the results the response is around 3-4 times smaller than for the instrumented front bracings. Secondly, the effect that the wave load acting on the columns will have on the bracings is going to be negligible.

For all these reasons although the area of the impact includes the corresponding column parts, for the fitting of the response on FTBF01, 02, 03 and 04 it will be only considered the wave load acting on the instrumented bracings within the impact area.

### 7.2.1 Interpretation of the study case

An initial overview of the response in the front bracings is indicated in Figures 7.4-7.5. To study it in more detail a time reference value ( $t=0$ ) is set to the original time: 132.95 s.

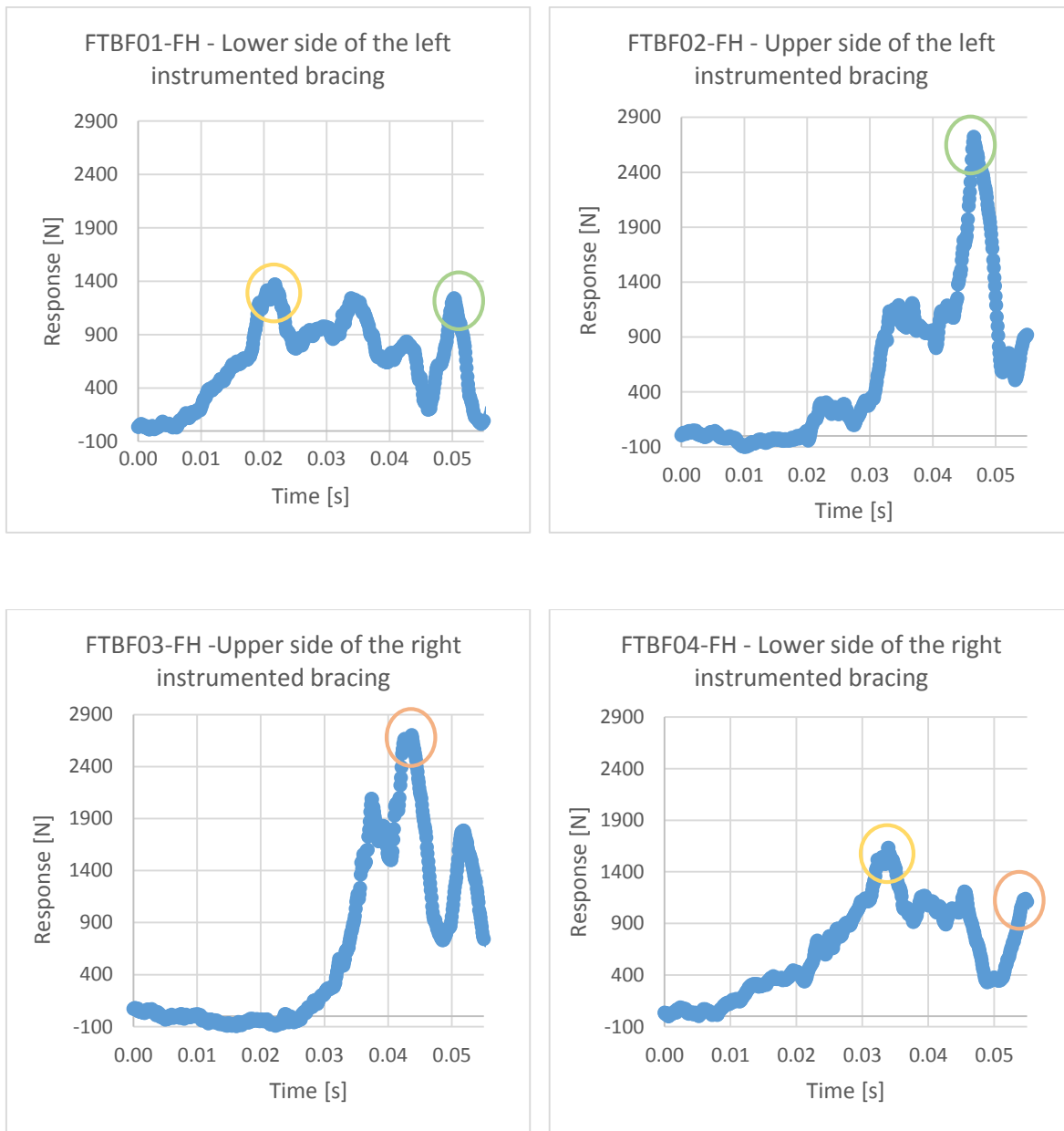


**Figure 7.6: Force response and correlations on the instrumented bracings for Wave test 2013061414 at 132-135s.**

A study in detail of the responses, Figure 7.6, shows how the wave is breaking and hitting the front of the structure:

The wave hits first FTBF01 at around 0.018 s and a peak value of 1300 N is recorded. The correlation between the wave impact at the lower part of the left instrumented bracing and its effect on the upper part is clearly shown around 0.005 s later on FTBF02, where the response is suddenly increased until 1050 N.

On the front right instrumented bracing the wave hits later on the lower side, FTBF04. The impact is observed from the response at around 0.029 s with a peak value of 1600 N similar as in FTBF01. That means as it was confirmed in the first chapter, that the wave is not acting simultaneously on the front side. The wave is asymmetrically hitting the structure. The time delay that exists between these two initial impact at the left and right side is quite larger, around 0.011 s. The distance in between these two force transducers is 1.560 m.

Focusing on the wave impact at the upper parts of the bracings the peak response is double than in the lower part of the bracings. The impact on FTBF02 is at 0.046 s whereas on FTBF03 is at 0.044. The distance in between these two force transducers is 0.716 m.

The correlation between the impacts at the upper part to the lower part is clearly observed as well. The impact on FTBF02 at 0.046 s has an effect 0.004 s later on FTBF01 at 0.05 s. An identical scenario can be described for the right bracing.

From this brief analysis the following conclusions can be highlighted:

- As the structure is almost completely symmetric both in geometry and boundary conditions, a symmetry is initially expected in the response if the front wave hits the structure at the same instant. Considering that the wave front does not hit it at exactly the same time the front of the structure, not completely symmetrical response is obtained.
- An existence time delay for the responses at the same height, FTBF01-04 and FTBF02-03, is found.

### 7.2.2 Treatment of the signal

Those responses are not only composed by the dynamic part coming from the breaking wave, but also a contribution from quasi static inertia and drag forces in which is called as Morison forces takes place.

The response on FTBF01 is a good example of that. There is an initial response that keeps a constant slope from 0 until 0.0179 s. From that instant the slope is quickly increased due to the action of the wave breaking.

Two different approaches can be done for dealing with this situation. The first approach would be to recreate not only the wave impact load, but also the Morison forces acting on the structure. Another approach would consider to deal directly with the response obtained and filtered it down with not a high cut-off frequency in order to remove these forces. Both have strengths and drawbacks that need to be considered.



- The Morison forces could have been recreated either defining another triangular load, but with a higher time duration or developing a CFD model which would simulate the wave conditions and the interaction structure-water. The Morison's coefficients should be extracted from there.
- Filtering it down the signal is a challenging issue because of the uncertainties in the cut-off frequency chosen. This cut-off frequency should be high enough to eliminate the Morison forces and low enough to no disturb the dynamic oscillations from the impact load.

Finally, the decision taken has been to filter down the signal and other approaches could be used in further analysis.

A first approach for the cut-off frequency shows that the Eigen frequency in Y direction, Wave direction, is around 34 Hz and corresponds to the vibration mode n°6 in the modal analysis. This as it has been shown from the modal analysis, is the lowest frequency of the structure in that direction.

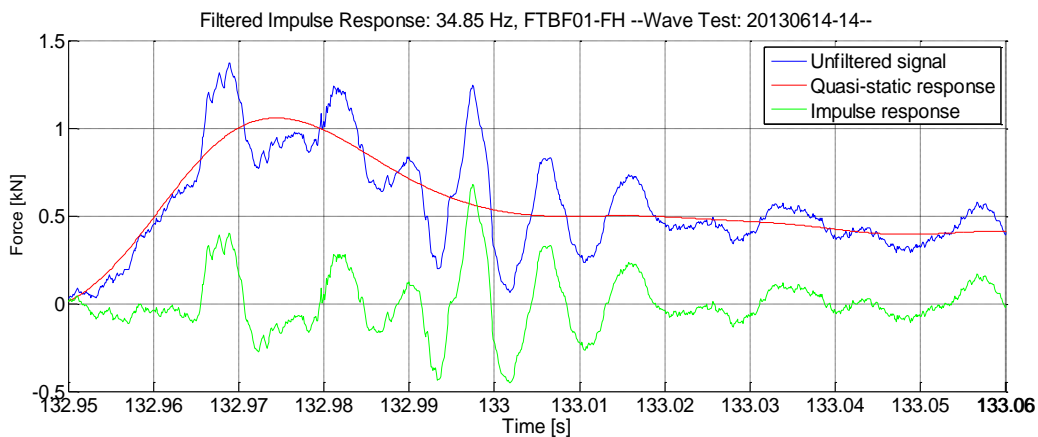


**Figure 7.7: Response decomposition at FTBF01-FH for a cut-off frequency of 34.85 Hz.**

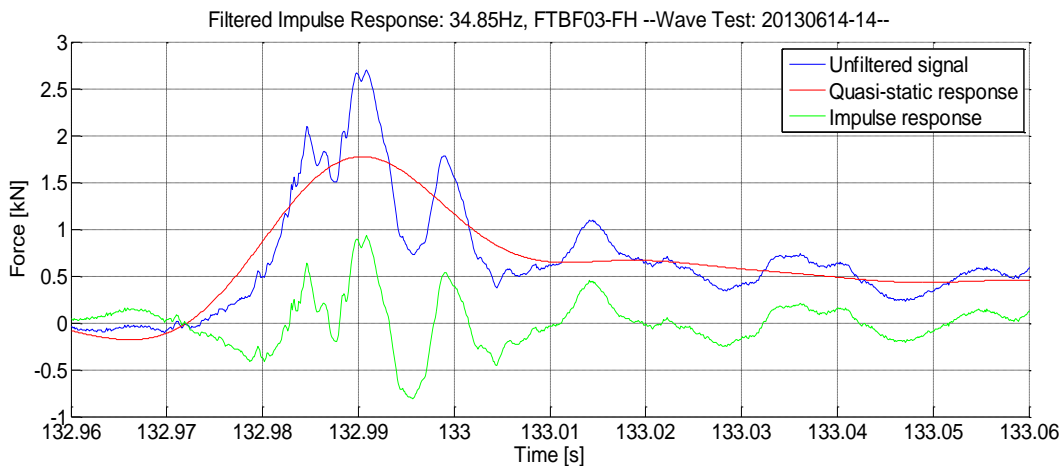


**Figure 7.8: Response decomposition at FTBF03-FH for a cut-off frequency of 34.85 Hz.**

From Figures 7.7-7.8 can be observed that for a cut-off frequency of 34.85 Hz the Morison forces are removed as is represented at the initial 0.015 s on FTBF01-FH in Figure 7.7.

On the other hand, the peak value has been reduced around 65% from the unfiltered response, which means that the impulse response only represents a 35% of the total response. In Figure 7.8 is shown that the frequency of the quasi static response seems too high and disturbs the impulse response.

The spectrum response of the bracings, see Figure 4.5, indicates that the peak value is around 90-100 Hz. Although the frequency of the peak value is about 3 times the defined cut-off frequency, the range frequencies that have a considerable contribution to the response spectrum of the bracings is ranged from 25 to 125 Hz.

Moreover the quasi static forces expected should not have such a pronounced peak and the response should follow the response signal but in a smoother way.

The response of FTBF01 is presented filtering down for three different cut-off frequencies:

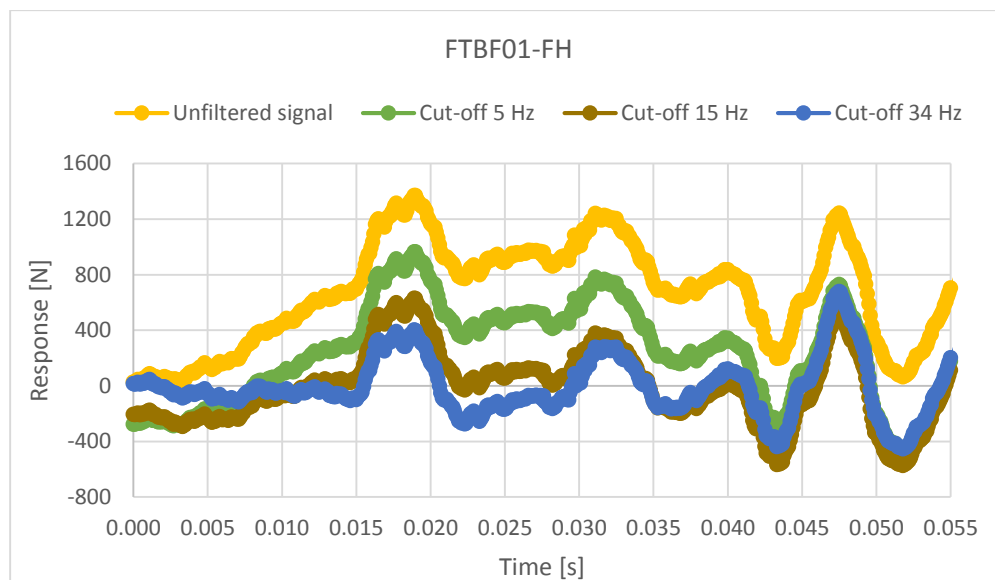


**Figure 7.9: Force response at FTBF01 for different cut-off frequencies**

It is observed from the above results that a cut-off frequency of 5 Hz does not completely remove the Morison contribution to the response. Otherwise, using a cut-off frequency of 34 Hz takes out the whole quasi-static component, but affects the dynamic response as it was seen before. For 15 Hz the quasi static forces are removed as well.

So a range of frequencies in between 15-25 Hz seems reasonable for taking out the Morison components.

In between these frequencies the dynamic response seems not be affected and the Morison forces removed.

Finally, the frequency selected for filtering down the signal is 18 Hz.

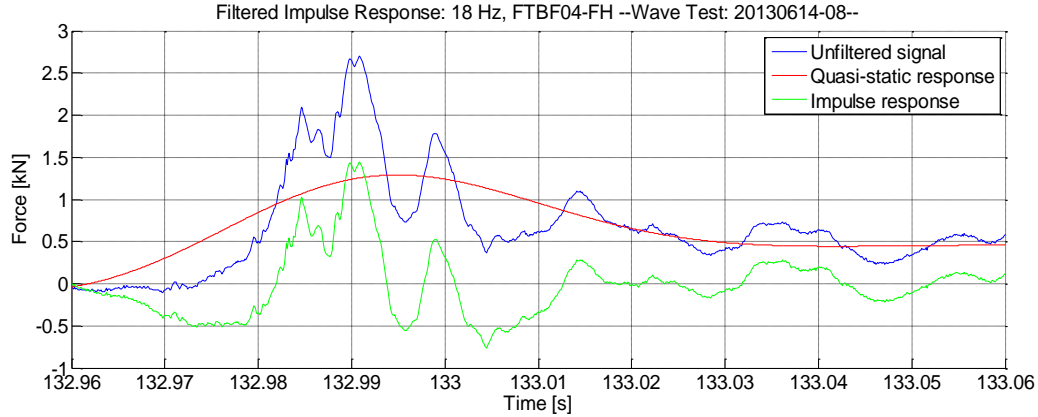


**Figure 7.10: Response decomposition at FTBF03-FH for a cut-off frequency of 18 Hz.**

### 7.2.3 Inverse Fast Fourier Transform, IFFT

The IFFT is an alternative method used to find the loads acting on any structure from measured response forces.

This procedure used by Määttänen (1979) was used to find ice forces acting from measured response forces and is applicable for wave slamming loads as well (Tørum 2013).

The measure response force  $f(t)$  can be expressed into Fourier integral as:

$$f(t) = \frac{1}{2\pi} \int_{-\infty}^{\infty} H(\omega) S_F(\omega) e^{i\omega t} d\omega \quad (38)$$

where  $S_F(\omega)$  is the linear spectrum of the impulse signal and can be calculated as:

$$S_F(\omega) = \frac{S_f(\omega)}{H(\omega)} \quad (39)$$

where  $S_f(\omega)$  is the linear spectrum of the measure signal  $f(t)$ ;  $H(\omega)$  is the transfer function or also called frequency response function. This function is obtained from the hammer tests applied at the instrumented bracings and defines the properties of the Structure. It and can be calculated as:

$$H(\omega) = \frac{S_{response\ hammer}(\omega)}{S_{hammer}(\omega)} \quad (40)$$

where  $S_{response\ hammer}(\omega)$  is the fast Fourier transform of the response due to the impact of the hammer load at any of the 4 bracing transducers, FTBF01-02-03-04. The  $S_{hammer}(\omega)$  represents the fast Fourier transform of the hammer load.

$$S_{response\ hammer}(\omega) = \int_{-\infty}^{\infty} f_{response\ hammer}(t) e^{-i\omega t} dt \quad (41)$$

$$S_{hammer}(\omega) = \int_{-\infty}^{\infty} f_{hammer}(t) e^{-i\omega t} dt \quad (42)$$

Finally, the Inverse Fast Fourier transform gives the slamming force.

$$F(t) = \frac{1}{2\pi} \int_{-\infty}^{\infty} \frac{S_F(\omega)}{H(\omega)} e^{i\omega t} d\omega \quad (43)$$

Although this method could be an alternative approach to get a first guess for the impulse load at the bracing transducers, is out of scope of this thesis. The idea behind it is to show and get an estimation about how the load time distribution is.

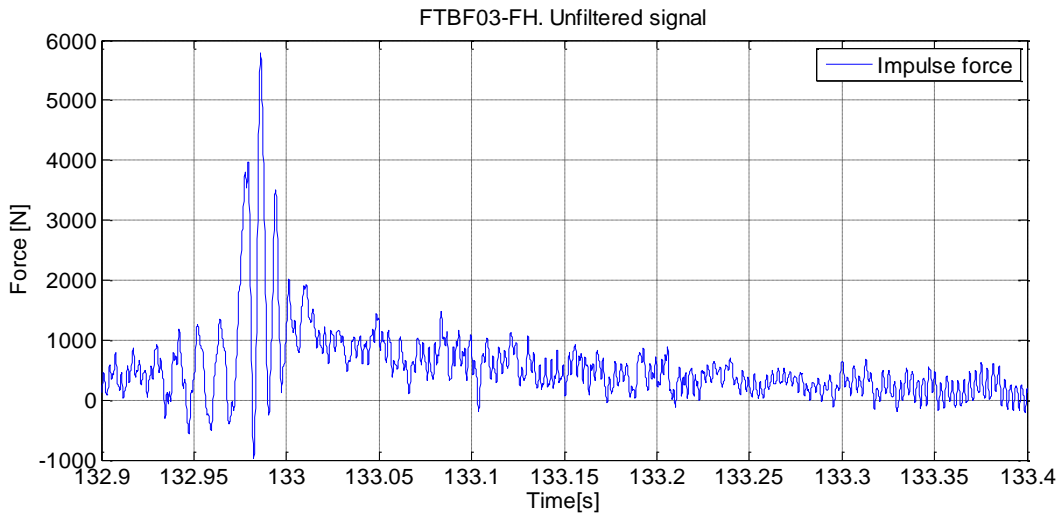


**Figure 7.11: IFFT of the response at FTBF03-FH.**

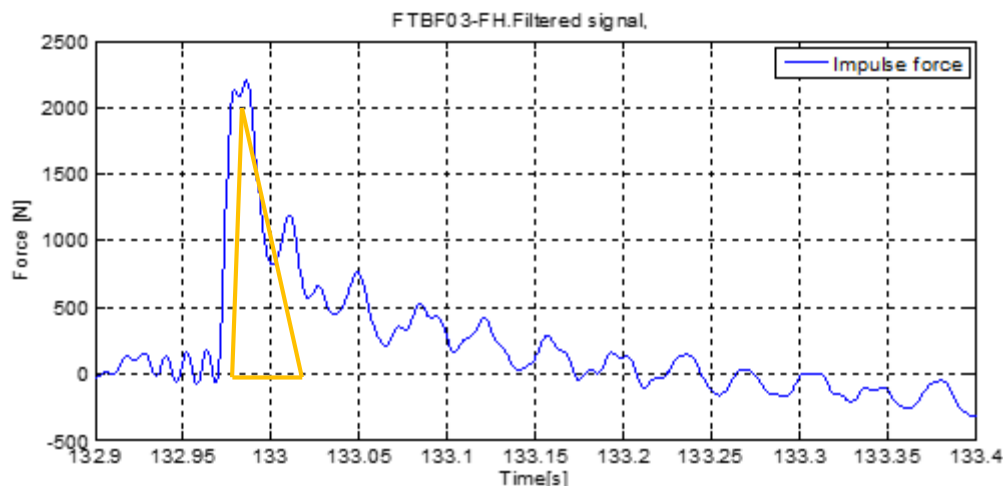


**Figure 7.12: Filtered response with a cut-off frequency of 150 Hz.**

From the above figure<sup>17</sup> is observed that the load acting has a quite defined triangular shape with a quick initial rising time from zero to the peak value and then the force decays more slowly.

The cutoff frequency has been set to 150 Hz because the load is expected to be smoother and not as spike as the unfiltered signal.

That situation reinforce the idea that the wave load can be defined as a triangular force time history governed by three main parameters such as: *total time of the load, peak force and rising time.*

#### 7.2.4 Sensitivity Analysis

From the interpretation of the study case: 20130614-14 it was found that the wave does not hit neither at the same time the front structure nor in the whole length of the instrumented bracings. The Figure 7.14 represents a scheme of the acting wave loads on the bracings.

So the hitting sequence is: 1 - FTBF01, 2 - FTBF04, 3 - FTBF03 and 4 - FTBF02.

In order to simulate this impact sequence a first uniform load will act from the lowest part of the left bracing until the middle of it, then the same situation will be at the right bracing with a certain offset time. After that, another uniform load will be defined from the middle until the upper part of the same bracing and finally the last load will act in the upper part of the left bracing. The wave load is defined as a uniform load, but with a triangular time history as it is shown in Figure 7.14

<sup>17</sup> The load showed on the figure includes the Morison forces as well. That explains why the load duration takes around 0.20 to decay completely.

The Figure 7.15 shows two different impact areas, where the impact area 1 corresponds to the loads acting on the lower part of the bracing. The impact area 2 refers to the loads that will act later on the upper points. See Figure 7.13 for the details of the first wave impact location.

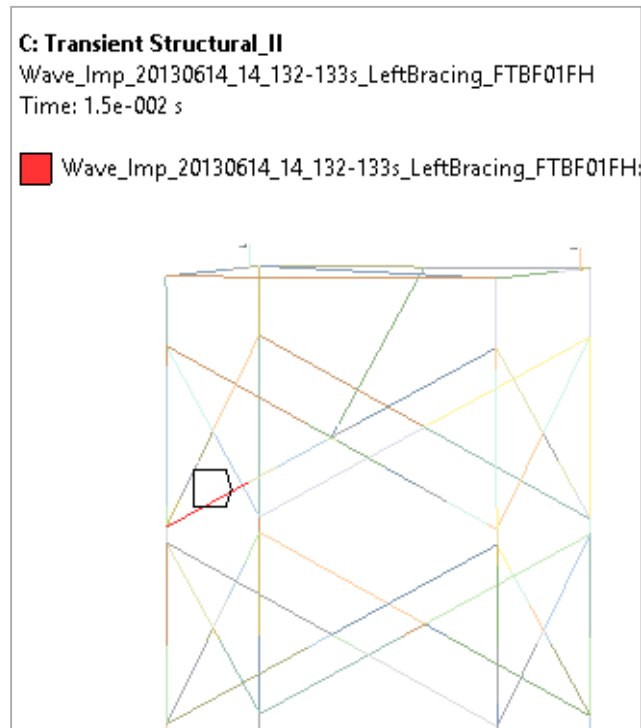


Figure 7.13. Location of the uniform wave load at the lower left front bracing.

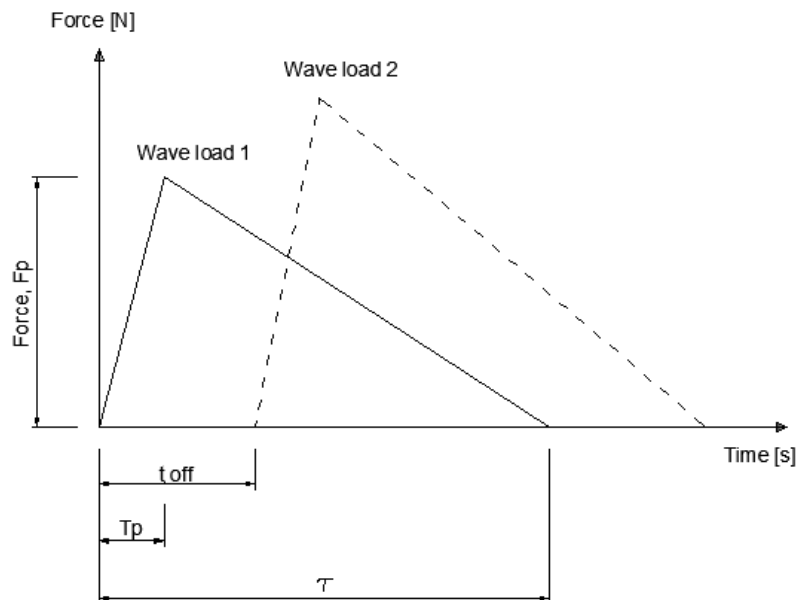


Figure 7.14: Characterization of the wave load.

#### 7.2.4.1 Parameters to calibrate

Summarizing, a total of four parameters have to be calibrated: Duration of the load ( $\tau$ ), Peak time ( $T_p$ ), Maximum force ( $F_p$ ) and the offset time ( $t_{off}$ ) from the impact of one wave load to another.

From different researches it has been found that the total time of the load is commonly approached by the following experimental formulas:

$$\tau = [0.25 - 0.5] \frac{D}{C_b}, \quad \text{Tanimoto (1986)} \quad (44)$$

$$\tau = \frac{13 D}{64 C_b}, \quad \text{Wienke and Oumeraci (2005)} \quad (45)$$

where  $D$  is the diameter of the element 0.1397 m and  $C_b$  is the celerity of the wave at the breaking moment. It is a very complex parameter to measure and in the literature is habitually calculated as:

$$C_b = \sqrt{g(d + \eta_b)} \quad (46)$$

where  $g = 9.81 \text{ m/s}^2$ ,  $d = 2 \text{ m}$  is the water depth and  $\eta_b$  is the wave crest height.

$\eta_{b1} = 1.34 \text{ m}$  For triangular loads applied to the upper part of the bracings

$\eta_{b2} = 1.06 \text{ m}$  For triangular loads applied to the lower part of the bracings

$l_{impact} = 0.635 \text{ m}$

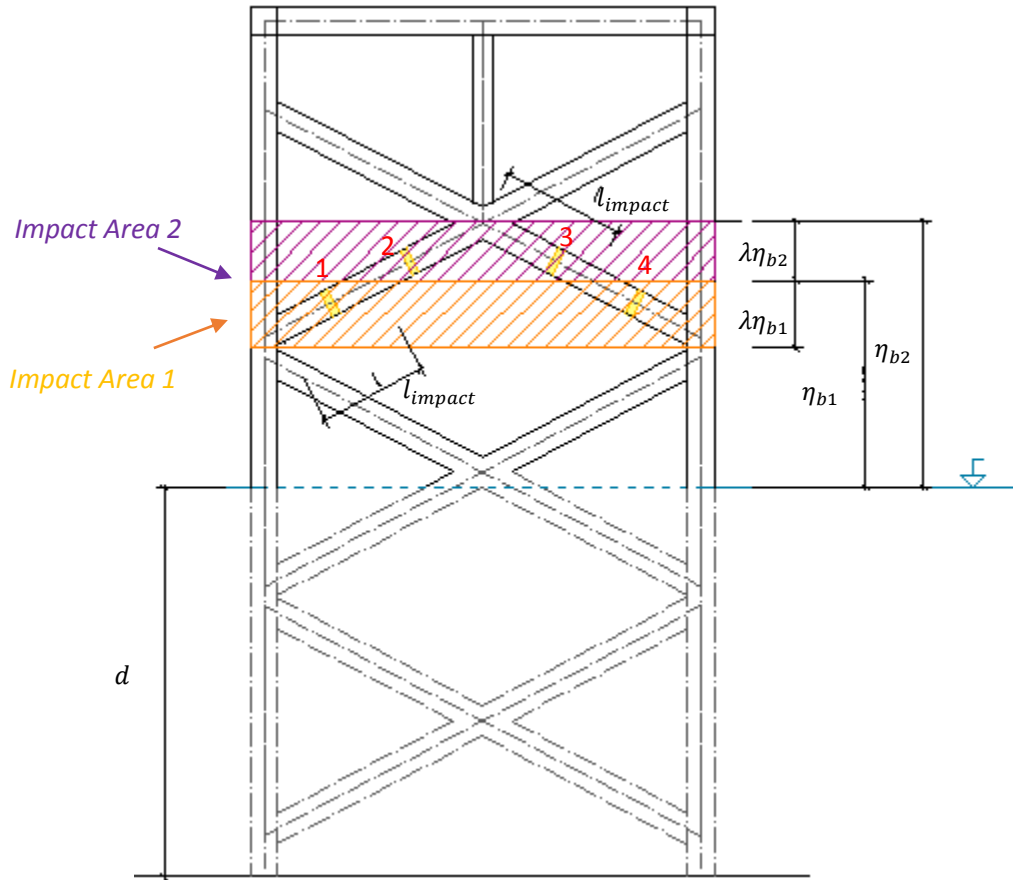


**Figure 7.15: Representation of the two impact areas produced by the delay on the impact along different points on the front bracings.**

*Impact Area 1 [FTBF01-04]*

In that area the wave celerity is:

$$c_b = \sqrt{g(d + \eta_{b1})} = \sqrt{g(2 + 1.06)} = 5.48 \text{ m/s} \quad (47)$$

And a first approach for the time of the load is limited between these two values:

$$\tau = [0.25 - 0.5] \frac{D}{c_b} = [0.25 - 0.5] \frac{0.1397}{5.48} = 0.006 - 0.0127s, \text{ Tanimato} \quad (48)$$

$$\tau = \frac{13}{64} \frac{D}{c_b} = 0.0051 \text{ s}, \quad \text{Wienke and Oumeraci} \quad (49)$$

Some simulations were done and it was found that the main parameters governing the response are the total load duration and obviously the peak force.



On the other hand, variations on the peak time does not show a high influence on the response. It is shown in Table 7.2 and Figure 7.16.

**Table 7.2: Wave’s cases studied with different peak time**

Load lower part of the left front bracing - FTBF01-			
Run Test	I	II	III
$\tau$ [s]	0.005	0.005	0.005
$F_p$ [N]	2300	2300	2300
$T_p$ [s]	0.001	0.0005	0.00005
$l_{impact}$ [m]	0.6351	0.6351	0.6351

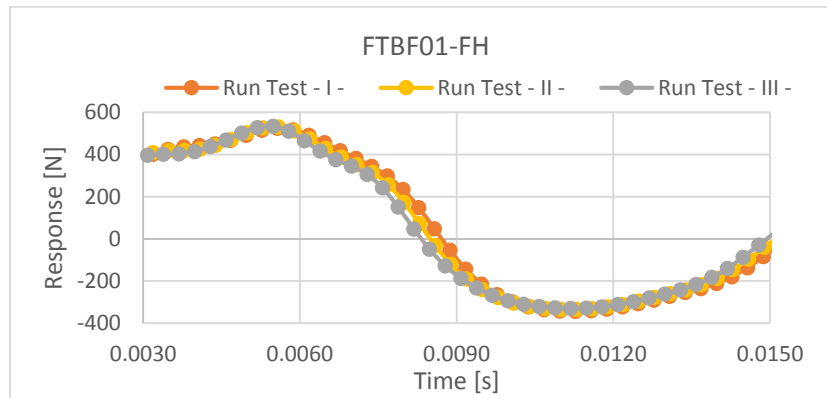


**Figure 7.16: Representation of the responses for different peak time values.**

The figure above shows slightly changes for different peak time values. For a very low peak time the response is produced earlier, but not important deviations are found. For this reason and to reduce the number of parameters to calibrate, from now on the peak time is defined as 10% of the total duration of the load.

Several combinations of triangular loads have been carried out but only three are going to be described in the report. This decision has been made in order to not overload with needless figures and to just describe the most important aspects. All the other combinations can be found in the Excel spreadsheet: “WaveSlam\_Forces\_LastV(I)”.

**Table 7.3: Characterization of wave loads studied for FTBF01**

Lower part of the left front bracing – FTBF01-			
Run Test	I	II	III
$\tau$ [s]	0.01	0.006	0.005
$F_p$ [N]	5000	5000	2800
$T_p$ [s]	0.001	0.0006	0.0005
$t_{off}$ [s]	0	0	0

The following figures represents the results from ANSYS and the data for the three different run-tests.

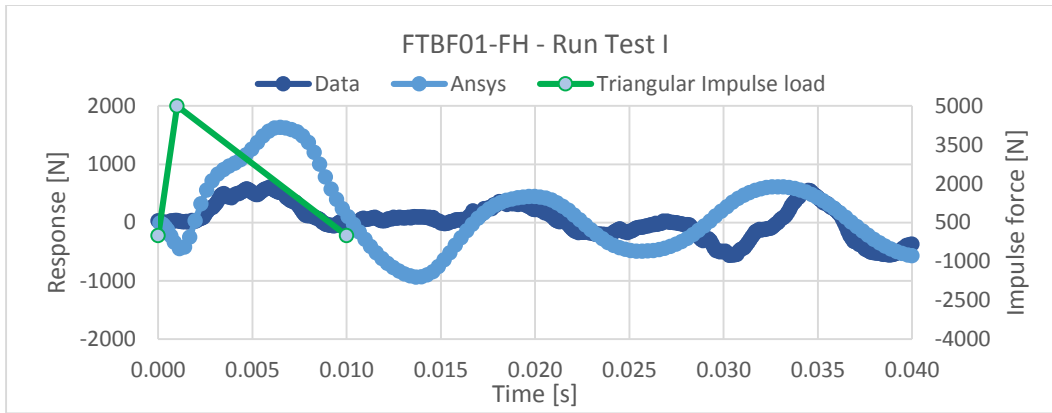


Figure 7.17: Comparison between the Data response and ANSYS at FTBF01-FH for run test I

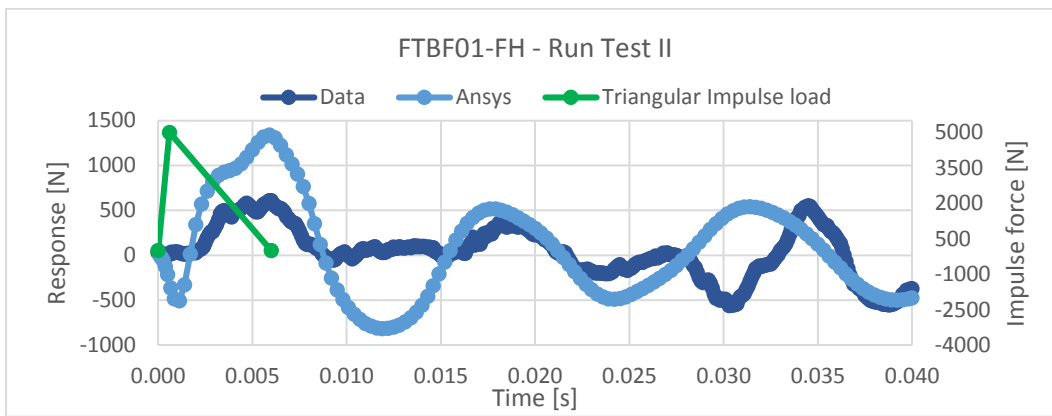


Figure 7.18: Comparison between the Data response and ANSYS at FTBF01-FH for run test II.

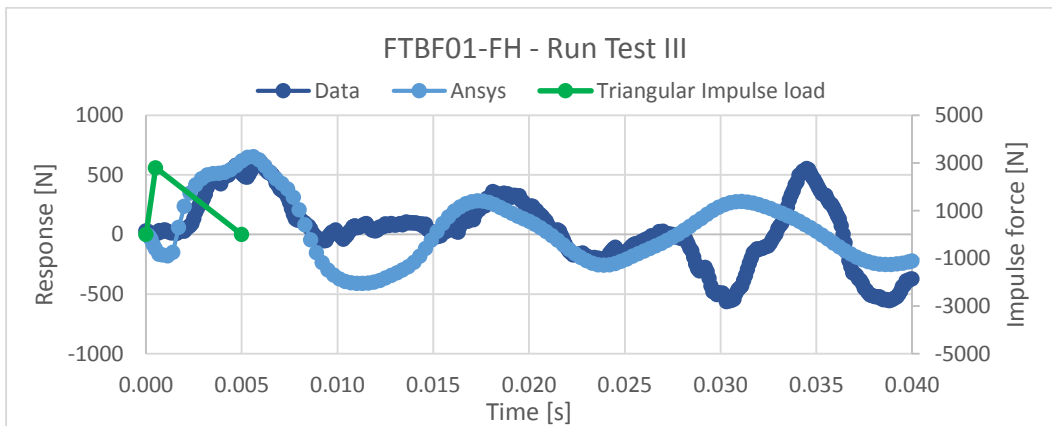
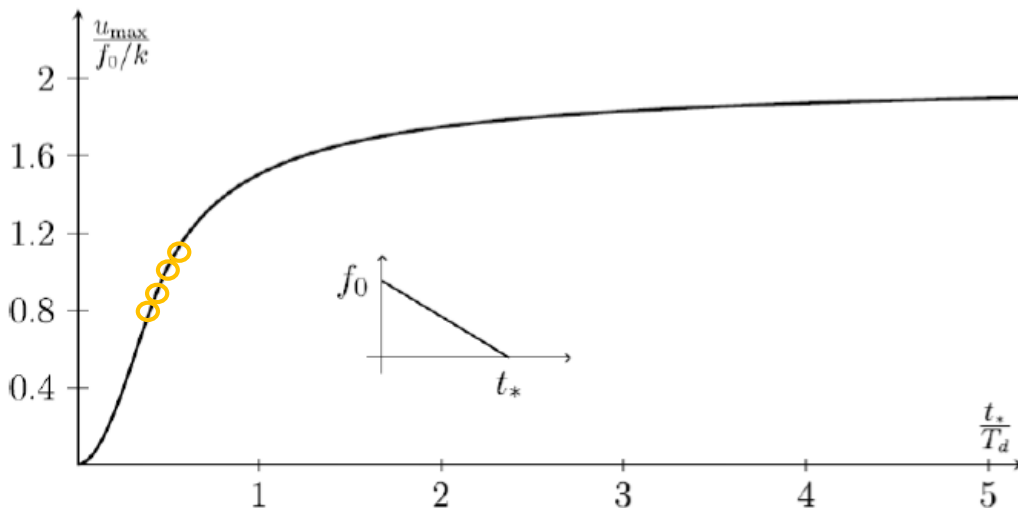


Figure 7.19: Comparison between the Data response and ANSYS at FTBF01-FH for run test III.

The above figures reflect how the dynamic response behaves for changes in the peak force intensity and load duration.

The influence of the duration of the wave load  $\tau$  ( $t_*$ ) is seen in Figure 7.20. The wave load is approached as a suddenly triangular force time history. As the Eigen frequency of the beam has found to be around 100 Hz, the maximum dynamic response obtained is in between the highlighted part of the curve for the run tests performed. Thus, a reduction in the wave duration load produces a high reduction of the response as it has seen from the results in ANSYS.



**Figure 7.20. The maximum response to a suddenly applied triangular force time history (Naess)**

The Run Test III exhibits a quite good response for the earlier highest peak. The focus of the analysis is concentrated in that initial highest peak because this will lead to the highest slamming factor  $C_s$ . The deviation for this test is around 5-7% for both force and time response. The Table 7.4 shows the results.

An overview of the response shows a good fit not only for the initial peak, but also in most parts of the signal. The analysis of the next peaks is more complex because is affected by the subsequent impacts of the wave along the front bracings. Specifically the response at 0.01 and 0.03s is affected for when the wave hits the right lower part of the bracing FTBF04, and left upper bracing FTBF02, respectively.

**Table 7.4: Sensitivity analysis of FTBF01-FH**

Sensitivity Analysis - FTBF01-FH			
Data	Peak value [N]	608.99	
	Time [s]	0.0059	
Run-Tests			Deviation [%]
I	Peak value [N]	1634.95	168.47
	Time [s]	0.00647	9.66
II	Peak value [N]	1338	119.71
	Time [s]	0.0059	0.00
III	Peak value [N]	651.69	7.01
	Time [s]	0.0056	5.08

The same procedure is done for the load acting on the lower part of the right front bracing. A new variable, offset time, has to be defined. The wave loads are defined in the Table 7.5 and the results are illustrated in Figures 7.21-7.23.

**Table 7.5: Characterization of wave loads studied for FTBF04**

Lower part of the right front bracing – FTBF04-			
Run Test	I	II	III
$\tau$ [s]	0.01	0.003	0.005
$F_p$ [N]	5000	3000	2800
$T_p$ [s]	0.001	0.0003	0.0005
$t_{off}$ [s]	0.0128	0.0128	0.0128

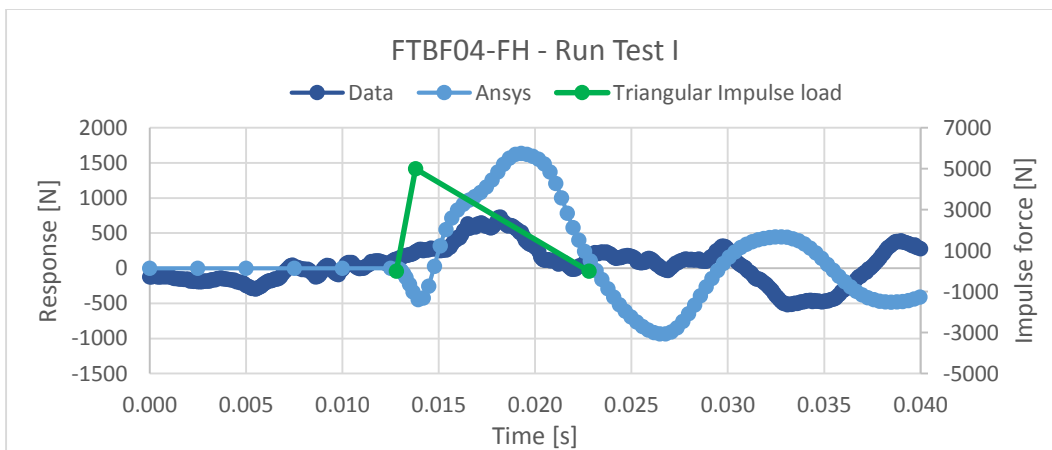


**Figure 7.21: Comparison between the Data response and ANSYS at FTBF04-FH for run test I**

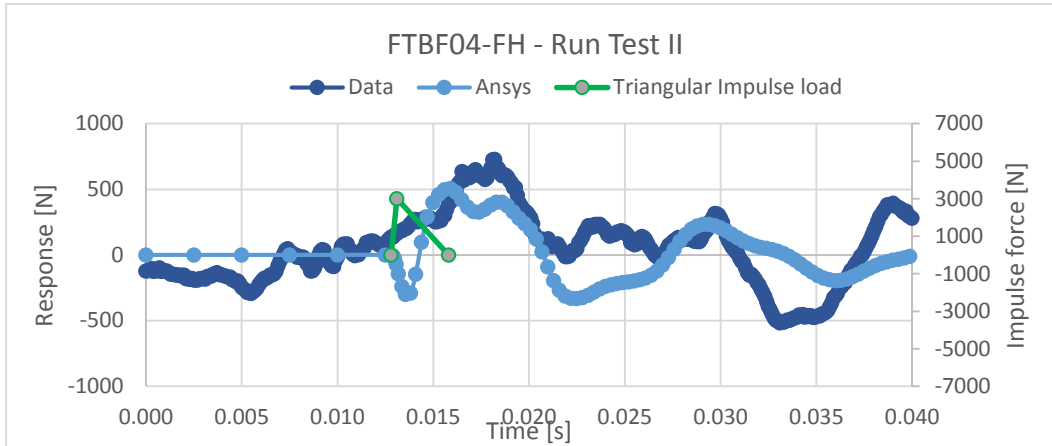


**Figure 7.22: Comparison between the Data response and ANSYS at FTBF04-FH for run test II.**

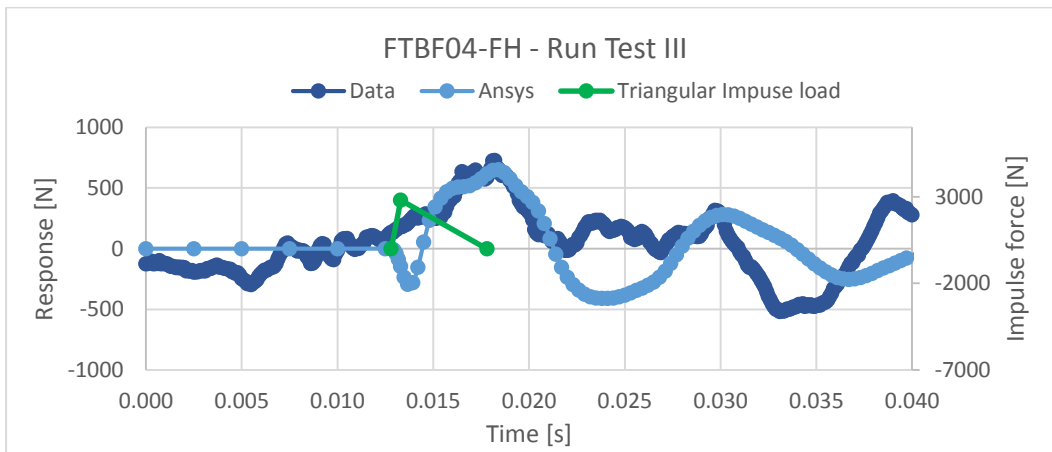


**Figure 7.23: Comparison between the Data response and ANSYS at FTBF04-FH for run test III.**

Regarding to the right bracing the response obtained for the same wave load than at FTBF01 offers an acceptable fit. The wave hits at this part around 0.0128s later but seemingly with the same intensity. Table 7.6 indicates a deviation for run test III of around 0.51% and 6.98 % for force and time response.

From the above figures is observed that the initial data response is initially affected (at around 0.010-0.015s) by some other forces not related to the impulse wave load at this point. This initial behavior might be explained either because of the remaining of some Morison's forces or is the effect produced by the wave that had hit the lower part of the left bracing, FTBF01.

In the first scenario where not all the Morison forces were removed, a higher cut-off frequency would be required. This frequency is around 20-21 Hz and would imply a reduction of the wave peak load of 6-8%.

**Table 7.6: Sensitivity analysis of FTBF04-FH**

Sensitivity Analysis - FTBF04-FH			
Data	Peak value [N]	649	
	Time [s]	0.0172	
Run-Tests			Deviation [%]
I	Peak value [N]	1637.3	152.28
	Time [s]	0.0193	12.21
II	Peak value [N]	506.135	22.01
	Time [s]	0.0159	7.56
III	Peak value [N]	652.315	0.51
	Time [s]	0.0184	6.98

Impact Area 2 [FTBF02-03]

In that area the wave celerity is:

$$C_b = \sqrt{g(d + \eta_{b2})} = \sqrt{g(2 + 1.35)} = 5.74 \text{ m/s} \quad (50)$$

And a first approach for the load duration is limited between these values:

$$\tau = [0.25 - 0.5] \frac{D}{C_b} = [0.25 - 0.5] \frac{0.1397}{5.74} = 0.006 - 0.012 \text{ s}, \quad \text{Tanimoto} \quad (51)$$

$$\tau = \frac{13}{64} \frac{D}{C_b} = 0.0049 \text{ s}, \quad \text{Wienke and Oumeraci} \quad (52)$$

Different run tests are defined and studied for FTBF02. See Table 7.7.

**Table 7.7: Characterization of wave loads studied for FTBF02**

Upper part of the left front bracing – FTBF02-			
Run Test	I	II	III
$\tau$ [s]	0.01	0.005	0.008
$F_p$ [N]	9000	7000	7000
$T_p$ [s]	0.001	0.0005	0.0008
$t_{off}$ [s]	0.025	0.025	0.025

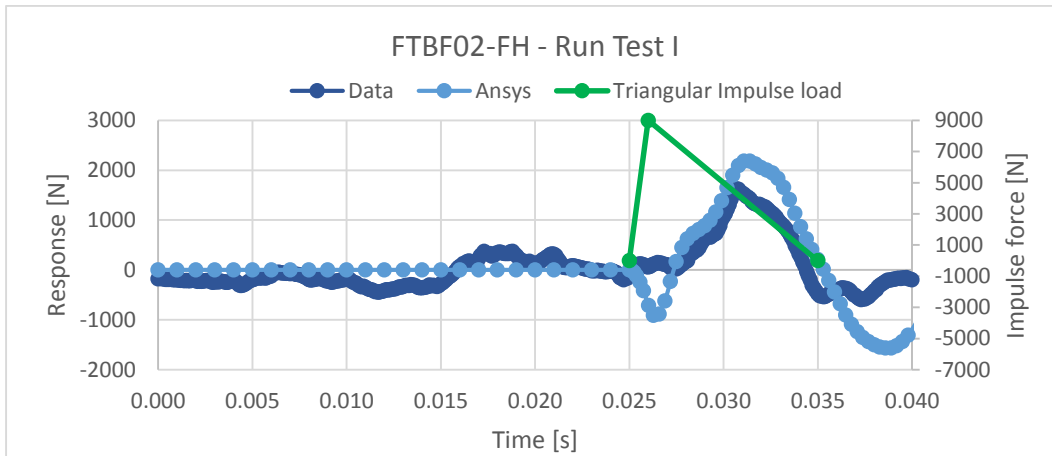


**Figure 7.24: Comparison between the Data response and ANSYS at FTBF02-FH for run test I**

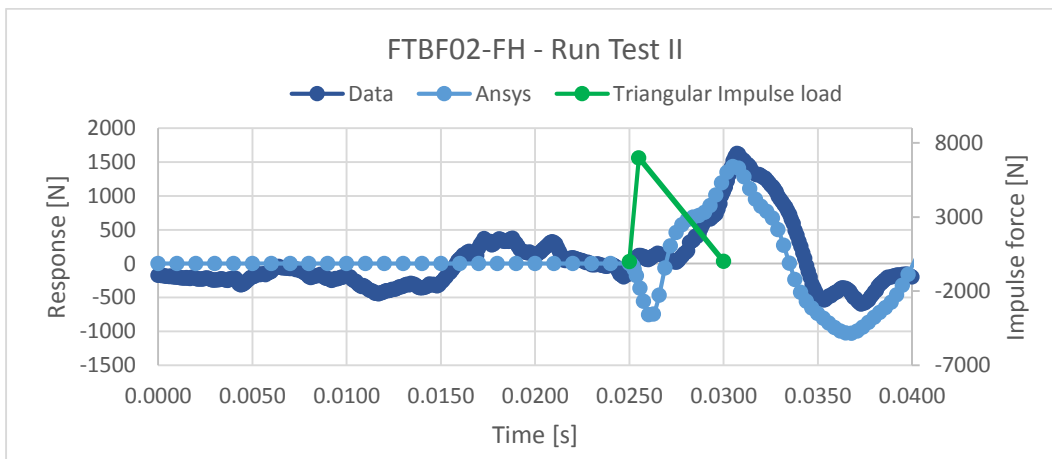


**Figure 7.25: Comparison between the Data response and ANSYS at FTBF02-FH for run test II.**

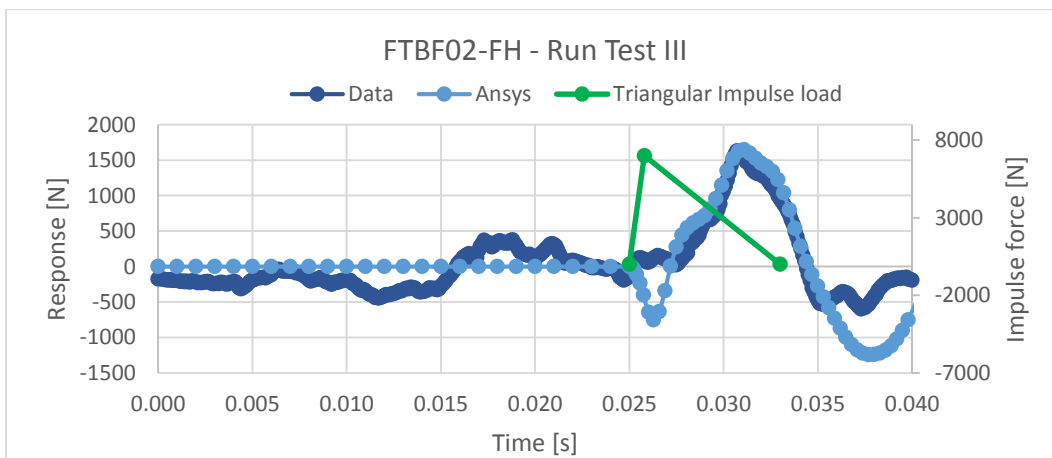


**Figure 7.26: Comparison between the Data response and ANSYS at FTBF02-FH for run test III.**

**Table 7.8: Sensitivity analysis of FTBF02-FH**

Sensitivity Analysis - FTBF02-FH			
<b>Data</b>	Peak value [N]	1626.73	
	Time [s]	0.0307	
<b>Run-Tests</b>			Deviation [%]
<b>I</b>	Peak value [N]	2183.15	34.20
	Time [s]	0.0311	1.30
<b>II</b>	Peak value [N]	1434	11.85
	Time [s]	0.0305	0.65
<b>III</b>	Peak value [N]	1646.85	1.24
	Time [s]	0.0311	1.30

The responses for the wave load acting on the upper part of the left front side bracing indicates that for a triangular load of 7000 N peak value and a total time duration of 0.008 s the response from ANSYS shows seems a really good approach. The response even reproduces the light changes on the shape of the highest peak.

At this side of the bracing is where the last impact of the wave is produced. The time delay with respect to the first hit is around 0.025s. The best results offer a deviation from the data at around 1% defined in Table 7.8.

**Table 7.9: Characterization of wave loads studied for FTBF03**

Upper part of the right front bracing – FTBF03-			
<i>Run Test</i>	<b>I</b>	<b>II</b>	<b>III</b>
$\tau$ [s]	0.01	0.008	0.006
$F_p$ [N]	9000	5000	7000
$T_p$ [s]	0.001	0.0008	0.0006
$t_{off}$ [s]	0.0217	0.0217	0.0217



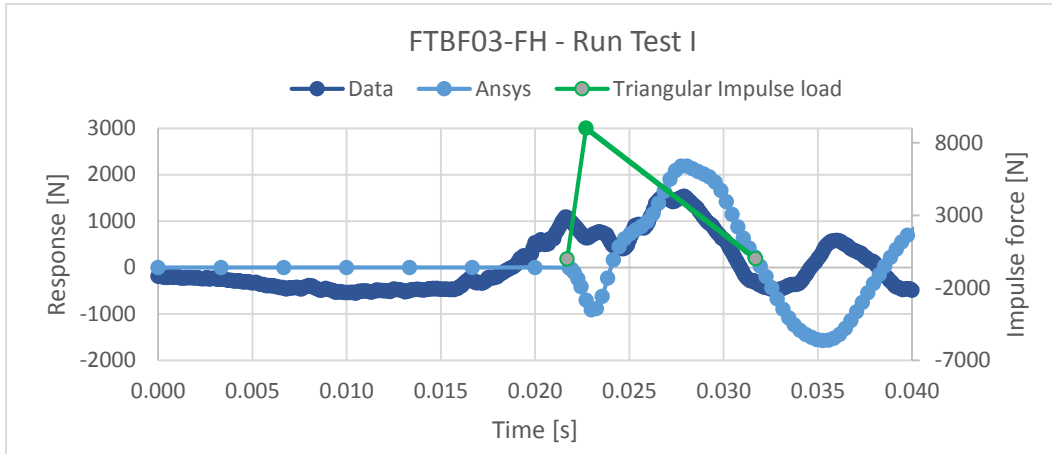


**Figure 7.27: Comparison between the Data response and ANSYS at FTBF03-FH for run test I**

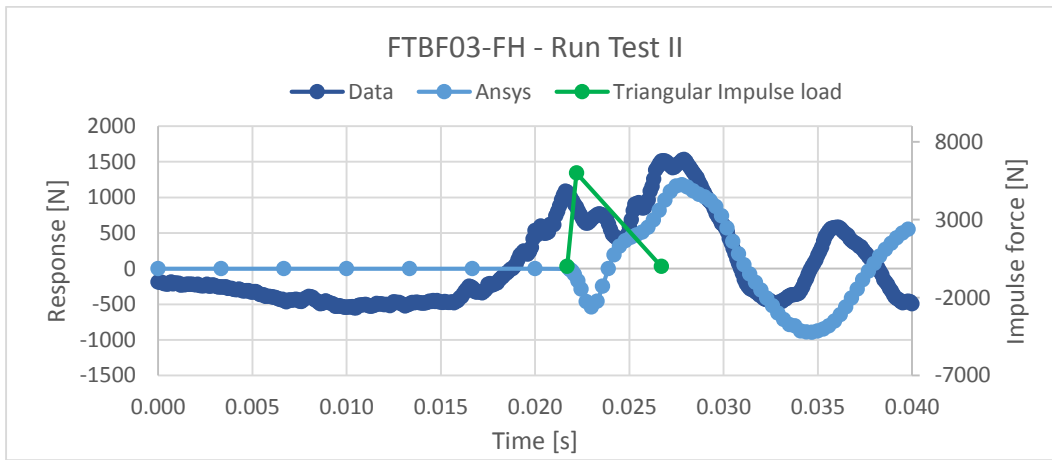


**Figure 7.28: Comparison between the Data response and ANSYS at FTBF03-FH for run test II.**

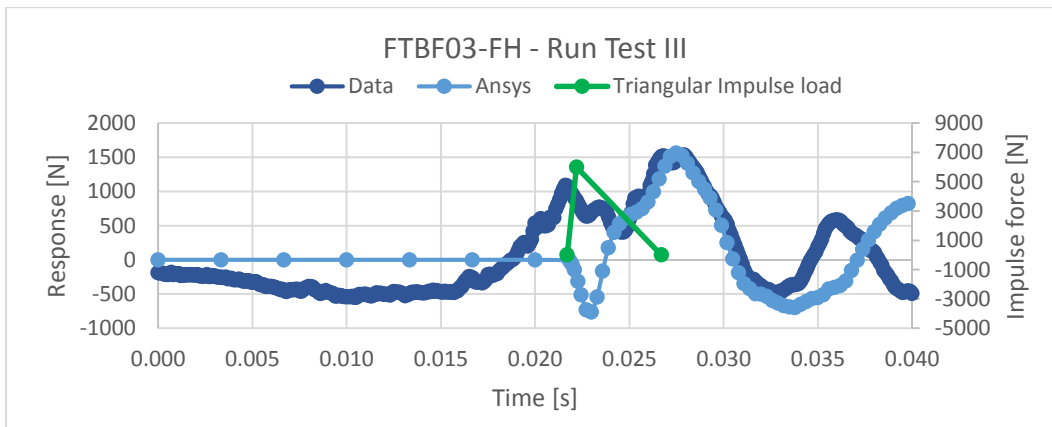


**Figure 7.29: Comparison between the Data response and ANSYS at FTBF03-FH for run test III.**

The impact at FTBF03 is preceded by the response from the hit at FTBF04 located on the same bracing.

The fit for the highest peak offers really low deviations as can be seen in Table 7.10. The intensity and the duration is the same as for the impact at FTBF02. Finally the time delay observed with respect to the first hit at FTBF01 is 0.0217s.

**Table 7.10: Sensitivity analysis of FTBF03-FH**

Sensitivity Analysis - FTBF03-FH			
<b>Data</b>	Peak value [N]	1534.326	
	Time [s]	0.0279	
<b>Run-Tests</b>			Deviation [%]
I	Peak value [N]	2186.6	42.51
	Time [s]	0.0281	0.72
II	Peak value [N]	1177.95	23.23
	Time [s]	0.0278	0.36
III	Peak value [N]	1563.05	1.87
	Time [s]	0.0275	1.43

### 7.2.5 Slamming coefficients

From the previous sensitivity analysis an estimation of the wave loadings acting on the different part of the instrumented bracings is extracted.

As described initially in equation (35) the slamming factor can be expressed as:

$$C_s = \frac{F_S}{\rho_w R C_b^2 l_{impact}} \quad (53)$$

where  $F_S$  is the wave force at the initial time of the load when the force is maximum;  $\rho_w$  is water density;  $R$  is the radius of the bracing element;  $C_b$  is the celerity of the wave;  $l_{impact}$  is defined as the part of the bracing element smashed by the wave.

The Tables 7.11 -7.12 summarize and define using equation (53) the slamming factors acting on the different parts.

7.2.5.1 Lower part of the front bracing, FTBF01-04.

In the tables below the results are presented for the best fit in all 4 force transducers that corresponds in all the cases for the Run Test n° III.

**Table 7.11: Slamming factors for the lower part of the bracings.**

FTBF01 – Run test III		FTBF04 - Run test III	
Wave crest, $\eta_b$ [m]	1.06	Wave crest, $\eta_b$ [m]	1.06
$d + \eta_b$ [m]	3.064	$d + \eta_b$ [m]	3.064
$C_b$ [m/s]	5.48	$C_b$ [m/s]	5.48
$\lambda \eta_b$ [m]	0.294	$\lambda \eta_b$ [m]	0.294
$l_{\text{impact}}$ [m]	0.635	$l_{\text{impact}}$ [m]	0.635
$\rho_w$ [kg/m <sup>3</sup> ]	1000	$\rho_w$ [kg/m <sup>3</sup> ]	1000
$D$ [m]	0.1397	$D$ [m]	0.1397
$F_s$ [N]	2800	$F_s$ [N]	2800
<b>Cs</b>	<b>2.09</b>	<b>Cs</b>	<b>2.09</b>

7.2.5.2 Upper part of the front bracing, FTBF02-03

**Table 7.12: Slamming factors for the upper part of the bracings.**

FTBF02 - Run test III		FTBF03 - Run test III	
Wave crest, $\eta_b$ [m]	1.35	Wave crest, $\eta_b$ [m]	1.35
$d + \eta_b$ [m]	3.35	$d + \eta_b$ [m]	3.35
$C_b$ [m/s]	5.74	$C_b$ [m/s]	5.74
$\lambda \eta_b$ [m]	0.294	$\lambda \eta_b$ [m]	0.294
$l_{\text{impact}}$ [m]	0.635	$l_{\text{impact}}$ [m]	0.635
$\rho_w$ [kg/m <sup>3</sup> ]	1000	$\rho_w$ [kg/m <sup>3</sup> ]	1000
$D$ [m]	0.1397	$D$ [m]	0.1397
$F_s$ [N]	7000	$F_s$ [N]	7000
<b>Cs</b>	<b>4.78</b>	<b>Cs</b>	<b>4.78</b>

## 8. CONCLUSIONS AND RECOMENDATIONS

The initial results of the analysis carried out for the dynamic responses on the front bracings and by extension, on some transducers at the columns for the crest height ranging from 1.09 m to 1.45 m, highlight several important features:

A preliminary analysis of the force response on the transducers installed at the same height describes that the maximum response is not given at the same time, which confirms in average that the wave is not hitting uniformly the front of the structure. This time delay is found around 0.003s in between FTBF01-04 and 0.002s in between FTBF02-03.

The existence of this light asymmetry on the front breaking wave produces a not completely symmetric response from most of the waves studied. Some implications of this behavior are:

An average peak force divergence of around 0.250 kN on the results for transducers placed at the same height. The study of the hammer test has shown the existence correlation among an impact on one side of the bracing and the response away from the hitting point. It might be plausible that the response on the bracings is amplified because for instance the wave hits first the left bracing and some milliseconds afterwards the wave reaches the right side. This existence time delay in the wave hitting could generate an augmentation of the response.

The responses along the columns and bracings are affected by the dynamics of the elements. The response is directly influenced by the ratio of the load impact duration and the natural oscillation period of the different parts of the structure. So different impact durations would generate different responses along the bracings. The duration of the wave impact might be influenced by where the wave breaks.

At that point is important to remark that there are several uncertainties involved during the force analysis, such as: the location where exactly the wave breaks (some distance before, in front of the structure or some distance away), the shape of the breaking front, curling factor, asymmetry of the impact, etc; which turns into a really complex problem and advanced statistics would be required for further analysis on this data.

Once the model has been built up and calibrated, the analysis for the *Wave test 2013061414* has been performed.

During the analysis of the wave response it was found a large time delay in the force response on the bracings for locations placed at the same height above SWL. That situation agrees with what was found in the previous force response and time analysis.

In order to just analyze the impulse response the signal has been filtered down. The election of the cut-off frequency plays an important role because it must take out the Morison forces and not disturb the frequency of the bracing produced by the impulse load.

The large existing time delay among the responses along the bracings has allowed separately model the wave load acting on the bracings.

The highest slamming factor  $C_s$  was found in the upper side of the front instrumented bracing with a value of  $C_s = 4.78$ . Smaller slamming factors were found in the lower parts of the front bracings  $C_s = 2.09$ , where the force recorded was almost three times less than on the upper parts.

These really low values on the lower sides of the bracings might be related to some wall effects. Even though the distance from the lower bracing transducers with respect to the wall side is around 1.50 m, it should be further investigated and would require more analysis in order to confirm or disregard it.

The  $C_s = 4.78$  found is smaller than the one found by Oumeraci (2005)  $C_s = 2\pi$ , but is quite similar to the slamming factor obtained by other authors as Aune (2011) who investigated the slamming factor in his Master's thesis on a truss support structure with a result of  $C_s = 4.77$  as well.

It was found that the duration of the load  $\tau$ , for the wave loads acting on the lower part of the bracing,  $\tau = 0.005$  s is the same as Wienke and Oumeraci (2005) derived for our study case  $\tau = 0.0049$  s. Regarding to the average load duration of the wave loads acting on the upper part,  $\tau = 0.007$  s is in between the values derived by Tanimoto (1986)  $\tau = 0.006 - 0.012$  s. So both expressions give really close values to the load duration previously found.

The model built up offers a good global initial response and a notable local response on the bracings simulating the wave loads as a uniform load with triangular force time history. The response from ANSYS gives an average error for the peak force magnitude of 2.65%, whereas the error related to at what time those peaks are produced with respect to the data values is around 3.45%. Moreover, the path described by the data response when the impulse occurs is faithfully described on ANSYS.

Based on that, the model built up on ANSYS seems a really promising tool in order to characterize the wave slamming forces acting on the bracings. In light of the randomness about the impact of waves in the structure it does not seem apparently plausible to automate the process to characterize the other breaking wave loads. At least an individual treatment for each wave is needed in order to consider the possible correlations and where the wave smashes first.

## 8.1 Recommendations for further work

The WaveSlam project is based on data that includes more than 15000 of both regular and irregular waves hitting the structure during 9 days. This master thesis represents a significant step forward with respect to get some understanding about slamming waves on a truss structure and slamming coefficients.

Based on the above conclusions, it is recommended to perform a complete analysis and use advanced statistics for the data to enlighten some aspects such as: (i) confirm or discard the existence of wall effects, (ii) reduce the uncertainty on the results, (iii) study the response considering where the wave breaks, (iv) detect whether there is a trend for the position where the wave hits first the front of the structure, etc.

Regarding to the model itself, it has not been fully validated and especially, if a complete validation of the structure would be required the focus should be put on the local behavior of the instrumented legs and the side instrumented bracings.

Further analysis might consider the development of a CFD model that will deal with the interaction of waves and structure. The recreation from a CFD model of the plunging breaking waves represents at the moment big challenges, but an estimation of the Morison forces (drag and inertia parameters) could be achieved from a fitting data analysis.

Once the model has been calibrated and accurate results have been obtained, is encouraged to analyze more waves in order to obtain a mean value for the highest slamming factors.

## REFERENCES

- Aashmar, M. (2012). *Wave slamming forces on truss support structures for wind turbines*. NTNU. Department of Civil and Transport Engineering. Trondheim: Norwegian University of Science and Technology
- American Bureau of Shipping (ABS,2010). *Guide for Building and Classing Offshore Wind Turbines*.
- American Petroleum Institute (API, 2007). *API RP 2A –WSD: Recommended Practice for Planning Designing and Construction Fixed Offshore structures – Working Stress Design, 21<sup>st</sup> Edition* (with Errata and Supplement in 2002,2005 and 2007)
- Aune, L. (2011). *Master thesis: Bølgeslag mot jacket på grunt vatn*. Department of Structural Engineering, Trondheim, Norwegian University of Science and Technology
- Christy Ushanth Navaratnam, Alf Tørum & Øivind A. Arntsen. (2013). *Preliminary analysis of wave slamming force response data from tests on a truss structure in Large Wave Flume, Hannover, Germany*. Department of Civil and Transport Engineering, Trondheim, Norwegian University of Science and Technology
- Det Norske Veritas (DNV, 2012a). *OS-J101 Design of Offshore wind turbine structures*
- Det Norske Veritas (DNV, 2010b). *RP-C205 Environmental conditions and Environmental loads*
- Germanischer Lloyd (GL, 2005). *Guideline for the Certification of Offshore Wind Turbines*.
- Goda, Y., Haranka, S., & Kitahata, M. (1996). Study of impulsive breaking wave forces on piles. *Port and Harbour Research Institute*, 5 (6), 1-30.
- International Electrotechnical Commission (IEC, 2009 ). *IEC 61400-3: Wind turbines Part 3: Design requirements for offshore Wind turbines, 1<sup>st</sup> Edition*.
- International Organization for Standardization (ISO, 2007). *ISO 19902: Petroleum and natural gas industries – Fixed Steel Offshore Structures*. Geneva, Switzerland.
- Morison, J., O'brien, M, Johnson, J., & Schaaf, S. (1950). The forces exerted by surface waves on piles. *Journal of petroleum Technology, Petroleum transactions, AMIE*, 189, 149-15
- Naess, A. (2011). *An introduction to random vibrations. Trondheim. Center for Ships and Ocean Structures*, Norwegian University of Science and Technology
- Ros Collados, X. (2011). *Master thesis: Impact forces on a vertical pile from plunging breaking waves*. Department of Civil and Transport Engineering. Trondheim: NTNU.

- Swaragi, T., & Nochino, M. (1984). Impact forces of nearly breaking waves on a vertical circular cylinder. *Coastal Engineering in Japan* (27), 249-263
- Tanimoto, K., Takahashi, S., Kaneko, T., & Shiota, K. (1986). Impulsive breaking wave forces on an inclined pile exerted by random waves. *Proceedings of 20<sup>th</sup> International Conference on Coastal Engineering*, (pp. 2288 -2302)
- Tørum, A (2013). *Analysis of force response data from tests on a model of truss structure subjected to plunging breaking waves*. Department of Civil and Transport Engineering. Trondheim, Norway. Norwegian University of Science and Technology
- Von Karman, T. (1929). *The impact on seaplane floats during landing*. Washington: National Advisory Committee for Aeronautics.
- Wagner, H. (1932). Über stoss-und gleitvorgänge an der oberfläche von flüssigkeiten. *Zeitschrift für Angewandte Mathematik und Mechanik*, 12(4), 193-215
- Wienke, J., & Oumeraci, H. (2005). Breaking wave impact force on a vertical an inclined slender pile – theoretical and large-scale model investigations. *Coastal Engineering* 52, 435-462



**LIST OF SYMBOLS**

$A$  = area

$b$  = mass forces

$C$  = Structural damping matrix

$C_a$  = added mass coefficient

$C_b$  = Breaking wave celerity

$C_D$  = Drag coefficient

$C_s$  = Slamming factor

$d$  = Water depth

$D$  = Diameter of the pile

$E$  = Young Modulus

$f$  = frequency

$f(t)$  = Force vector

$f_0$  = Impulse load

$f_s(t)$  = Line slamming force

$F_D$  = Drag force

$F_M$  = Inertia force

$F_p$  = Peak force

$F_s$  = Slamming force

$g$  = gravity acceleration

$(\omega)$  = Frequency response function

$I$  = Inertia

$k$  = Stiffness

$K$  = Structural stiffness matrix

$K_c$  = Keulegan – Carpenter number

$l_{\text{impact}}$  = length of the bracing within the impact.

$m$  = mass

$m_a$  = added mass

$M$  = Structural mass matrix

$N_i$  = Interpolation functions

$R$  = Radius of the pile

$Sf(\omega)$  = Linear spectrum of applied force

$t$  = Time

$T$  = wave period

$T_d$  = natural period of oscillation

$T_{off}$  = Offset time

$T_p$  = Peak time

$t^*$  = Duration of impulse impact

$u$  = Wave velocity

$u_{max}$  = Maximum response

$V$  = Relative velocity between water and the body

$w$  = angular frequency

$X_i$  = Point force

$\rho_w$  = Density of water

$\eta_b$  = Breaking crest height

$\lambda$  = Curling factor

$\delta\xi$  = Virtual strain

$\delta u$  = Virtual displacement

$\xi$  = Damping ratio

$\alpha$  = mass coefficient

$\beta$  = stiffness coefficient

$\tau$  = Duration of wave load

## APPENDICES

## APPENDIX A

## **MASTER DEGREE THESIS**

Spring 2014

for

Student: Rausa Heredia, Ignacio Eugenio

### **Characterization of wave slamming forces on a truss structures within the framework of WaveSlam project**

#### **BACKGROUND**

The wind power is one of the most fast growing energy source. The first offshore wind project around the world was set up in Denmark during the beginning of the 1990s. Since that time, Europe has become the world leader in offshore energy production.

When the installation of these wind turbines are referred to shallow water (20 -30 m water depth) the foundations might be exposed to slamming forces from breaking waves, typically plunging breaking waves. The determination of wave slamming forces remains still today, after more than 85 years of study, a challenging topic. The main difficulties are related to the uncertainties and singularities of pressure and fluid velocity in the waterfront.

Nowadays the mains models available to estimate the slamming forces arising from breaking waves are monopods. Reinertsen A/S, Trondheim, has been involved in the design of truss support structures for wind turbines on the Thornton Bank, Belgian Coast. Calculations based on monopods show that the impulsive forces from the plunging waves might be governing factors of the truss structure and the foundations.

#### **TASK**

The goal of the proposed project is to investigate the slamming forces from plunging breaking waves on truss structures placed in shallow water and to improve the method to calculate those forces through model tests.

For this purpose large scale (1:8) tests were carried out at the Large Wave Flume in Hannover, Germany in 2013, in order to recreate plunging breaking waves and to study the responses from these wave breaking forces.

The simulation of the model tested using a finite element method software will allow to study and characterize through a fitting analysis, which have been the wave forces acting on the structure and determine the respective slamming coefficients. So far only monopod structures have been extensively studied so this project undoubtedly represents a significant step for the study of the slamming forces on truss structures.

An overview about the main tasks to be developed in this project are:

- Statistical analysis of local measurements on the bracings
- To develop a finite element model for a transient analysis in ANSYS. This part is the core of the Master Thesis and will be developed in collaboration with Reinertsen SA.
- Validating and updating the numerical model for the local response on the bracings and a global response as well.
- Estimating wave forces.
- Characterization of slamming factors in the front bracings.

### **General about content, work and presentation**

The text for the master thesis is meant as a framework for the work of the candidate. Adjustments might be done as the work progresses. Tentative changes must be done in cooperation and agreement with the professor in charge at the Department.

In the evaluation thoroughness in the work will be emphasized, as will be documentation of independence in assessments and conclusions. Furthermore the presentation (report) should be well organized and edited; providing clear, precise and orderly descriptions without being unnecessary voluminous.

The report shall include:

- Standard report front page (from DAIM, <http://daim.idi.ntnu.no/>)
- Title page with abstract and keywords.(template on: <http://www.ntnu.no/bat/skjemabank>)
- Preface
- Summary and acknowledgement. The summary shall include the objectives of the work, explain how the work has been conducted, present the main results achieved and give the main conclusions of the work.
- The main text.
- Text of the Thesis (these pages) signed by professor in charge as Attachment 1.

The thesis can as an alternative be made as a scientific article for international publication, when this is agreed upon by the Professor in charge. Such a report will include the same points as given above, but where the main text includes both the scientific article and a process report.

Advice and guidelines for writing of the report is given in “Writing Reports” by Øivind Arntsen, and in the departments “Råd og retningslinjer for rapportskrivning ved prosjekt og masteroppgave” (In Norwegian) located at <http://www.ntnu.no/bat/studier/oppgaver>.

### **Submission procedure**

Procedures relating to the submission of the thesis are described in DAIM (<http://daim.idi.ntnu.no/>).

Printing of the thesis is ordered through DAIM directly to Skipnes Printing delivering the printed paper to the department office 2-4 days later. The department will pay for 3 copies, of which the institute retains two copies. Additional copies must be paid for by the candidate / external partner.

On submission of the thesis the candidate shall submit a CD with the paper in digital form in pdf and Word version, the underlying material (such as data collection) in digital form (e.g. Excel). Students must submit the submission form (from DAIM) where both the Ark-Bibl in SBI and Public Services (Building Safety) of SB II has signed the form. The submission form including the appropriate signatures must be signed by the department office before the form is delivered Faculty Office.

Documentation collected during the work, with support from the Department, shall be handed in to the Department together with the report.

According to the current laws and regulations at NTNU, the report is the property of NTNU. The report and associated results can only be used following approval from NTNU (and external cooperation partner if applicable). The Department has the right to make use of the results from the work as if conducted by a Department employee, as long as other arrangements are not agreed upon beforehand.

### **Tentative agreement on external supervision, work outside NTNU, economic support etc.**

Separate description is to be developed, if and when applicable. See <http://www.ntnu.no/bat/skjemabank> for agreement forms.

### **Health, environment and safety (HSE) <http://www.ntnu.edu/hse>**

NTNU emphasizes the safety for the individual employee and student. The individual safety shall be in the forefront and no one shall take unnecessary chances in carrying out the work. In particular, if the student is to participate in field work, visits, field courses, excursions etc. during the Master Thesis work, he/she shall make himself/herself familiar with “Fieldwork

HSE Guidelines". The document is found on the NTNU HMS-pages at <http://www.ntnu.no/hms/retningslinjer/HMSR07E.pdf>

The students do not have a full insurance coverage as a student at NTNU. If you as a student want the same insurance coverage as the employees at the university, you must take out individual travel and personal injury insurance.

---

**Startup and submission deadlines**

The work on the Master Thesis starts in January 16<sup>th</sup>, 2014

The thesis report shall be submitted digitally in DAIM at the latest at 23:59:59 pm 16, 2014

**Professor in charge:** Michael Muskulus

**Other supervisors:** Øivind Arntsen, Sebastian Schafhirt

Department of Civil and Transport Engineering, NTNU

Trondheim, January 16<sup>th</sup>, 2014, (revised: dd.mm.yyyy)



---

(signature)



## **APPENDIX B**

In the following appendix several figures are provided with more details about the location of bracing transducers and dimensions of the structure.

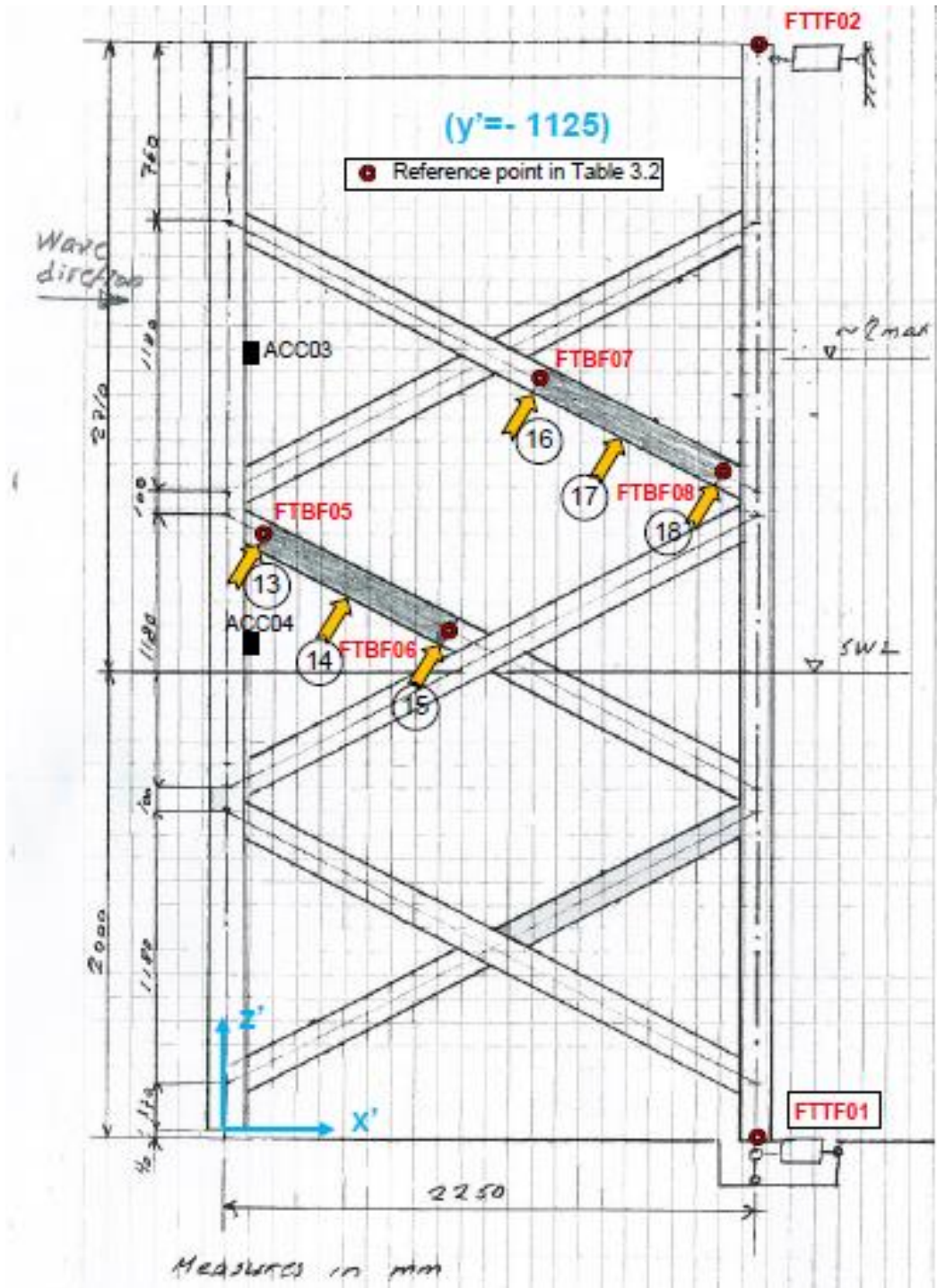


Figure 0.1: Right lateral view of the truss structure taking as reference the wave direction

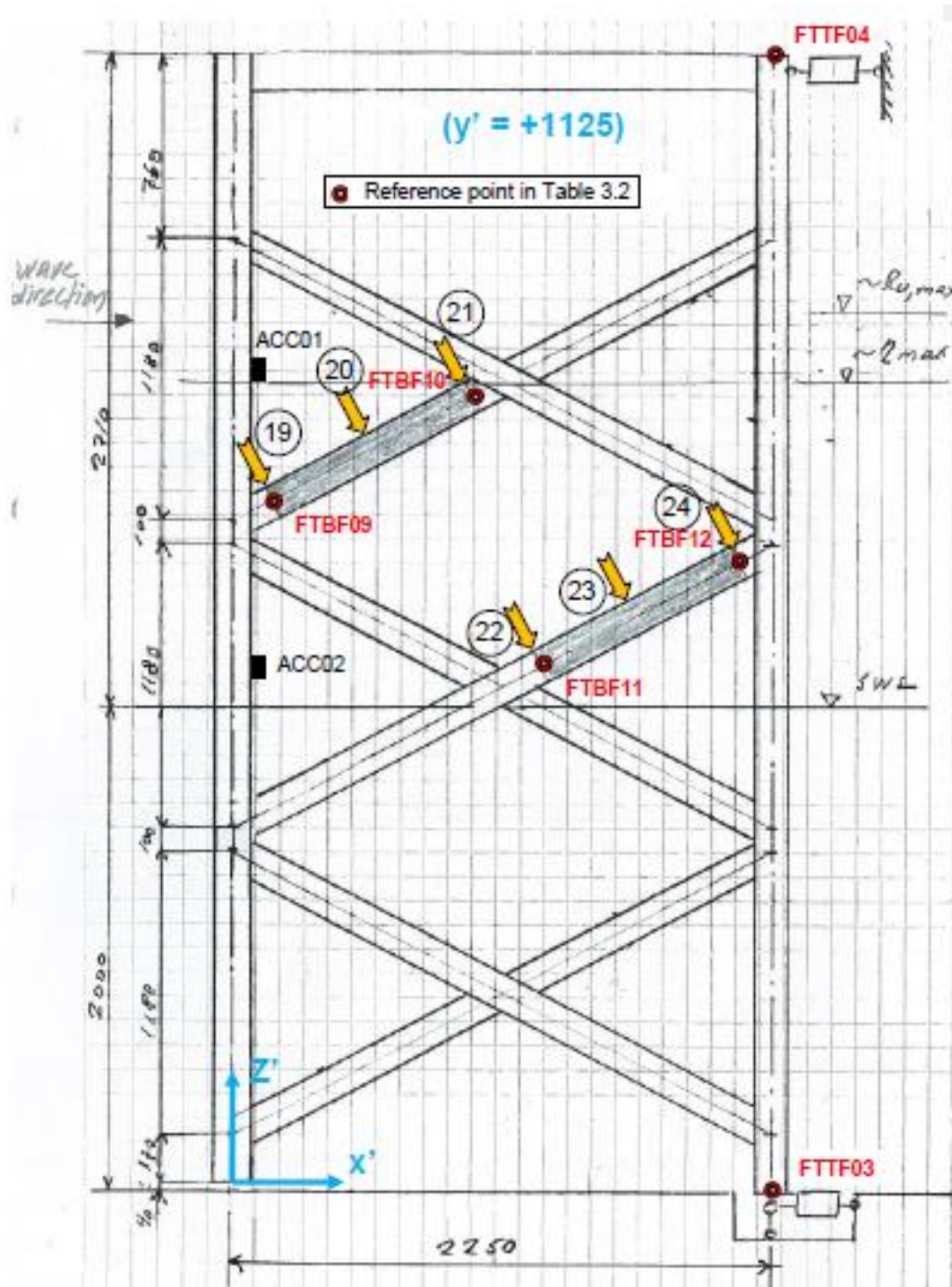


Figure 0.2: Left lateral view of the truss structure taking as reference the wave direction



## APPENDIX C

The results of force and time analysis can be found in this appendix. A complete table of the results is attached to this report in the Excel spreadsheet: “*Data\_Analaysis\_Bracings.xlsx*”

**Table 0.1. Maximum impulse response values in the front bracings transducers for tests n°11 and 13 on the 13 June, 2013**

Force analysis						
Date			<i>Instrumented front bracings</i>			
		WGS9	FTBF01-FH	FTBF02-FH	FTBF03-FH	FTBF04-FH
13.06	Time of study [s]	H. at structure [m]	Max. Impulse [kN]	Max. Impulse [kN]	Max. Impulse [kN]	Max. Impulse [kN]
11	77-79	1.1	0.369	0.431	1.25	0.5212
	81-82	1.153	1.2612	0.3558	0.4313	0.2916
	109-111	1.065	0.5077	0.2354	0.3291	0.7645
	133-135	1.059	0.2651	0.5632	0.3656	0.2449
	137-139	1.041	0.4943	0.3117	0.6407	0.3885
	129-131	1.065	0.2584	0.3808	0.9818	0.3033
	89-91	1.139	0.401	0.318	0.6544	0.5385
	101-103	1.101	0.424	0.3872	0.5706	0.3216
13	78-81	1.15	1.019	0.406	0.8242	1.204
	83-84	1.186	0.5824	0.294	0.3314	0.426
	98-100	1.162	0.563	0.3845	0.3538	0.3416
	123-124	1.15	0.443	0.3801	1.06	0.6015
	103-105	1.133	0.541	0.3562	0.5512	0.7868
	119-121	1.178	0.3035	0.294	0.9915	0.3206
	135-136	1.09	0.7	0.3684	0.442	0.53
	87-88	1.159	0.8982	0.3496	0.3555	0.442

**Table 0.2. Maximum impulse response values in the front bracings transducers for tests n°2-4-8 and 13 on the 14 June, 2013**

Force analysis						
Date			<i>Instrumented front bracings</i>			
	WGS9		<i>FTBF01-FH</i>	<i>FTBF02-FH</i>	<i>FTBF03-FH</i>	<i>FTBF04-FH</i>
<b>14.06</b>	H. at structure [m]	Time of study [s]	Max. Impulse [kN]	Max. Impulse [kN]	Max. Impulse [kN]	Max. Impulse [kN]
	1.235	73-75	0.693	1.855	0.9603	0.5767
	1.15	78-79	0.4236	0.8272	1.434	1.068
	1.16	152-154	0.7538	0.84	0.6927	1.264
	1.16	156-158	1.35	0.5271	0.9802	1.383
	1.228	119-121	0.6027	1.952	1.041	0.3622
	1.26	92-93	0.6543	1.556	0.9589	0.5362
	1.228	106-107	0.7252	0.3265	0.9264	0.3825
2	1.177	133-134	0.3716	0.8869	1.444	0.5035
	1.246	66-69	1.428	0.6138	0.9397	1.169
	1.268	79-81	0.9396	2.53	1.312	0.8658
	1.254	98-99	0.4996	1.201	0.7808	0.6824
	1.131	149-151	2.074	0.9461	0.4753	1.914
	1.237	75-76	0.8653	1.941	1.582	0.6402
	1.245	112-113	1.285	0.2731	0.7429	1.38
	1.229	130-132	1.389	1.322	0.8534	0.8424
4	1.22	117-118	1.375	0.7658	0.6216	0.3972
	1.212	72-74	0.5776	0.4457	0.2708	0.4021
	1.275	81-83	2.669	0.8258	1.016	1.948
	1.343	85-87	0.9488	0.6677	0.8482	1.526
	1.256	136-138	1.691	2.011	2.216	0.9247
	1.274	76-77	1.774	1.208	0.583	1.939
	1.254	122-123	0.8144	1.556	0.8212	0.4304
	1.213	141-142	0.7985	1.615	2.431	1.134
8	1.221	146-147	2.124	1.097	0.4628	1.192
	1.231	66-68	2.797	1.627	0.732	2.544
	1.35	115-117	1.489	2.148	1.747	1.697
	1.306	125-127	0.9	1.374	1.333	1.843
	1.344	140-141	0.8841	2.012	1.804	0.5576
	1.307	71-72	0.9004	1.66	1.192	0.6732
	1.381	76-77	0.3937	1.608	1.33	0.3644
	1.217	106-107	1.697	1.212	1.511	2.042
13	1.177	155-156	0.9281	0.3653	0.5613	2.008

**Table 0.3. Maximum impulse response values in the front bracings transducers for tests n°23-16-25 and 24 on the 14 June, 2013**

Force analysis						
Date	Instrumented front bracings					
	WGS9		FTBF01-FH	FTBF02-FH	FTBF03-FH	FTBF04-FH
<b>14.06</b>	H. at structure [m]	Time of study [s]	Max. Impulse [kN]	Max. Impulse [kN]	Max. Impulse [kN]	Max. Impulse [kN]
23	1.298	58-59	0.883	1.877	0.5465	1.687
	1.369	63-66	0.8346	1.704	1.025	1.511
	1.402	69-72	0.5009	1.336	1.246	0.4032
	1.518	80-81	0.7923	1.78	1.662	0.6664
	1.353	86-87	0.5579	0.7234	0.3766	0.3109
	1.366	92-93	0.2607	0.444	0.8978	0.8509
	1.477	141-142	0.243	0.7326	0.8504	0.2288
	1.432	147-148	0.2292	0.6868	0.3764	0.277
16	1.324	61-63	1.48	1.617	1.979	2.844
	1.397	105-107	1.127	1.93	1.971	0.7057
	1.452	115-117	1.153	2.849	2.577	0.944
	1.441	135-137	0.983	1.349	3.107	0.9799
	1.348	71-72	2.068	1.413	0.8363	2.745
	1.346	101-102	1.335	0.4714	0.9834	1.383
	1.399	125-126	0.75428	1.569	1.169	1.154
	1.469	145-146	1.651	1.447	1.609	0.9501
25	1.35	62-64	1.023	1.212	1.265	1.023
	1.49	79-81	3.182	1.386	1.071	1.723
	1.488	140-142	3.399	1.231	2.094	3.573
	1.495	151-153	4.316	1.222	1.151	1.443
	1.401	107-108	2.786	1.116	0.9794	1.038
	1.472	113-114	2.435	1.152	0.8433	1.796
	1.444	135-136	2.336	1.767	1.907	2.271
	1.514	146-147	1.544	1.135	1.145	2.501
24	1.377	67-69	3.596	2.367	1.425	1.653
	1.402	122-124	2.524	2.321	2.587	0.6487
	1.543	139-141	1.29	2.915	2.66	1.835
	1.551	144-147	2.193	4	3.406	1.231
	1.444	72-73	3.2018	4.112	2.902	1.552
	1.512	78-79	1.65	2.185	2.589	1.486
	1.43	128-129	4.397	2.847	2.525	1.726
	1.433	133-135	1.665	4.443	1.464	1.096



**Table 0.4. Time response values for the highest force response in the front bracings transducers and columns for tests n°11 and 13 on the 13 June, 2013**

<i>Time response [s]</i>						
<b>Date</b>	<i>Bracings</i>				<i>Legs</i>	
<b>13.06</b>	<i>FTBF01</i>	<i>FTBF02</i>	<i>FTBF03</i>	<i>FTBF04</i>	<i>FTLF04</i>	<i>FTLF08</i>
<i>11</i>	77.416	77.409	77.416	77.416	77.422	77.426
	81.503	81.504	81.509	81.511	81.515	81.507
	109.635	109.634	109.621	109.622	109.642	109.618
	133.741	133.731	133.736	133.703	133.716	133.699
	137.882	137.881	137.872	137.873	137.868	137.831
	129.654	129.651	129.656	129.659	129.63	129.612
	89.56	89.558	89.559	89.558	89.559	89.548
	101.615	101.616	101.621	101.621	101.601	101.604
<i>13</i>	79.131	79.132	79.127	79.126	79.121	79.126
	83.144	83.146	83.142	83.142	83.142	83.14
	99.233	99.233	99.24	99.241	99.218	99.209
	123.173	123.172	123.178	123.179	123.18	123.128
	103.242	103.243	103.237	103.236	103.24	103.225
	119.196	119.187	119.181	19.182	119.214	119.168
	135.531	135.531	135.52	135.519	135.488	135.492
	87.18	87.181	87.186	87.175	87.1752	87.1623

**Table 0.5. Time response values for the highest force response in the front bracings transducers and columns for tests n°2 -4-8 and 13 on the 14 June, 2013**

Time response [s]						
Date	Bracings				Legs	
14/06	FTBF01	FTBF02	FTBF03	FTBF04	FTLF04	FTLF08
2	73.95	73.959	73.964	73.966	73.948	73.947
	78.467	78.473	78.462	78.465	78.446	78.461
	152.364	152.375	152.396	152.367	152.361	152.364
	157.311	157.311	157.318	157.316	157.298	157.306
	119.976	119.973	119.979	119.979	119.947	119.96
	92.414	92.412	92.417	92.419	92.383	92.374
	106.288	106.306	106.292	106.292	106.266	106.26
	133.779	133.783	133.775	133.777	133.754	133.754
4	66.617	66.62	66.629	66.626	66.608	66.617
	80.425	80.423	80.428	80.439	80.421	80.419
	98.966	98.966	98.961	98.961	98.934	98.9
	150.055	150.065	150.058	150.056	150.054	150
	75.82	75.818	75.814	75.826	75.796	75.796
	112.51	112.518	112.604	112.604	112.511	112.598
	131.067	131.067	131.062	131.061	131.041	131.05
	117.208	117.21	117.209	117.209	117.2	117.196
8	71.982	71.983	71.996	72.109	71.988	71.99
	81.302	81.304	81.312	81.31	81.239	81.26
	85.957	85.958	85.96	85.958	85.948	85.957
	136.713	136.708	136.707	136.716	136.685	136.682
	76.688	76.7	76.695	76.692	76.655	76.673
	122.821	122.822	122.826	122.829	122.802	122.79
	141.348	141.371	141.365	141.369	141.331	141.324
	146.197	146.199	146.203	146.189	146.2	146.234
13	66.79	66.802	66.769	66.794	66.775	66.775
	115.832	115.831	115.838	115.838	115.826	115.831
	125.665	125.669	125.66	125.672	125.66	125.66
	140.378	140.376	140.372	140.372	140.36	140.363
	71.718	71.718	71.716	71.716	71.698	71.7086
	76.624	76.646	76.646	76.646	76.625	76.637
	106.049	106.04	106.058	106.057	106.044	106.048
	155.798	155.814	155.808	155.804	155.813	155.787

**Table 0.6. Time response values for the highest force response in the front bracings transducers and columns for tests n°23 16-25-and 24 on the 14 June, 2013**

Time response [s]						
Date	Bracings				Legs	
14/06	FTBF01	FTBF02	FTBF03	FTBF04	FTLF04	FTLF08
23	58.622	58.645	58.634	58.613	58.632	58.619
	64.122	64.158	64.163	64.119	64.127	64.117
	69.741	69.741	69.746	69.75	69.719	69.724
	80.91	80.9316	80.937	80.939	80.92	80.913
	86.555	86.586	86.588	86.59	86.551	86.553
	92.01	92.07	92.095	92.029	92.055	92.053
	141.76	141.757	141.763	141.766	141.733	141.734
	147.153	147.155	147.164	147.159	147.136	147.132
16	62.089	62.086	62.095	62.088	62.082	62.091
	106.145	106.146	106.145	106.138	106.142	106.14
	115.92	115.918	115.915	115.918	115.904	115.902
	135.65	135.662	135.658	135.659	135.645	135.646
	71.793	71.805	71.8	71.796	71.795	71.769
	101.301	101.301	101.288	101.298	101.294	101.299
	125.79	125.798	125.793	125.783	125.779	125.774
	145.336	145.334	145.34	145.341	145.33	145.323
25	63.264	63.22	63.216	63.256	63.25	63.23
	79.947	79.949	79.955	79.939	79.917	79.92
	141.039	141.036	141.031	141.028	141.005	141.006
	151.752	151.755	151.756	151.75	151.729	151.742
	107.691	107.693	107.699	107.69	107.673	107.665
	113.252	113.257	113.243	113.248	113.238	113.23
	135.546	135.55	135.545	135.543	135.533	135.523
	146.361	146.365	146.349	146.347	146.342	146.336
24	67.132	67.133	67.129	67.128	67.115	67.116
	122.772	122.782	122.785	122.787	122.766	122.771
	139.431	139.421	139.424	139.428	139.401	139.405
	144.775	144.774	144.768	144.771	144.764	144.757
	72.737	72.735	72.741	72.741	72.7301	72.7288
	78.293	78.298	78.296	78.298	78.2841	78.2827
	128.385	128.383	128.392	128.383	128.374	128.379
	133.939	133.936	133.929	133.921	133.93	133.921

**Table 0.7. Average values for the response and deviation associated to each one**

Filtered signal											
Crest height		FTBF01		FTBF02		FTBF03		FTBF04			
Value [m]	Deviation (±)	Response [kN]	Deviation (±)	Response [kN]	Deviation (±)	Response [kN]	Deviation (±)	Response [kN]	Deviation (±)	Response [kN]	Deviation (±)
1.090	0.040	0.498	0.322	0.373	0.097	0.653	0.318	0.422	0.175		
1.151	0.030	0.631	0.234	0.354	0.041	0.614	0.301	0.582	0.293		
1.200	0.042	0.697	0.298	1.096	0.612	1.055	0.258	0.760	0.412		
1.229	0.042	1.232	0.471	1.199	0.736	0.913	0.365	0.986	0.485		
1.256	0.044	1.425	0.750	1.178	0.529	1.081	0.804	1.187	0.600		
1.289	0.073	1.249	0.743	1.501	0.551	1.276	0.443	1.466	0.815		
1.402	0.071	0.538	0.276	1.160	0.578	0.873	0.445	0.742	0.571		
1.397	0.054	1.319	0.413	1.58	0.661	1.779	0.793	1.463	0.844		
1.457	0.056	2.628	1.045	1.278	0.215	1.307	0.449	1.921	0.850		
1.462	0.065	2.565	1.085	3.149	0.902	2.445	0.679	1.403	0.32		

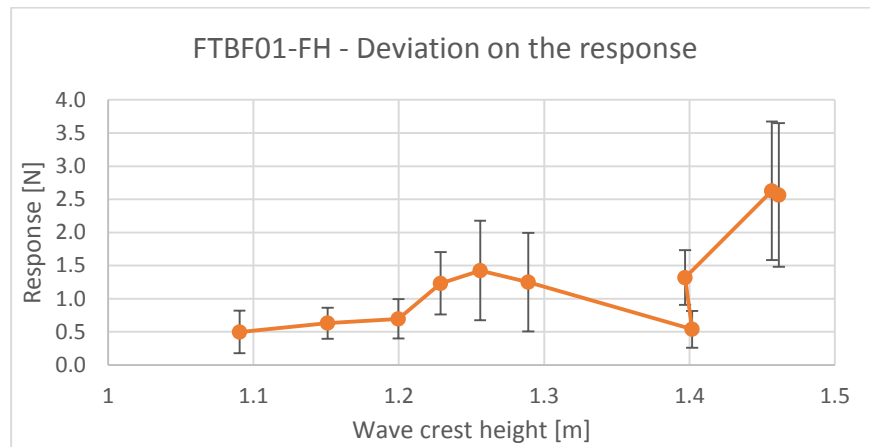


**Figure 0.4: Deviation on the response for samplings analyzed at FTBF01-FH**

## APPENDIX D

A complete table for the proportional damping is described in this appendix.

**Table 0.8 Proportional damping ratios for different frequencies**

<b>F</b> <b>[Hz]</b>	<b>W</b> <b>[rad/s]</b>	<b>Damping Ratio (Mass</b> <b>propt)</b>	<b>Damping Ratio (Stiff</b> <b>propt)</b>	<b>Damping</b> <b>Ratio</b>
0.50	3.14	0.042320	0.000074	0.042394
1.00	6.28	0.021160	0.000147	0.021307
1.50	9.42	0.014107	0.000221	0.014328
2.00	12.57	0.010580	0.000294	0.010874
2.50	15.71	0.008464	0.000368	0.008832
3.00	18.85	0.007053	0.000441	0.007495
3.50	21.99	0.006046	0.000515	0.006561
4.00	25.13	0.005290	0.000589	0.005879
4.50	28.27	0.004702	0.000662	0.005364
5.00	31.42	0.004232	0.000736	0.004968
5.50	34.56	0.003847	0.000809	0.004657
6.00	37.70	0.003527	0.000883	0.004410
6.50	40.84	0.003255	0.000956	0.004212
7.00	43.98	0.003023	0.001030	0.004053
7.50	47.12	0.002821	0.001104	0.003925
8.00	50.27	0.002645	0.001177	0.003822
8.50	53.41	0.002489	0.001251	0.003740
9.00	56.55	0.002351	0.001324	0.003675
9.50	59.69	0.002227	0.001398	0.003625
10.00	62.83	0.002116	0.001471	0.003587
10.50	65.97	0.002015	0.001545	0.003560
11.00	69.12	0.001924	0.001619	0.003542
11.50	72.26	0.001840	0.001692	0.003532
12.00	75.40	0.001763	0.001766	0.003529
12.50	78.54	0.001693	0.001839	0.003532
13.00	81.68	0.001628	0.001913	0.003541
13.50	84.82	0.001567	0.001986	0.003554
14.00	87.96	0.001511	0.002060	0.003572
14.50	91.11	0.001459	0.002134	0.003593
15.00	94.25	0.001411	0.002207	0.003618
15.50	97.39	0.001365	0.002281	0.003646
16.00	100.53	0.001323	0.002354	0.003677
16.50	103.67	0.001282	0.002428	0.003710
17.00	106.81	0.001245	0.002502	0.003746
17.50	109.96	0.001209	0.002575	0.003784
18.00	113.10	0.001176	0.002649	0.003824
18.50	116.24	0.001144	0.002722	0.003866
19.00	119.38	0.001114	0.002796	0.003909
19.50	122.52	0.001085	0.002869	0.003955

20.00	125.66	0.001058	0.002943	0.004001
20.50	128.81	0.001032	0.003017	0.004049
21.00	131.95	0.001008	0.003090	0.004098
21.50	135.09	0.000984	0.003164	0.004148
22.00	138.23	0.000962	0.003237	0.004199
22.50	141.37	0.000940	0.003311	0.004251
23.00	144.51	0.000920	0.003384	0.004304
23.50	147.65	0.000900	0.003458	0.004358
24.00	150.80	0.000882	0.003532	0.004413
24.50	153.94	0.000864	0.003605	0.004469
25.00	157.08	0.000846	0.003679	0.004525
25.50	160.22	0.000830	0.003752	0.004582
26.00	163.36	0.000814	0.003826	0.004640
26.50	166.50	0.000798	0.003899	0.004698
27.00	169.65	0.000784	0.003973	0.004757
27.50	172.79	0.000769	0.004047	0.004816
28.00	175.93	0.000756	0.004120	0.004876
28.50	179.07	0.000742	0.004194	0.004936
29.00	182.21	0.000730	0.004267	0.004997
29.50	185.35	0.000717	0.004341	0.005058
30.00	188.50	0.000705	0.004414	0.005120
30.50	191.64	0.000694	0.004488	0.005182
31.00	194.78	0.000683	0.004562	0.005244
31.50	197.92	0.000672	0.004635	0.005307
32.00	201.06	0.000661	0.004709	0.005370
32.50	204.20	0.000651	0.004782	0.005433
33.00	207.35	0.000641	0.004856	0.005497
33.50	210.49	0.000632	0.004929	0.005561
34.00	213.63	0.000622	0.005003	0.005625
34.50	216.77	0.000613	0.005077	0.005690
35.00	219.91	0.000605	0.005150	0.005755
35.50	223.05	0.000596	0.005224	0.005820
36.00	226.19	0.000588	0.005297	0.005885
36.50	229.34	0.000580	0.005371	0.005951
37.00	232.48	0.000572	0.005444	0.006016
37.50	235.62	0.000564	0.005518	0.006082
38.00	238.76	0.000557	0.005592	0.006148
38.50	241.90	0.000550	0.005665	0.006215
39.00	245.04	0.000543	0.005739	0.006281
39.50	248.19	0.000536	0.005812	0.006348



40.00	251.33	0.000529	0.005886	0.006415
40.50	254.47	0.000522	0.005959	0.006482
41.00	257.61	0.000516	0.006033	0.006549
41.50	260.75	0.000510	0.006107	0.006616
42.00	263.89	0.000504	0.006180	0.006684
42.50	267.04	0.000498	0.006254	0.006752
43.00	270.18	0.000492	0.006327	0.006819
43.50	273.32	0.000486	0.006401	0.006887
44.00	276.46	0.000481	0.006474	0.006955
44.50	279.60	0.000476	0.006548	0.007024
45.00	282.74	0.000470	0.006622	0.007092
45.50	285.88	0.000465	0.006695	0.007160
46.00	289.03	0.000460	0.006769	0.007229
46.50	292.17	0.000455	0.006842	0.007297
47.00	295.31	0.000450	0.006916	0.007366
47.50	298.45	0.000445	0.006989	0.007435
48.00	301.59	0.000441	0.007063	0.007504
48.50	304.73	0.000436	0.007137	0.007573
49.00	307.88	0.000432	0.007210	0.007642
49.50	311.02	0.000427	0.007284	0.007711
50.00	314.16	0.000423	0.007357	0.007781
50.50	317.30	0.000419	0.007431	0.007850
51.00	320.44	0.000415	0.007505	0.007919
51.50	323.58	0.000411	0.007578	0.007989
52.00	326.73	0.000407	0.007652	0.008059
52.50	329.87	0.000403	0.007725	0.008128
53.00	333.01	0.000399	0.007799	0.008198
53.50	336.15	0.000396	0.007872	0.008268
54.00	339.29	0.000392	0.007946	0.008338
54.50	342.43	0.000388	0.008020	0.008408
55.00	345.58	0.000385	0.008093	0.008478
55.50	348.72	0.000381	0.008167	0.008548
56.00	351.86	0.000378	0.008240	0.008618
56.50	355.00	0.000375	0.008314	0.008688
57.00	358.14	0.000371	0.008387	0.008759
57.50	361.28	0.000368	0.008461	0.008829
58.00	364.42	0.000365	0.008535	0.008899
58.50	367.57	0.000362	0.008608	0.008970
59.00	370.71	0.000359	0.008682	0.009040
59.50	373.85	0.000356	0.008755	0.009111
60.00	376.99	0.000353	0.008829	0.009182

<i>Half power band with method -24062013-</i>									
<i>Test run</i>	19	49	36	15	22	32	39	25	
<i>Point</i>	2	25	5	1	3	4	6	8	
<i>Peak frequency</i>	25.33	25.02	25.63	25.024	25.63	25.63	25.63	25.63	25.63
<i>f1<sup>18</sup></i>	25.09	24.26	24.98	24.72	25.19	25.16	25.35	24.2	
<i>f2</i>	25.79	25.46	25.91	25.62	25.83	25.8	25.86	26.07	
<i>ξ</i>	0.0138	0.0240	0.0181	0.0180	0.0125	0.0125	0.0099	0.0099	0.0099

**Figure 0.5: Summarize of the Half power bandwidth method applied using different hammer tests**

<sup>18</sup> This value is the frequency that corresponds to  $x_{max}/2$ , where  $x_{max}$  is the relative value that corresponds to the peak frequency. See figure 5.25 for more details

## **APPENDIX E**

This appendix contains the four scripts coded in MATLAB for the analysis of the response on the instrumented bracings and columns, the calculation of the spectrums and finally the script that calculates the impulse forces using the so called Frequency Response Method.

### *Bracing analysis*

```

close all
clear all

%----This script is only used for the HORIZONTAL forces on the bracings--
--

%Call the script preston2mate to get the data from the WG S9 -----

Ch_01_21=ans;
clear ans

WG_S9_01(:,2)=Ch_01_21(:,19);

fs=200; %Sampling frequency of water gauges
n=length(WG_S9_01);
WG_S9_01(1,1)=0;

for t=1:n-1
    WG_S9_01(t+1,1)=WG_S9_01(t,1)+(1/fs);
end

figure(1)
plot(WG_S9_01(:,1),WG_S9_01(:,2))
title('water surface at structure__2013061423')

%Analysis of the bracings forces.

filename='20130614_08_FTBF_FH.dat';
delimiterIn=' ';
headerlinesIn=7;

FTBF=importdata(filename,delimiterIn,headerlinesIn);

t_b(:,1)=FTBF.data(:,1); %Time column for the bracings. They are sampled
at a frequency of 10000 Hz

t_w(:,1)=WG.data(:,1); %Time column for the water gauges. They are
sampled at a frequency of 200 Hz

%Importing the values for either bracers or water gauges into a Matrix M
M(:,1)=FTBF.data(:,1);

for i=2:5
    M(:,i)=FTBF.data(:,i);
end

%Range values
Dmin=1410000;
    
```

```
Dmax=1420000;

Dmin_w=15801;
Dmax_w=16401;

M_r(:,1)=M(Dmin:Dmax,1);

for j=2:5
    M_r(:,j)=M(Dmin:Dmax,j);
end

WG_S9_01_ranged(:,1)=WG_S9_01(Dmin_w:Dmax_w,1);
WG_S9_01_ranged(:,2)=WG_S9_01(Dmin_w:Dmax_w,2);

%Filtering it down
[b a]=butter(4,25/5000,'low');

M_r_f(:,1)=filtfilt(b,a,M_r(:,2));
M_r_f(:,2)=filtfilt(b,a,M_r(:,3));
M_r_f(:,3)=filtfilt(b,a,M_r(:,4));
M_r_f(:,4)=filtfilt(b,a,M_r(:,5));

%Dynamic response
for l=2:5
    M_r_d(:,l-1)=M_r(:,l)-M_r_f(:,l-1);
end

%Filtered Dynamic response
[d c]=butter(4,400/5000,'low'); %Take out the noise

M_r_n(:,1)=filtfilt(d,c,M_r_d(:,1));
M_r_n(:,2)=filtfilt(d,c,M_r_d(:,2));
M_r_n(:,3)=filtfilt(d,c,M_r_d(:,3));
M_r_n(:,4)=filtfilt(d,c,M_r_d(:,4));

%Plots
figure(2)
hold on
plot(M_r(:,1),M_r(:,2))
plot(M_r(:,1),M_r_f(:,1),'r')
plot(M_r(:,1),M_r_n(:,1),'g')

figure(3)
hold on
plot(M_r(:,1),M_r(:,3))
plot(M_r(:,1),M_r_f(:,2),'r')
plot(M_r(:,1),M_r_n(:,2),'g')

figure(4)
hold on
plot(M_r(:,1),M_r(:,4))
plot(M_r(:,1),M_r_f(:,3),'r')
plot(M_r(:,1),M_r_n(:,3),'g')
```

```

figure(5)
hold on
plot(M_r(:,1),M_r(:,5))
plot(M_r(:,1),M_r_f(:,4),'r')
plot(M_r(:,1),M_r_n(:,4),'g')

grid on
t=title('Filtered Impulse Response: 400 Hz, FTBF04-FH --Wave Test:
20130614-08--');
x_1=xlabel('Time [s]');
y_1=ylabel('Force [kN]');
h_legend=legend('Unfiltered signal', 'Quasi-static response', 'Impulse
response');
set(set(x_1,'FontSize',14), set(y_1,'FontSize',14)
set(gca,'FontSize',14)

```

### *Column Analysis*

```

clear all
close all

%----This script is only used for the response at FTLF04-08----

%Call the script preston2matg to get the data from any wave test we are
%interested in

%FTLF04-FTLF08
Ch_22_72=ans;
clear ans
for r=17:21,
s(:,r)=Ch_22_72(1,r);
end

FTLF04=s{1,17};          FTLF08=s{1,21};
FTLF04(:,2)=FTLF04;    FTLF08(:,2)=FTLF08;

n_1=length(FTLF04);
fs_1=10000; %Sampling frequency
FTLF04(1,1)=0;

for i=1:n_1-1
    FTLF04(i+1,1)=FTLF04(i,1)+(1/fs_1);
end

figure(2)
plot(FTLF04(:,1),FTLF04(:,2))
title('FTLF04_unfiltered__2013061408')

FTLF08(1,1)=0;

for i=1:n_1-1

```

```

    FTLF08(i+1,1)=FTLF08(i,1)+(1/fs_1);
end

figure(3)
plot(FTLF08(:,1),FTLF08(:,2))
title('FTLF08_unfiltered__2013061408')

%Study range points
Dmin=1460000;
Dmax=1470000;

FTLF04_ranged(:,2)=FTLF04(Dmin:Dmax,2);
FTLF04_ranged(:,1)=FTLF04(Dmin:Dmax,1);

FTLF08_ranged(:,2)=FTLF08(Dmin:Dmax,2);
FTLF08_ranged(:,1)=FTLF08(Dmin:Dmax,1);

figure(3)
plot(FTLF04_ranged(:,1),FTLF04_ranged(:,2))
title('FTLF06-unfiltered. Data points: 665000-668000--2013061423--')
x_2=xlabel('t[s]');
y_2=ylabel('[kN]');

%Filtering

[b a]=butter(4,25/5000,'low');
FTLF04_filtered=filtfilt(b,a,FTLF04_ranged(:,2));
FTLF08_filtered=filtfilt(b,a,FTLF08_ranged(:,2));

FTLF04_dyn=FTLF04_ranged(:,2)-FTLF04_filtered;
FTLF08_dyn=FTLF08_ranged(:,2)-FTLF08_filtered;

[c d]=butter(4,400/5000,'low');
FTLF04_filtered_1=filtfilt(c,d,FTLF04_dyn);
FTLF08_filtered_1=filtfilt(c,d,FTLF08_dyn);

figure(4)
hold on
plot(FTLF04_ranged(:,1),FTLF04_ranged(:,2))
plot(FTLF04_ranged(:,1),FTLF04_filtered,'r')
plot(FTLF04_ranged(:,1),FTLF04_filtered_1,'g')

figure(5)
hold on
plot(FTLF08_ranged(:,1),FTLF08_ranged(:,2))
plot(FTLF08_ranged(:,1),FTLF08_filtered,'r')
plot(FTLF08_ranged(:,1),FTLF08_filtered_1,'g')

grid on
t=title('Filtered Impulse Response: 400 Hz, FTLF08 --Wave Test: 20130614-08--');
x_1=xlabel('Time [s]');
y_1=ylabel('Force [kN]');

```

```
h_legend=legend('Unfiltered signal', 'Quasi-static response', 'Impulse
response');
set(set(x_1,'FontSize',14), set(y_1,'FontSize',14)
set(gca,'FontSize',14)
```

### *Spectrum Analysis*

*%This script calculates the Spectrum for any signal.*

```
clear all
close all

filename='20130624_26_FTBF01_Response_Hammer.dat';
delimiterIn=' ';
headerlinesIn=4;

FTBF_imp=importdata(filename,delimiterIn,headerlinesIn);

Dmin=62000;
Dmax=66000;

FTFB01(:,1)=FTBF_imp.data(Dmin:Dmax,1);
FTFB01(:,2)=FTBF_imp.data(Dmin:Dmax,2);

fs=10000; %Hz
Channel_2_Data_d=detrend(FTFB01(:,2));
n=length(Channel_2_Data_d);
FTFB01(:,2)=Channel_2_Data_d;

NFFT=2^nextpow2(n);

Y=fft(FTFB01(:,2),NFFT);
Power=(Y.*conj(Y))/NFFT;
f=(0:NFFT/2).*fs/NFFT;

figure(1)
grid on
plot(f(1:end),Power(1:(end/2)+1))
title('Spectrum at FTBF01-FH / Hammer test at position 9. Data
points=62000:66000')
x_1=xlabel('Frequency [Hz]');
y_1=ylabel('Relative values');
h_legend=legend('Response');
set(h_legend, 'FontSize',14), set(x_1,'FontSize',14),
set(y_1,'FontSize',14)
set(gca,'FontSize',14)
```



### *Frequency response method (FRF).*

```
%This script calculates the impulse load on the bracings using the FRF
method.

%We have to calculate first the transfer functions assuming that H(w) for
%FTBF01 is equal to FTBF04 and the same occurs for FTBF02 and FTBOF03. So
%only two transfer functions are calculated.

%First we import the response from the hammer test on
FTTBF01/02/03/04_FH.

filename='2013061133_FTBF02_FH_ImpulseResponse.dat';
delimiterIn=' ';
headerlinesIn=4;

Response_FTBF1_FH=importdata(filename,delimiterIn,headerlinesIn);

R(:,1)=Response_FTBF1_FH.data(:,1); %Extract the data for the response
Hammer. This data have been sampled at 20000 Hz.
R(:,2)=Response_FTBF1_FH.data(:,2);

fs=9600; %Initial frequency for the Hammer Impulse
I(:,2)=Channel_15_Data;
I(1,1)=0;
for i=1:length(Channel_15_Data)-1
    I(i+1,1)=I(i,1)+1/fs;
end

%Range of data that is going to be analyzed for the impulse
Dmin_i=8600;
Dmax_i=14600;
n=Dmax_i-Dmin_i;

I_r(:,1)=I(Dmin_i:Dmax_i,1);
I_r(:,2)=I(Dmin_i:Dmax_i,2);

%As the hammer impulse and the response are recorded in different
%frequencies, we decide to get both in 20000 Hz. So we apply a linear
%interpolation to the impulse data.

fs1=20000; %Hz, new frequency sampling for the Impulse Hammer
I_1(1,1)=I_r(1,1);

for i=1:n
    I_1(i+1,1)=I_1(i,1)+(1/fs1);
end

I_1(:,2)=interp1(I_r(:,1),I_r(:,2),I_1(:,1),'linear');

%Range of data that is going to be analyzed for the response from the
%hammer test
Dmin_r=1100;
```

```

Dmax_r=7100; %To make it the same size as the impulse data

R_1(:,1)=R(Dmin_r:Dmax_r,1);
R_1(:,2)=R(Dmin_r:Dmax_r,2)-mean(R(:,2));

fs=20000;
R_1d(:,2)=R_1(:,2)*1000; %We convert the response to Newtons.
R_1d(1,1)=0+0.894;
for i=1:length(R_1)-1
    R_1d(i+1,1)=R_1d(i,1)+1/fs;
end

plot(R_1d(:,1),R_1d(:,2),'r')
hold on
plot(I_1(:,1),I_1(:,2))

n_1=Dmax_i-Dmin_i; %This n_1 has the same size as the length of the
Response from the hammer test
NFFT=2^nextpow2(n_1);

Y1=fft(R_1d(:,2),NFFT);
Y2=fft(I_1(:,2),NFFT);

Power1=(Y1.*conj(Y1)/NFFT);
Power2=(Y2.*conj(Y2)/NFFT);
f=(0:NFFT/2).*fs1/NFFT; %Up to the nyquist frequency

figure(1)
plot(f(1:end),Power1(1:(end/2)+1))
hold on
plot(f(1:end),Power2(1:(end/2)+1),'r')

%Transfer function. It is assumed that H(w) for FTBF01 and 04 are equal.
%The same occurs for FTBF02 and 03.
%So, two different transfer functions needs to be defined, one for
FTBF01-04
%and the other for FTBF02-03. Y2 keeps the same for both. Y1 varies
%for FTBF01 and FTBF02.

H=Y1./Y2; %Transfer function

SFF1= Y1./H;
SFF2= Y2.*H;

FFF=ifft(SFF1); %It gives back the value for the Impulse Response
FFF1=ifft(SFF2); %It gives back the value for the Response

%-----
%Now we are going to analyze what are the impulse at the different points
%for the different wave tests.

filename='2013061414_FTBF_FH_ResponseWave(III).dat';
delimiterIn=' ';

```

```
headerlinesIn=7;

FTBF=importdata(filename,delimiterIn,headerlinesIn);
t_b(:,1)=FTBF.data(:,1);

M(:,1)=FTBF.data(:,1);
M(:,2)=FTBF.data(:,2);
M(:,3)=FTBF.data(:,3);
M(:,4)=FTBF.data(:,4);
M(:,5)=FTBF.data(:,5);

%Range values
Dmin1=4000;
Dmax1=10000;

M_r(:,1)=M(Dmin1:Dmax1,1);
M_r(:,2)=M(Dmin1:Dmax1,2);
M_r(:,3)=M(Dmin1:Dmax1,3);
M_r(:,4)=M(Dmin1:Dmax1,4);
M_r(:,5)=M(Dmin1:Dmax1,5);

%Spectrum of the response on FTLF02

fs1=10000; %Hz
n1=Dmax1-Dmin1;

FTBF01=M_r(:,2)*1000;
FTBF02=M_r(:,3)*1000;
FTBF03=M_r(:,4)*1000;
FTBF04=M_r(:,5)*1000;

NFFT1=2^nextpow2(n1);

%Defining the length for the FFT.

if NFFT1<=NFFT;
    NFFT1;
else NFFT1=NFFT;
end

Y3=fft(FTBF01,NFFT1);
Power3=(Y3.*conj(Y3)/NFFT1);
f1=(0:NFFT1/2).*fs1/NFFT1;

Y4=fft(FTBF02,NFFT1);
Power4=(Y4.*conj(Y4)/NFFT1);
f2=(0:NFFT1/2).*fs1/NFFT1;

Y5=fft(FTBF03,NFFT1);
Power5=(Y5.*conj(Y5)/NFFT1);
f3=(0:NFFT1/2).*fs1/NFFT1;

Y6=fft(FTBF04,NFFT1);
```

```

Power6=(Y6.*conj(Y6)/NFFT1);
f4=(0:NFFT1/2).*fs1/NFFT1;

figure(2)
plot(f1(1:end),Power3(1:(end/2)+1))

figure(3)
plot(f2(1:end),Power4(1:(end/2)+1))

%The acting load is found dividing the Response by the Transfer
%function.The transfer function H is not the same for FTBF01 and FTBF02.
%There is one transfer function for FTBF01-04 and another for FTBF02-03.

r1=Y3./H; %load at FTBF01
FTBF01_Imp=ifft(r1);

r2=Y4./H; %load at FTBF02.
FTBF02_Imp=ifft(r2);

r3=Y5./H; %load at FTBF03
FTBF03_Imp=ifft(r3);

r4=Y6./H; %load at FTBF04
FTBF04_Imp=ifft(r4);

t_br=t_b(Dmin1:Dmax1);
if length(t_br)>=NFFT1;
    t_br1=t_br(1:NFFT1,1);
else tx=(t_br(1):1/10000:(NFFT1-length(t_br))/10000+t_br(end));
    t_br1=tx;
end

figure(4)
plot(t_br1,FTBF01_Imp)
title('FTBF01-FH. Unfiltered signal')
x_1=xlabel('Time[s]');
y_1=ylabel('Force [N]');
h_legend=legend('Impulse force');
set(h_legend, 'FontSize',14), set(x_1, 'FontSize',14),
set(y_1, 'FontSize',14)
set(gca, 'FontSize',14)
grid on

figure(5)
plot(t_br1,FTBF04_Imp)
title('FTBF04-FH. Unfiltered signal')
x_1=xlabel('Time[s]');
y_1=ylabel('Force [N]');
h_legend=legend('Impulse force');
set(h_legend, 'FontSize',14), set(x_1, 'FontSize',14),
set(y_1, 'FontSize',14)
set(gca, 'FontSize',14)
grid on
    
```

```
[c1 d1]=butter(4,70/5000,'low'); %Filtering it down to smooth the signal
FTBF01_filt=filtfilt(c1,d1,FTBF01_Imp(:,1));
FTBF02_filt=filtfilt(c1,d1,FTBF02_Imp(:,1));
FTBF03_filt=filtfilt(c1,d1,FTBF03_Imp(:,1));
FTBF04_filt=filtfilt(c1,d1,FTBF04_Imp(:,1));

FTBF01_c=FTBF01_filt-200; %Calibration of the load
figure(6)
plot(t_br1,FTBF01_c)
title('FTBF01-FH. Filtered signal, Low pass filter: cutoff freq:70 Hz')
x_1=xlabel('Time[s]');
y_1=ylabel('Force [N]');
h_legend=legend('Impulse force');
set(h_legend, 'FontSize',14), set(x_1,'FontSize',14),
set(y_1,'FontSize',14)
set(gca,'FontSize',14)
grid on

FTBF02_c=FTBF02_filt-350; %Calibration of the load
figure(7)
plot(t_br1,FTBF02_c)
title('FTBF02-FH.Filtered signal, Low pass filter: cutoff freq:70 Hz')
x_1=xlabel('Time[s]');
y_1=ylabel('Force [N]');
h_legend=legend('Impulse force');
set(h_legend, 'FontSize',14), set(x_1,'FontSize',14),
set(y_1,'FontSize',14)
set(gca,'FontSize',14)
grid on

FTBF03_c=FTBF03_filt-350; %Calibration of the load
figure(8)
plot(t_br1,FTBF03_c)
title('FTBF03-FH.Filtered signal, Low pass filter: cutoff freq:70 Hz')
x_1=xlabel('Time[s]');
y_1=ylabel('Force [N]');
h_legend=legend('Impulse force');
set(h_legend, 'FontSize',14), set(x_1,'FontSize',14),
set(y_1,'FontSize',14)
set(gca,'FontSize',14)
grid on

FTBF04_c=FTBF04_filt-200; %Calibration of the load
figure(9)
plot(t_br1,FTBF04_c)
title('FTBF04-FH.Filtered signal, Low pass filter: cutoff freq:70 Hz')
x_1=xlabel('Time[s]');
y_1=ylabel('Force [N]');
h_legend=legend('Impulse force');
set(h_legend, 'FontSize',14), set(x_1,'FontSize',14),
set(y_1,'FontSize',14)
set(gca,'FontSize',14)
```

